E-ISSN: 2147-1959

MIRT

Molecular Imaging and Radionuclide Therapy

June 2021 Volume 30 Issue 2 www.tsnm.org

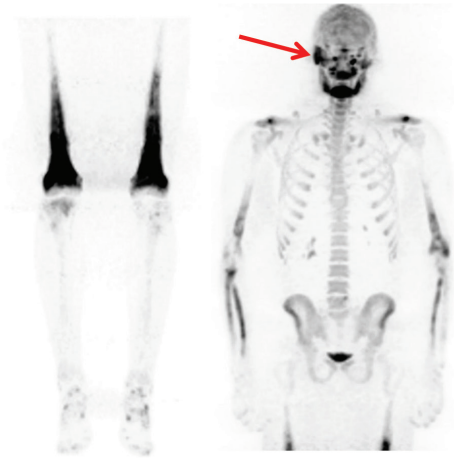

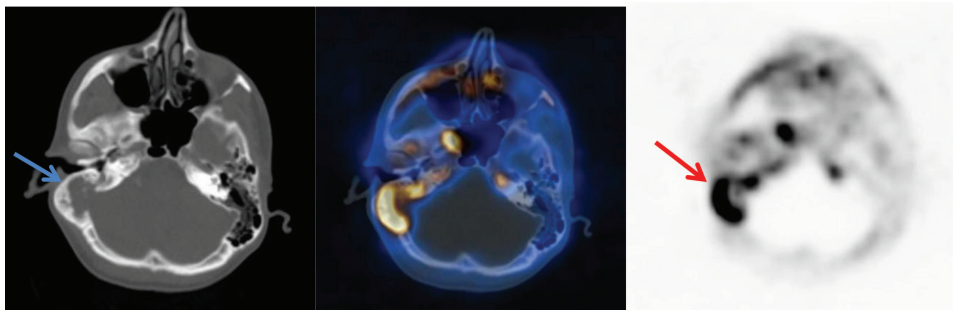

"Official Journal of the Turkish Society of Nuclear Medicine"

galenos yayınevi

TURKISH SOCIETY OF NUCLEAR MEDICINE 1975

MIRT

Molecular Imaging and Radionuclide Therapy

MIRT

Molecular Imaging and Radionuclide Therapy

Turkish Society of Nuclear Medicine
Cinnah Caddesi Pilot Sokak No: 10/12 Çankaya 06650 Ankara, Turkey **Phone:** +90 312 441 00 45 **Fax:** +90 312 441 12 95 **Web:** www.tsnm.org **E-mail:** dernekmerkezi@tsnm.org
"Formerly Turkish Journal of Nuclear Medicine"

Reviewing the articles' conformity to the publishing standards of the Journal, typesetting, reviewing and editing the manuscripts and abstracts in English, creating links to source data, and publishing process are realized by Galenos.

Galenos Publishing House
Owner and Publisher
Derya Mor
Erkan Mor

Publication Coordinator
Burak Sever

Web Coordinators
Fuat Hocalar
Turgay Akpınar

Graphics Department
Ayda Alaca
Çiğdem Birinci
Gülşah Özgül

Finance Coordinator
Sevinç Çakmak

Project Coordinators
Aysel Balta
Duygu Yıldırm
Gamze Aksoy
Gülay Akın
Hatice Sever
Melike Eren
Meltem Acar
Özlem Çelik Çekil
Pınar Akpınar
Rabia Palazoğlu

Research&Development
Melisa Yiğitoğlu
Nihan Karamanlı

Digital Marketing Specialist
Seher Altundemir

Publisher Contact
Address: Molla Gürani Mah. Kaçamak Sk. No: 21/1
34093 İstanbul, Turkey
Phone: +90 (212) 621 99 25 **Fax:** +90 (212) 621 99 27
E-mail: info@galenos.com.tr/yayin@galenos.com.tr
Web: www.galenos.com.tr
Publisher Certificate Number: 14521

Online Publication Date: June 2021
ISSN: 2146-1414 **E-ISSN:** 2147-1959
International scientific journal published quarterly.

MIRT

Molecular Imaging and Radionuclide Therapy

ABOUT US

Molecular Imaging and Radionuclide Therapy (formerly Turkish Journal of Nuclear Medicine) is the official publication of Turkish Society of Nuclear Medicine.

Focus and Scope

Molecular Imaging and Radionuclide Therapy (Mol Imaging Radionucl Ther, MIRT) is a double-blind peer-review journal published in English language. It publishes original research articles, invited reviews, editorials, short communications, letters, consensus statements, guidelines and case reports with a literature review on the topic, in the field of molecular imaging, multimodality imaging, nuclear medicine, radionuclide therapy, radiopharmacy, medical physics, dosimetry and radiobiology. MIRT is published three times a year (February, June, October). Audience: Nuclear medicine physicians, medical physicists, radiopharmaceutical scientists, radiobiologists.

The editorial policies are based on the "Recommendations for the Conduct, Reporting, Editing, and Publication of Scholarly Work in Medical Journals (ICMJE Recommendations)" by the International Committee of Medical Journal Editors (2016, archived at http://www.icmje.org/) rules.

Molecular Imaging and Radionuclide Therapy is indexed in **Pubmed, Pubmed Central (PMC), Emerging Sources Citation Index (ESCI), TUBITAK-ULAKBIM, DOAJ, Scopus, Gale/Cengage Learning, EBSCO databases, Embase, ProQuest Health & Medical Complete, CINAHL, Index Copernicus, J-Gate, IdealOnline, ROOT INDEXING, Türkiye Atıf Dizini-Turkiye Citation Index, Turk Medline, EuroPub, Hinari, GOALI, ARDI, OARE** and **AGORA.**

Open Access Policy

This journal provides immediate open access to its content on the principle that making research freely available to the public supports a greater global exchange of knowledge.

Open Access Policy is based on rules of Budapest Open Access Initiative (BOAI) (http://www.budapestopenaccessinitiative.org/). By "open access" to [peer-reviewed research literature], we mean its free availability on the public internet, permitting any users to read, download, copy, distribute, print, search, or link to the full texts of these articles, crawl them for indexing, pass them as data to software, or use them for any other lawful purpose, without financial, legal, or technical barriers other than those inseparable from gaining access to the internet itself. The only constraint on reproduction and distribution, and the only role for copyright in this domain, should be to give authors control over the integrity of their work and the right to be properly acknowledged and cited.

Subscription Information

Manuscripts can only be submitted electronically through the Journal Agent website (http://www.journalagent.com/mirt/?plng=eng) after creating an account. This system allows online submission and review.

All published volumes in full text can be reached free of charge through the website http://mirt.tsnmjournals.org

Copyright Statement

Turkish Society of Nuclear Medicine holds the international copyright of all the content published in the journal.

Republication and reproduction of images or tables in any published material should be done with proper citation of source providing authors names; article title; journal title; year (volume) and page of publication; copyright year of the article.

The author(s) hereby affirms that the manuscript submitted is original, that all statement asserted as facts are based on author(s) careful investigation and research for accuracy, that the manuscript does not, in whole or part, infringe any copyright, that it has not been published in total or in part and is not being submitted or considered for publication in total or in part elsewhere.

Completed Copyright Statement form should be submitted to the online article system.

By signing this form,

1. Each author acknowledge that he/she participated in the work in a substantive way and is prepared to take public responsibility for the work.

2. Each author further affirms that he or she has read and understands the "Ethical Guidelines for Publication of Research".

3. The author(s), in consideration of the acceptance of the manuscript for publication, does hereby assign and transfer to the Molecular Imaging and Radionuclide Therapy all of the rights and interest in and the copyright of the work in its current form and in any form subsequently revised for publication and/or electronic dissemination.

Instructions for Authors

Instructions for authors are published in the journal and on the website http://mirt.tsnmjournals.org

Material Disclaimer

Scientific and legal responsibilities pertaining to the papers belong to the authors. Contents of the manuscripts and accuracy of references are also the author's responsibility. The Turkish Society of Nuclear Medicine, the Editor, the Editorial Board or the publisher do not accept any responsibility for opinions expressed in articles.

Financial expenses of the journal are covered by Turkish Society of Nuclear Medicine.

Correspondence Address

Editor in Chief Prof. Murat Fani Bozkurt, MD, FEBNM Hacettepe University, Medical School, Department of Nuclear Medicine, Ankara, Turkey

E-mail: fanibozkurt@gmail.com

Web page: http://mirt.tsnmjournals.org/

Publisher Corresponding Address

Galenos Yayınevi Tic. Ltd. Şti.
Address: Molla Gürani Mah. Kaçamak Sk. No: 21/1 34093 Fındıkzade, İstanbul, Turkey
Phone: +90 212 621 99 25
Fax: +90 212 621 99 27
E-mail: info@galenos.com.tr

MIRT

Molecular Imaging and Radionuclide Therapy

INSTRUCTIONS TO AUTHORS

Molecular Imaging and Radionuclide Therapy (Mol Imaging Radionucl Ther, MIRT) publishes original research articles, short communications, invited reviews, editorials, case reports with a literature review on the topic, interesting images, consensus statements, guidelines, letters in the field of molecular imaging, multimodality imaging, nuclear medicine, radionuclide therapy, radiopharmacy, medical physics, dosimetry and radiobiology. MIRT is published by the Turkish Society of Nuclear Medicine three times a year (February, June, October).

Molecular Imaging and Radionuclide Therapy does not charge any article submission or processing fees.

GENERAL INFORMATION

MIRT commits to rigorous peer review, and stipulates freedom from commercial influence, and promotion of the highest ethical and scientific standards in published articles. Neither the Editor(s) nor the publisher guarantees, warrants or endorses any product or service advertised in this publication. All articles are subject to review by the editors and peer reviewers. If the article is accepted for publication, it may be subjected to editorial revisions to aid clarity and understanding without changing the data presented.

Manuscripts must be written in English and must meet the requirements of the journal. The journal is in compliance with the uniform requirements for manuscripts submitted to biomedical journals published by the International Committee of Medical Journal Editors (NEJM 1997; 336:309-315, updated 2016). Manuscripts that do not meet these requirements will be returned to the author for necessary revision before the review. Authors of manuscripts requiring modifications have a maximum of two months to resubmit the revised text. Manuscripts returned after this deadline will be treated as new submissions.

It is the authors' responsibility to prepare a manuscript that meets ethical criteria. The Journal adheres to the principles set forth in the Helsinki Declaration October 2013 (https://www.wma.net/policies-post/wma-declaration-of-helsinki-ethical-principles-for-medical-research-involving-human-subjects/) and holds that all reported research involving "Human beings" conducted in accordance with such principles.

Reports describing data obtained from research conducted in human participants must contain a statement in the MATERIALS AND METHODS section indicating approval by the ethical review board (including the approval number) and affirmation that INFORMED CONSENT was obtained from each participant.

All manuscripts reporting experiments using animals must include a statement in the MATERIALS AND METHODS section giving assurance that all animals have received humane care in compliance with the Guide for the Care and Use of Laboratory Animals (www.nap.edu) and indicating approval by the ethical review board.

If the study should have ethical approval, authors asked to provide ethical approval in order to proceed the review process. If they provide approval, review of the manuscript will continue.

In case report(s) and interesting image(s) a statement regarding the informed consent of the patients should be included in the manuscript and the identity of the patient(s) should be hidden.

Subjects must be identified only by number or letter, not by initials or names. Photographs of patients' faces should be included only if scientifically relevant. Authors must obtain written consent from the patient for use of such photographs. In cases of image media usage that potentially expose patients' identity requires obtaining permission for publication from the patients or their parents/guardians.

If the proposed publication concerns any commercial product, the author must include in the cover letter a statement indicating that the author(s) has (have) no financial or other interest with the product or explaining the nature of any relations (including consultancies) between the author(s) and editor the manufacturer or distributor of the product.

All submissions will be screened by Crossref Smilarity Check powered by "iThenticate". Manuscripts with an overall similarity index of greater than 25%, or duplication rate at or higher than 5% with a single source will be returned back to authors.

MANUSCRIPT CATEGORIES

1. Original Articles

2. Short Communications are short descriptions of focused studies with important, but very straightforward results.

3. Reviews address important topics in the field. Authors considering the submission of uninvited reviews should contact the editor in advance to determine if the topic that they propose is of current potential interest to the Journal. Reviews will be considered for publication only if they are written by authors who have at least three published manuscripts in the international peer reviewed journals and these studies should be cited in the review. Otherwise only invited reviews will be considered for peer review from qualified experts in the area.

4. Editorials are usually written by invitation of the editor by the editors on current topics or by the reviewers involved in the evaluation of a submitted manuscript and published concurrently with that manuscript.

5. Case Report and Literature Reviews are descriptions of a case or small number of cases revealing a previously undocumented disease process, a unique unreported manifestation or treatment of a known disease process, unique unreported complications of treatment regimens or novel and important insights into a condition's pathogenesis, presentation, and/or management. The journal's policy is to accept case reports only if it is accompanied by a review of the literature on the related topic. They should include an adequate number of images and figures.

6. Interesting Image

One of the regular parts of Molecular Imaging and Radionuclide Therapy is a section devoted to interesting images. Interesting image(s) should describe case(s) which are unique and include interesting findings adding insights into the interpretation of patient images, a condition's pathogenesis, presentation, and/or management.

7. Consensus Statements or Guidelines may be submitted by professional societies. All such submissions will be subjected to peer review, must be modifiable in response to criticisms, and will be published only if they meet the Journal's usual editorial standards.

8. Letters to the Editor may be submitted in response to work that has been published in the Journal. Letters should be short commentaries related to specific points of agreement or disagreement with the published work.

Note on Prior Publication

Articles are accepted for publication on the condition that they are original, are not under consideration by another journal, or have not been previously published. Direct quotations, tables, or illustrations that have appeared in

MIRT
Molecular Imaging and Radionuclide Therapy

copyrighted material must be accompanied by written permission for their use from the copyright owner and authors. Materials previously published in whole or in part shall not be considered for publication. At the time of submission, authors must report that the manuscript has not been published elsewhere. Abstracts or posters displayed at scientific meetings need not be reported.

MANUSCRIPT SUBMISSION PROCEDURES

MIRT only accepts electronic manuscript submission at the web site http://www.journalagent.com/mirt/. After logging on to the website Click the 'online manuscript submission' icon. All corresponding authors should be provided with a password and a username after entering the information required. If you already have an account from a previous submission, enter your username and password to submit a new or revised manuscript. If you have forgotten your username and/or password, please send an e-mail to the editorial office for assistance. After logging on to the article submission system please read carefully the directions of the system to give all needed information and attach the manuscript, tables and figures and additional documents.

All Submissions Must Include:

1. Completed Copyright Assignment & Disclosure of Potential Conflict of Interest Form; This form should be downloaded from the website (provided in the author section), filled in thoroughly and uploaded to the website during the submission.
2. All manuscripts describing data obtained from research conducted in human participants must be accompanied with an approval document by the ethical review board.
3. All manuscripts reporting experiments using animals must include approval document by the animal ethical review board.
4. All submissions must include the authorship contribution form which is signed by all authors.

Authors must complete all online submission forms. If you are unable to successfully upload the files please contact the editorial office by e-mail.

MANUSCRIPT PREPARATION

General Format

The Journal requires that all submissions be submitted according to these guidelines:

- Text should be double spaced with 2.5 cm margins on both sides using 12-point type in Times Roman font.
- All tables and figures must be placed after the text and must be labeled.
- Each section (abstract, text, references, tables, figures) should start on a separate page.
- Manuscripts should be prepared as a word document (*.doc) or rich text format (*.rtf).
- Please make the tables using the table function in Word.
- Abbreviations should be defined in parenthesis where the word is first mentioned and used consistently thereafter.
- Results should be expressed in metric units. Statistical analysis should be done accurately and with precision. Please consult a statistician if necessary.
- Authors' names and institutions should not be included in the manuscript text and should be written only in the title page.

Title Page

The title page should be a separate form from the main text and should include the following:

- Full title (in English and in Turkish). Turkish title will be provided by the editorial office for the authors who are not Turkish speakers.
- Authors' names and institutions.
- Short title of not more than 40 characters for page headings.
- At least three and maximum eight keywords. (in English and in Turkish). Do not use abbreviations in the keywords. Turkish keywords will be provided by the editorial office for the authors who are not Turkish speakers. If you are not a native Turkish speaker, please reenter your English keywords to the area provided for the Turkish keywords. English keywords should be provided from http://www.nlm.nih.gov/mesh (Medical Subject Headings) while Turkish keywords should be provided from http://www.bilimterimleri.com.
- Word count (excluding abstract, figure legends and references).
- Corresponding author's e-mail and address, telephone and fax numbers.
- Name and address of person to whom reprint requests should be addressed.

Original Articles

Authors are required to state in their manuscripts that ethical approval from an appropriate committee and informed consents of the patients were obtained.

Original Articles should be submitted with a structured abstract of no more than 250 words. All information reported in the abstract must appear in the manuscript. The abstract should not include references. Please use complete sentences for all sections of the abstract. Structured abstract should include background, objective, methods, results and conclusions. Turkish abstract will be provided by the editorial office for the authors who are not Turkish speakers. If you are not a native Turkish speaker, please reenter your English abstract to the area provided for the Turkish abstract.

- Introduction
- Materials and Methods
- Results
- Discussion
- Study Limitations
- Conclusion

May be given for contributors who are not listed as authors, or for grant support of the research.

References should be cited in numerical order (in parentheses) in the text and listed in the same numerical order at the end of the manuscript on a separate page or pages. The author is responsible for the accuracy of references. Examples of the reference style are given below. Further examples will be found in the articles describing the Uniform Requirements for Manuscripts Submitted to Biomedical Journals (Ann Intern Med.1988; 208:258-265, Br Med J. 1988; 296:401-405). The titles of journals should be abbreviated according to the style used in the Index Medicus. Journal Articles and Abstracts: Surnames and initials of author's name, title of the article, journal name, date, volume number, and pages. All authors should be listed regardless of number. The citation of unpublished papers, observations or personal communications is not permitted. Citing an abstract is not recommended. Books: Surnames and initials of author's names, chapter title, editor's name, book title, edition, city, publisher, date and pages.

MIRT
Molecular Imaging and Radionuclide Therapy

INSTRUCTIONS TO AUTHORS

Sample References

Journal Article: Sayit E, Söylev M, Capa G, Durak I, Ada E, Yilmaz M. The role of technetium-99m-HMPAO-labeled WBC scintigraphy in the diagnosis of orbital cellulitis. Ann Nucl Med 2001;15:41-44.

Erselcan T, Hasbek Z, Tandogan I, Gumus C, Akkurt I. Modification of Diet in Renal Disease equation in the risk stratification of contrast induced acute kidney injury in hospital inpatients. Nefrologia 2009 doi: 10.3265/Nefrologia.2009.29.5.5449.en.full.

Article in a journal published ahead of print: Ludbrook J. Musculovenous pumps in the human lower limb. Am Heart J 2009;00:1-6. (accessed 20 February 2009).

Lang TF, Duryea J. Peripheral Bone Mineral Assessment of the Axial Skeleton: Technical Aspects. In: Orwoll ES, Bliziotes M (eds). Osteoporosis: Pathophsiology and Clinical Management. New Jersey, Humana Pres Inc, 2003;83-104.

Books: Greenspan A. Orthopaedic Radiology a Pratical Approach. 3th ed. Philadelphia, Lippincott Williams Wilkins 2000, 295-330.

Website: Smith JR. 'Choosing Your Reference Style', Online Referencing 2(3), http://orj.sagepub.com (2003, accessed October 2008).

- Tables

Tables must be constructed as simply as possible. Each table must have a concise heading and should be submitted on a separate page. Tables must not simply duplicate the text or figures. Number all tables in the order of their citation in the text. Include a title for each table (a brief phrase, preferably no longer than 10 to 15 words). Include all tables in a single file following the manuscript.

– Figure Legends

Figure legends should be submitted on a separate page and should be clear and informative.

– Figures

Number all figures (graphs, charts, photographs, and illustrations) in the order of their citation in the text. At submission, the following file formats are acceptable: AI, EMF, EPS, JPG, PDF, PPT, PSD, TIF. Figures may be embedded at the end of the manuscript text file or loaded as separate files for submission. All images MUST be at or above intended display size, with the following image resolutions: Line Art 800 dpi, Combination (Line Art + Halftone) 600 dpi, Halftone 300 dpi. Image files also must be cropped as close to the actual image as possible.

Short Communications:

Short communications should be submitted with a structured abstract of no more than 200 words. These manuscripts should be no longer than 2000 words, and include no more than two figures and tables and 20 references. Other rules which the authors are required to prepare and submit their manuscripts are the same as described above for the original articles.

Invited Review Articles:

- Title page (see above)
- Abstract: Maximum 250 words; without structural divisions; in English and in Turkish . Turkish abstract will be provided by the editorial office for the authors who are not Turkish speakers. If you are not a native Turkish speaker, please reenter your English abstract to the area provided for the Turkish abstract.
- Text
- Conclusion
- Acknowledgements (if any)
- References

Editorial:

- Title page (see above)
- Abstract: Maximum 250 words; without structural divisions; in English and in Turkish. Turkish abstract will be provided by the editorial office for the authors who are not Turkish speakers. If you are not a native Turkish speaker, please re enter your English abstract to the area provided for the Turkish abstract.
- Text
- References

Case Report and Literature Review

- Title page (see above)
- Abstract: Approximately 100-150 words; without structural divisions; in English and in Turkish. Turkish abstract will be provided by the editorial office for the authors who are not Turkish speakers. If you are not a native Turkish speaker, please re-enter your English abstract to the area provided for the Turkish abstract.
- Introduction
- Case report
- Literature Review and Discussion
- References

Interesting Image:

No manuscript text is required. Interesting Image submissions must include the following:

Title Page: (see Original article section)

Abstract: Approximately 100-150 words; without structural divisions; in English and in Turkish. Turkish abstract will be provided by the editorial office for the authors who are not Turkish speakers. If you are not a native Turkish speaker, please re-enter your English abstract to the area provided for the Turkish abstract.

Image(s): The number of images is left to the discretion of the author. (See Original article section)

Figure Legend: Reference citations should appear in the legends, not in the abstract. Since there is no manuscript text, the legends for illustrations should be prepared in considerable detail but should be no more than 500 words total. The case should be presented and discussed in the Figure legend section.

References: Maximum eight references (see original article section).

Letters to the Editor:

- Title page (see above)
- Short comment to a published work, no longer than 500 words, no figures or tables.
- References no more than five.

Consensus Statements or Guidelines: These manuscripts should typically be no longer than 4000 words and include no more than six figures and tables and 120 references.

Proofs and Reprints

Proofs and a reprint orders are sent to the corresponding author. The author should designate by footnote on the title page of the manuscript the name and

MIRT
Molecular Imaging and Radionuclide Therapy

address of the person to whom reprint requests should be directed. The manuscript when published will become the property of the journal.

Archiving

The editorial office will retain all manuscripts and related documentation (correspondence, reviews, etc.) for 12 months following the date of publication or rejection.

Submission Preparation Checklist

As part of the submission process, authors are required to check off their submission's compliance with all of the following items, and submissions may be returned to authors that do not adhere to these guidelines.

1. The submission has not been previously published, nor is it before another journal for consideration (or an explanation has been provided in Comments to the Editor).
2. The submission file is in Microsoft Word, RTF, or WordPerfect document file format. The text is double-spaced; uses a 12-point font; employs italics, rather than underlining (except with URL addresses); and the location for all illustrations, figures, and tables should be marked within the text at the appropriate points.
3. Where available, URLs for the references will be provided.
4. All authors should be listed in the references, regardless of the number.
5. The text adheres to the stylistic and bibliographic requirements outlined in the Author Guidelines, which is found in About the Journal.
6. English keywords should be provided from http://www.nlm.nih.gov/mesh(Medical Subject Headings), while Turkish keywords should be provided fromhttp://www.bilimterimleri.com
7. The title page should be a separate document from the main text and should be uploaded separately.
8. The "Affirmation of Originality and Assignment of Copyright/The Disclosure Form for Potential Conflicts of Interest Form" and Authorship Contribution Form should be downloaded from the website, filled thoroughly and uploaded during the submission of the manuscript.

TO AUTHORS

Copyright Notice

The author(s) hereby affirms that the manuscript submitted is original, that all statement asserted as facts are based on author(s) careful investigation and research for accuracy, that the manuscript does not, in whole or part, infringe any copyright, that it has not been published in total or in part and is not being submitted or considered for publication in total or in part elsewhere. Completed Copyright Assignment & Affirmation of Originality Form will be uploaded during submission. By signing this form;

1. Each author acknowledges that he/she participated in the work in a substantive way and is prepared to take public responsibility for the work.
2. Each author further affirms that he or she has read and understands the "Ethical Guidelines for Publication of Research".
3. The author(s), in consideration of the acceptance of the manuscript for publication, does hereby assign and transfer to the Molecular Imaging and Radionuclide Therapy all of the rights and interest in and the copyright of the work in its current form and in any form subsequently revised for publication and/or electronic dissemination.

Privacy Statement

The names and email addresses entered in this journal site will be used exclusively for the stated purposes of this journal and will not be made available for any other purpose or to any other party.

Peer Review Process

1. The manuscript is assigned to an editor, who reviews the manuscript and makes an initial decision based on manuscript quality and editorial priorities.
2. For those manuscripts sent for external peer review, the editor assigns at least two reviewers to the manuscript.
3. The reviewers review the manuscript.
4. The editor makes a final decision based on editorial priorities, manuscript quality, and reviewer recommendations.
5. The decision letter is sent to the author.

Contact Address

All correspondence should be directed to the Editorial Office:
Cinnah Caddesi Pilot Sokak No:10/12 06650 Çankaya / Ankara, Turkey
Phone: +90 312 441 00 45
Fax: +90 312 441 12 97
E-mail: info@tsnmjournals.org

MIRT
Molecular Imaging and Radionuclide Therapy

CONTENTS

Original Articles

Interesting Images

MIRT
Molecular Imaging and Radionuclide Therapy

CONTENTS

TURKISH SOCIETY OF NUCLEAR MEDICINE 1975

Original Article
Mol Imaging Radionucl Ther 2021;30:69-78 DOI:10.4274/mirt.galenos.2021.08831

Pharmacokinetic Modeling of ^{18}F-FDOPA PET in the Human Brain for Early Parkinson's Disease

Erken Parkinson Hastalığının İnsan Beyninde ^{18}F-FDOPA PET Yöntemiyle Farmakokinetik Modellemesi

Wirunpatch Buratachwatanasiri[1,2], Maythinee Chantadisai[3], Jaruwan Onwanna[2,4], Yuda Chongpison[5], Yothin Rakvongthai[1,2,3], Kitiwat Khamwan[1,2,3]

[1]*Medical Physics Program, Department of Radiology, Faculty of Medicine, Chulalongkorn University, Bangkok, Thailand*
[2]*Chulalongkorn University Biomedical Imaging Group, Department of Radiology, Faculty of Medicine, Chulalongkorn University, Bangkok, Thailand*
[3]*Division of Nuclear Medicine, Department of Radiology, Faculty of Medicine, Chulalongkorn University and King Chulalongkorn Memorial Hospital, The Thai Red Cross Society, Bangkok, Thailand*
[4]*Biomedical Engineering Program, Faculty of Engineering, Chulalongkorn University, Bangkok, Thailand*
[5]*Center of Excellence in Biostatistics, Research Affairs, Faculty of Medicine, Chulalongkorn University, Bangkok, Thailand*

Abstract

Objectives: Early detection is essential for the treatment approaches of Parkinson's disease (PD). Clinical criteria alone may be insufficient to distinguish early PD from other conditions. This study aimed to investigate the transfer rate constants of 6-^{18}F-fluoro-L-dopa (^{18}F-FDOPA) in positron emission tomography (PET) brain images as a sensitive parameter to detect early PD.

Methods: Retrospective ^{18}F-FDOPA PET data of five patients with early PD were collected. PET data were acquired for 90 min after intravenous injection of 306-379 MBq ^{18}F-FDOPA, and reconstructed into a series of 18 five-minute frames. Reoriented PET images were coregistered and normalized with the PET brain template on the statistical parametric mapping. The ^{18}F-FDOPA activity concentrations were measured in the striatum, caudate, and putamen on both sides: Contralateral (as PD) and ipsilateral (as control) to the main motor symptoms. The pharmacokinetic model was generated using the SAAM II simulation software. The transfer rate constants across the blood-brain barrier (forward, K_1 and reverse, k_2) and decarboxylation rate constants (k_3) were estimated in these regions.

Results: The activity uptakes in the contralateral striatum (0.0323%±0.0091%) and putamen (0.0169%±0.0054%) were significantly lower than the control (0.0353%±0.0086%, 0.0199%±0.0054%, respectively). The K_1 and k_3 were significantly lower in the contralateral striatum and putamen ($p<0.05$). There were no significant differences in any transfer rate constants in the caudate.

Conclusion: The transfer rate constants (K_1 and k_3) of ^{18}F-FDOPA on the contralateral striatum and putamen were significantly lower than the control. These biokinetic data could be potential indicators for quantitative detection of early PD diagnosis.

Keywords: ^{18}F-FDOPA, early Parkinson's disease detection, pharmacokinetic model, statistical parametric mapping, quantitative analysis

Address for Correspondence: Kitiwat Khamwan PhD, Division of Nuclear Medicine, Department of Radiology, Faculty of Medicine, Chulalongkorn University and King Chulalongkorn Memorial Hospital, The Thai Red Cross Society, 1873 Rama IV Road, Pathumwan, Bangkok 10330, Thailand
Phone: +66-61-9325919 **E-mail:** kitiwat.k@chula.ac.th ORCID ID: orcid.org/0000-0001-6247-2829
Received: 14.12.2020 **Accepted:** 01.04.2021

Öz

Amaç: Parkinson hastalığının (PH) tedavi yaklaşımında erken tanı önemlidir. Klinik kriterler tek başına erken PH'yi diğer nedenlerden ayırt etmek için yetersiz olabilir. Bu çalışmada, 6-^{18}F-floro-L-dopa (^{18}F-FDOPA) pozitron emisyon tomografisi (PET) beyin görüntülemede transfer hızı sabitlerinin erken PH saptanmasında duyarlı bir parametre olup olmadığının araştırılması amaçlanmıştır.

Yöntem: Erken PH'li beş hastanın geriye dönük ^{18}F-FDOPA PET verileri toplandı. PET verileri, 306-379 MBq ^{18}F-FDOPA'nın intravenöz enjeksiyonundan sonra 90 dakika süreyle alındı ve 18 adet beşer dakikalık bir dizi halinde rekonstrükte edildi. Reoryante edilen PET görüntüleri istatistiksel parametrik haritalama üzerindeki beyin PET şablonu ile birleştirildi ve normalize edildi. ^{18}F-FDOPA aktivite konsantrasyonları her iki tarafta striatum, kaudat ve putamende ölçüldü: Ana motor semptomlara karşı kontralateral (PH olarak) ve ipsilateral (kontrol olarak). Farmakokinetik model SAAM II simülasyon yazılımı kullanılarak geliştirildi. Bu bölgelerde kan-beyin bariyeri boyunca transfer hızı sabitleri (ileri, K_1 ve geri, k_2) ve dekarboksilasyon hızı sabitleri (k_3) tahmini ölçümleri yapıldı.

Bulgular: Kontralateral striatumda (%0,0323±%0,0091) ve putamende (%0,0169±%0,0054) aktivite alımları kontrolden anlamlı derecede düşüktü (sırasıyla; 0,0353%±0,0086%, 0,0199%±0,0054%). K_1 ve k_3 kontralateral striatum ve putamenlerde anlamlı derecede düşüktü ($p<0,05$). Kaudattaki herhangi bir transfer hızı sabitinde anlamlı bir fark yoktu.

Sonuç: Kontralateral striatum ve putamendeki ^{18}F-FDOPA'nın transfer hızı sabitleri (K_1 ve k_3) kontrolden anlamlı derecede düşüktü. Bu biyokinetik veriler, erken evre PH tanısının kantitatif tespiti için potansiyel göstergeler olabilir.

Anahtar kelimeler: ^{18}F-FDOPA, erken Parkinson hastalığı tespiti, farmakokinetik model, istatistiksel parametrik haritalama, kantitatif analiz

Introduction

Parkinson's disease (PD) is the second most common neurodegenerative disorder. Degeneration of dopamine neurons in the mesencephalic substantia nigra causes the progressive impairment of dopaminergic innervations of the caudate or putamen. When over 50% of the nigrostriatal dopamine neurons have degenerated, PD symptoms are usually distinctly expressed, such as resting tremor, bradykinesia, and rigidity (1,2,3,4). In the early PD stage, clinical criteria alone may be insufficient to distinguish PD from other conditions such as parkinsonism-related disorders or other drug-related conditions. Furthermore, it is more difficult to diagnose PD at this early stage since its clinical signs may be mild and unnoticed (5,6). Therefore, *in vivo* markers of dopaminergic degeneration are essential for early diagnosis and disease progression monitoring. A radioactive tracer, 6-^{18}F-fluoro-L-dopa (^{18}F-FDOPA), has been extensively used in positron emission tomography (PET) brain image studies to assess the presynaptic nigrostriatal dopaminergic function. The uptake of ^{18}F-FDOPA PET demonstrates the activity of the dopa-decarboxylase enzyme in the striatal nerve terminals of dopamine neurons and is correlated with the dopamine storage capacity (7,8,9).

A nuclear medicine physician interprets the ^{18}F-FDOPA PET imaging based on the visualization of the relative radioactivity distribution in the striatum. A decreased ^{18}F-FDOPA uptake in the striatum contralateral to the side of the main or first motor symptoms (due to crossing of the pyramidal pathway) has been reported in early PD patients (10,11,12,13,14,15). The depletion is more severe in the putamen than in the caudate nucleus. The most prominent depletion is in the dorsal parts of the putamen because of the topographic organization of the nigrostriatal projection (4,11,16). Most previous studies differentiate PD from non-PD based on the qualitative assessment or semi-quantitative analysis, such as the standardized uptake value or reference tissue-uptake ratio as an imaging biomarker. However, these studies have not identified any sensitive parameters derived from kinetic modeling in the striatal subregion. The quantitative analysis of biokinetic data in ^{18}F-FDOPA PET brain imaging may provide additional clinical usefulness to the routine qualitative assessment, especially when the qualitative analysis could not differentiate PD from non-PD conditions.

There are several pharmacokinetic (PK) approaches in PET imaging techniques, of which compartmental modeling has been used to simulate the physiologically significant parameters. In compartmental models, the organ of interest is composed of many interacting subsystems (compartments) with a set of transfer rate constants describing the exchanges of mass or material between the compartments (17,18,19,20,21,22). Wahl and Nahmias (22) published a simplified two-tissue compartment, three-rate constant ^{18}F-FDOPA kinetic model by eliminating the fourth transfer rate constant and the number of compartments. The significant difference between normal subjects and PD patients was found in the dopa-decarboxylase rate constant (k_3). However, only two patients were investigated, and the stages of the PD were not clearly defined.

This study aimed to investigate the transfer rate constants of ^{18}F-FDOPA in the brain PET images of patients with early-stage PD, based on the compartmental modeling of Wahl and Nahmias, and to identify optimal quantitative parameters that could differentiate between normal and pathological FDOPA metabolism. Furthermore, we aimed

to re-evaluate if a two-tissue compartment, three-rate constant PK model could adequately describe the FDOPA kinetics and its metabolite in the striatal, caudate, and putamen of patients with early PD.

Materials and Methods

Patients and ^{18}F-FDOPA Image Acquisition

This study was approved by the Institutional Review Board (IRB) of the Faculty of Medicine, Chulalongkorn University (IRB no. 361/61). In consultation with the IRB, the use of already collected and anonymized imaging data for this study was deemed exempt from formal informed consent. Retrospective data were collected from five patients who underwent an ^{18}F-FDOPA PET brain scan at the Division of Nuclear Medicine, King Chulalongkorn Memorial Hospital (KCMH). All patients were diagnosed with stage II PD according to the Hoehn and Yahr (HY) staging (23) and the UK PD Society Brain Bank Clinical Diagnosis Criteria (24). Patients' demographic and clinical data are shown in Table 1. All patients fasted for 4-6 h before the FDOPA injection. Patients who had drug-induced parkinsonian syndrome or vascular causes of parkinsonian syndrome were excluded from this study. All patients were treated with levodopa in combination with FDOPA decarboxylase inhibitor (carbidopa). The patient preparation protocol for the ^{18}F-FDOPA PET neurological imaging at the KCMH was followed the joint practice guideline developed collaboratively by the European Association of Nuclear Medicine (EANM) and the Society of Nuclear Medicine and Molecular Imaging (SNMMI) (25,26). The protocol required that carbidopa and other anti-parkinsonian drugs must be discontinued 2 days before the examination to ensure that there is no interpretation bias because of the carbidopa effect from the FDOPA accumulation in the striatal region. A nuclear medicine physician interpreted the PET images. Typical early PD was identified when the visual assessment revealed a relatively unilateral decrease in ^{18}F-FDOPA uptake in the dorsal part of the putamen.

Three-dimensional list-mode brain PET data were acquired for 90 min using the Siemens Biograph 16 HI-REZ PET/CT system (CTI/Siemens Medical Solutions, Knoxville, TN, USA) immediately after patients were intravenously injected with 306-379 MBq ^{18}F-FDOPA. A series of PET images were reconstructed using an ordered subset expectation maximization algorithm with four iterations and 14 subsets, matrix size of 168x168, and voxel size of 4.0627x4.0627x3 mm^3 to obtain a 90-min dynamic image with the framing scheme of 18x5 min frames. Decay, attenuation, model-based scatter corrections, and 5-mm Gaussian filter of convolution kernel were applied for all PET image reconstruction.

Striatal Segmentation using the Statistical Parametric Mapping (SPM)

To achieve the consistency of region of interest (ROI) contouring in the striatum, caudate, and putamen, all subsequent image manipulations and data analyses were performed using the SPM software. Before the contouring process, Digital Imaging and Communications in Medicine image files were converted into an interfile format using the MRICRON software to create SPM-compatible images. The images were then imported into the SPM software version 12 (27), which was operated on the MATLAB software version R2018a (Mathworks, Natick, MA, USA). The images were reoriented as close as possible to the magnetic resonance (MR) reference images by adjusting the individual movement parameters (pitch, roll, and yaw), and the crosshair origin (0, 0, 0) was checked to be closed to the anterior commissure.

The series of reoriented images were coregistered and stereotactically normalized with the International Consortium for Brain Mapping (ICBM) using 16 iterations of nonlinear warping, a frequency cut-off at 25, and 8-mm full-width at half maximum Gaussian filter as a smoothing filter. The initial image parameters were 168x168x109, which resulted in a 16-bit final image format with a size of 181x217x181 and a voxel size of 1x1x1 mm^3. The normalized images were then segmented automatically

Table 1. The patient' demographic and clinical data

Patient	Age (years)	Weight (kg)	Sex	Administered activity (MBq)	Severity (HY scale)	Lower uptake striatum (side)[a]	Affected side	Initial symptom
1F	75	80	Female	358	II	Left	Right	Tremor
2F	64	57	Female	306	II	Left	Right	Tremor
3F	62	54	Female	323	II	Left	Right	Rigidity/tremor
4M	44	76	Male	379	II	Left	Right	Tremor
5F	71	50	Female	349	II	Left	Right	Bradykinesia/rigidity

[a]Lower uptake level of ^{18}F-FDOPA, HY: Hoehn and Yahr, ^{18}F-FDOPA: ^{18}F-fluoro-L-dopa

into the striatum, caudate, and putamen by making a binary mask image from the Automated Anatomical Labeling-VOIs atlas, which was derived from the Montreal Neurological Institute (MNI) T1-MR imaging (MRI) data set. The image segmentation was performed in each single frame of the patient data set. A PET template of the ICBM used in the coregistration and stereotactical normalization was derived from the perfusion ^{15}O-labeled water. The overall orientation was matched with MNI space templates, and a nuclear medicine physician visually validated the delineation results in these striatal subregions to confirm that the segmentation utilizing the SPM was performed appropriately. The overall process of the semi-automated segmentation in the striatum, caudate, and putamen using SPM is illustrated in Figure 1.

Determination of the Scaling Factor for Activity Concentration

Changes in pixel values during the SPM processing may occur on the original and normalized images after applying the coregistration and normalization. The scaling factor was determined to correct the changes. A whole-brain image histogram was computed at each time point using the ImageJ program. The histogram provided the mean and count values, which referred to the activity concentration (Bq/mL) and the total number of voxels, respectively. The whole-image activity (Bq) in each time frame was determined by multiplying these values and the voxel volume (0.0248 and 0.001 mL in the original and normalized images, respectively). The whole-brain image activity from the original images was then divided by the respective normalized images to determine the mean value from all time frames, and the mean scaling factors were computed.

To determine the radioactivity in the striatum, caudate, and putamen, the rectangular ROIs were manually drawn over these three regions on each side to compute the histogram in each time frame as illustrated in Figure 2. The whole-region activity (Bq) was calculated by multiplying the activity concentration with the total voxel number, voxel volume (0.001 mL), and mean scaling factor. The whole-region activity (Bq) in every time frame of the striatum,

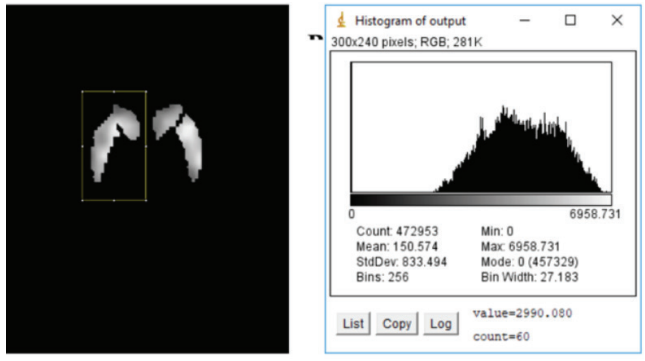

Figure 2. (Left) region of interest over right side of the striatum, and (right) the histogram output

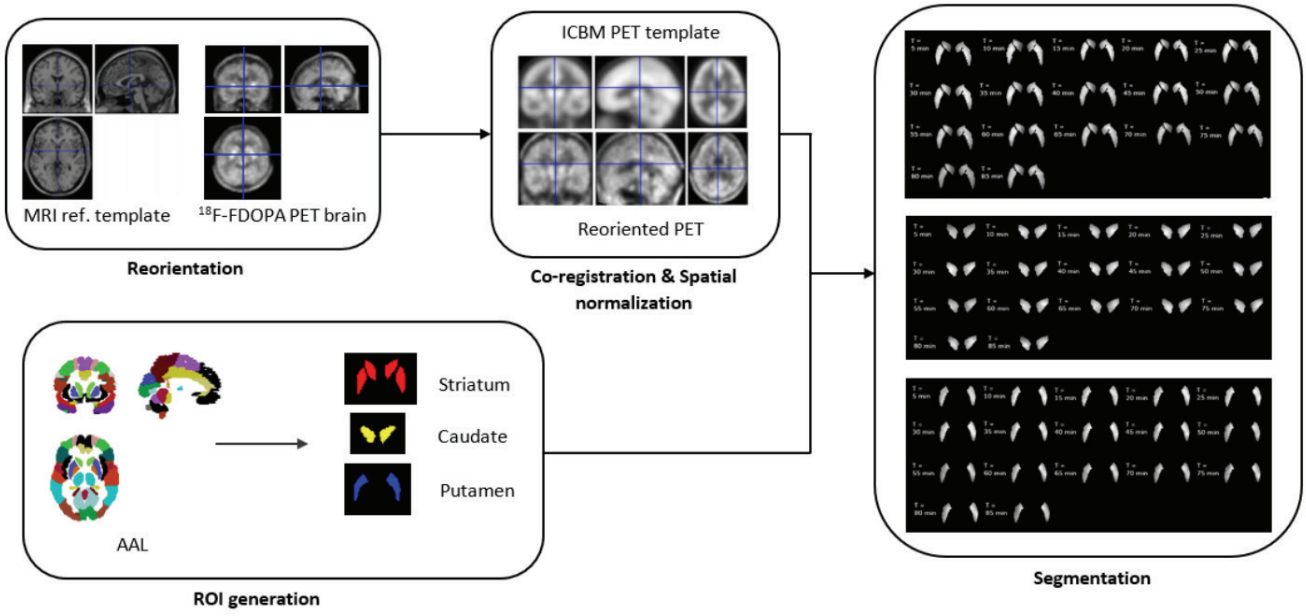

Figure 1. Schematic flowchart showing the semi-automated segmentation in the striatum, caudate, and putamen regions using the statistical parametric mapping (SPM)

MRI: Magnetic resonance imaging, ^{18}F-FDOPA: ^{18}F-fluoro-L-dopa, PET: Positron emission tomography, ICBM: International Consortium for Brain Mapping

caudate, and putamen was obtained from each side. The results of the ipsilateral versus contralateral to the predominant motor symptoms were calculated separately. The analysis between the PD and control was performed within the same patient. The contralateral side that had lower uptake was identified as the PD, and the ipsilateral side (normal uptake) as the control.

^{18}F-FDOPA Compartmental Model for PD Patients

A two-tissue compartment, three-rate constant model was chosen for a PK ^{18}F-FDOPA model in this study. The percentage of the injected radioactivity was calculated every 5 min after injection in each region. Data were imported into the SAAM II compartmental modeling software (The Epsilon Group, Charlottesville, VA, USA) (28). The FDOPA PK compartmental model was created and followed the Wahl and Nahmias'(22) model as shown in Figure 3. The model was fitted to the PD patient data. The model fitting was initially performed using the rate constants reported by Wahl and Nahmias (22). Then, the SAAM II software computationally created a system of ordinary differential equations, according to the specified compartmental model structure, and simulated the solutions based on the provided parameters and model inputs. The image-based input function to the model (bolus injection into the blood) for the compartment analysis in this study can be defined as follows:

$$\text{Input function} = ((q_3+q_4)*BVF*(a*q_1+(1-a)*q_2))*\exp(-\log(2)*t/110), \quad (1)$$

where q_i is the ^{18}F-FDOPA activity in the i^{th} compartment; q_1, q_2, q_3, and q_4 are the ^{18}F-FDOPA activities that internally solved differential equations by SAAM II in plasma, erythrocytes, FDOPA brain tissue, and its metabolite compartments, respectively. BVF refers to an estimate of blood volume fraction in the brain tissue, and *a* is the coefficient value assumed to be 0.6; t is the ^{18}F physical half-life of 109.7 min. The general assumption in SAAM II was that the flux of material between compartments depended only on the amount of material presented in the starting compartment (29). This corresponded to the assumption of first-order kinetics. The transfer rate constants of FDOPA exchanging between the compartments, which were created internally and solved by SAAM II, were described by the following set of differential equations:

$$\frac{dC_{Tissue}(t)}{d(t)} = K_1C_{plasma}(t)-k_2C_{Tissue}(t)-k_3C_{Tissue}(t), \quad (2)$$

$$\frac{dC_{FDA}(t)}{d(t)} = k_3C_{Tissue}(t), \quad (3)$$

where C_{Tissue} and C_{FDA} represent radioactivity concentrations of the tissue FDOPA and 6-[^{18}F] fluorodopamine (FDA) and its metabolites compartment, respectively. K_1 and k_2 are the forward and reverse transport rate constants of plasma FDOPA across the blood–brain barrier to the tissue FDOPA compartment, whereas k_3 represents the FDOPA decarboxylation rate constant from the tissue FDOPA compartment to the combined compartment of FDA and its metabolites. The SAAM II then generated a time-integrated activity curve of the model and fitted it to the patient data based upon a nonlinear least square regression algorithm. The transfer rate constants (K_1, k_2, and k_3) in each patient were determined accordingly.

To assess the performance of model fitting, the Akaike information criterion (AIC) and the Bayes information criterion (BIC) were used to assess which of the rate constants would best fit the patient's data. The AIC is a technique based on in-sample fit to estimate the likelihood of a model to predict the values. The BIC is another criterion for model selection that measures the trade-off between the model fit and complexity of the model. Lower AIC and BIC values indicated a better fit. The AIC and BIC values can be determined using equations as follows (30,31):

$$AIC = 2k-2(\ln)(L), \quad (4)$$

$$BIC = k(\ln)(N)-2(\ln)(L), \quad (5)$$

where L is the value of the likelihood, N is the number of recorded measurements, and k is the number of estimated parameters. As a result, the parameter with minimum AIC and BIC values was chosen as the best fitting model among several competing models.

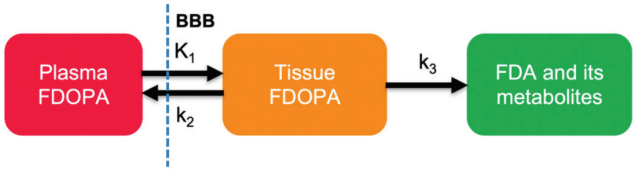

Figure 3. Two-tissue-compartment and three-rate constant for describing the FDOPA kinetics in early PD patients following Wahl and Nahmias (22)

FDOPA: Fluoro-L-dopa, PD: Parkinson's disease, FDA: Fluorodopamine

Statistical Analysis

The transfer rate constants (K_1, k_2, and k_3) in each region were determined. The comparisons between the ipsilateral and contralateral sides of the striatum, caudate, and putamen were performed using a non-parametric statistic, the Wilcoxon signed-rank test. Data analysis was performed using the Statistical Package for Social Sciences program version 23 (IBM Corp, Armonk, NY, USA). The differences

between groups were considered significant when p values were less than 0.05.

Results

Figure 4 depicts the mean time-activity curves after the ^{18}F-FDOPA injection obtained from both the ipsilateral and contralateral sides of the striatum (Figure 4A), caudate (Figure 4B), and putamen (Figure 4C). The activity uptake in each region was expressed as a percentage of the injected radioactivity and represented by a range (mean ± standard deviation) as follows: (a) The striatum 0.0225%-0.0453% (0.0323±0.0091) and 0.0263%-0.0457% (0.0353±0.0086) for the contralateral and ipsilateral sides, respectively, (b) the caudate 0.0112-0.0204% (0.0155±0.0038) and 0.0118%-0.0191% (0.0154±0.0034), and (c) the putamen 0.0113%-0.0249% (0.0169±0.0054) and 0.0139%-0.0273% (0.0199±0.0054). The highest average percentage of injected activity was at 15 min after injection in every region.

According to the PK model fitting, the measured FDOPA curves fitted well to a two-tissue compartment, three-rate constant model (mean AIC of -5.72 and BIC of -5.62). The time-activity curves of both sides initially increased after the injection, reached the maximum uptake activity at 15 min after injection, and then decreased slightly thereafter. The activity uptakes on the contralateral side of the striatum and putamen were significantly lower than the ipsilateral side. However, the caudate time-activity curves were nearly superimposed on each other (Figure 4).

The details of the transfer rate constants on the contralateral and ipsilateral sides are presented in Table 2. Figures 5A and 5B depict the box plot of the transfer rate constants for both sides of the striatum and putamen. There were statistically significant differences in K_1 and k_3 between the contralateral and ipsilateral sides of the striatum and putamen ($p<0.05$). However, there were no significant differences in the k values between both sides of the caudate region (not shown).

Figure 6 illustrates the ^{18}F-FDOPA PET transaxial images from a patient suspected of idiopathic parkinsonism with right-hand resting tremor (patient no: 1). Based on visual interpretation, there was a subtle change of relatively mild decreased ^{18}F-FDOPA uptake at the dorsal part of the left putamen and symmetrical uptakes at the bilateral caudate nuclei. After quantitative analysis using the PK model was applied for further confirmation, the K_1 (0.0109 vs. 0.0124) and k_3 (0.0098 vs. 0.0146) of the contralateral putamen were significantly lower than that of the ipsilateral side. This quantitative analysis provided the results that supported the visual assessment.

Discussion

This study investigated the transfer rate constants of ^{18}F-FDOPA in the PET brain images of five early PD patients. The PK model in this study was a two-compartmental, three-transfer rate constants model, which was based on compartmental modeling in accordance with Wahl and Nahmias (22). The results demonstrated the differences between the contralateral and ipsilateral sides of the striatum, including the caudate and putamen, which was in agreement with Wahl and Nahmias (22). The mean transfer rate constants K_1 and k_3 on the contralateral (PD) striatum and putamen were significantly lower than those on the ipsilateral (normal) side ($p<0.05$). In addition, the difference was more pronounced in the putamen. In contrast, no significant differences were found in the caudate. These findings agreed with the results of previous PD imaging studies, which suggested that the dopamine

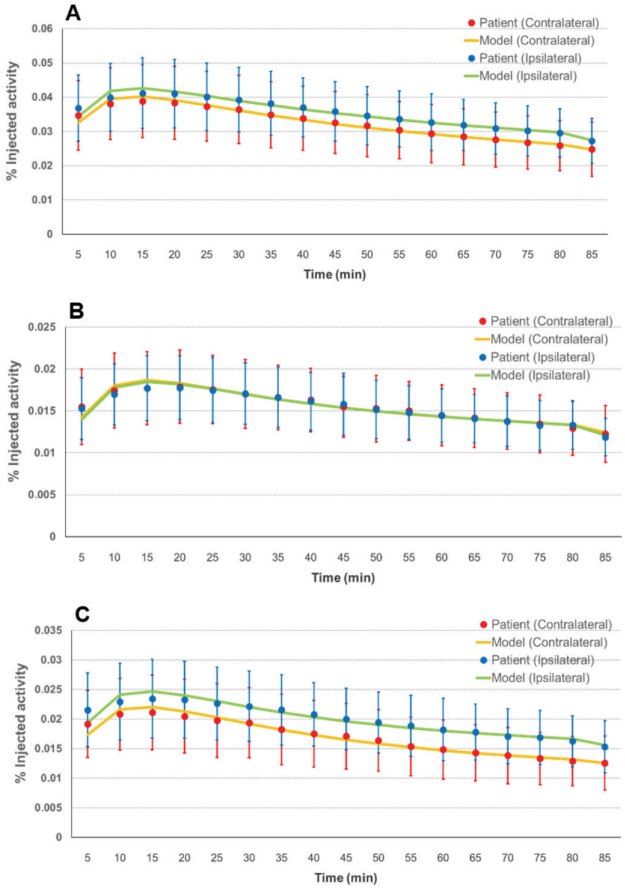

Figure 4. Mean (± 1 SD) time-activity curves in the (A) striatum, (B) caudate, and (C) putamen. Blue and red round markers represent patient's data obtained from the contralateral and ipsilateral side, respectively. Green and yellow lines represent the model fitted from the contralateral and ipsilateral side, respectively

SD: Standard deviation

depletion began in the dorsal parts of the putamen and proceeded to the caudate nucleus and other parts of the dopaminergic system during disease progression (4,11,16). The decreased ^{18}F-FDOPA uptake in this work was more significant in the contralateral striatum, which was in accordance with an observation that the motor symptoms were more severe on the contralateral side to the striatum that had decreased dopaminergic activity (3). However, our results may only represent patients with stage two of PD who had right-side predominant symptoms (Table 1) or loss of activity uptake in the left striatum.

Table 3 illustrates the transfer rate constants of this work compared with previous reports by Huang et al. (21) and Wahl and Nahmias (22). Wahl and Nahmias (22) found a significant difference in the dopa-decarboxylase rate constant between normal subjects and PD patients, although only two PD patients were investigated. The FDOPA transfer rate constants for K_1 and k_2 of the ipsilateral (normal) side in our study were approximately two-fold lower than those of Wahl and Nahmias' study but were comparable with Huang's study. The patient characteristics could be the cause of the differences in these transfer rate constants. The k_3 of the contralateral (PD) striatum in our study was 2.6-fold higher than in Wahl and Nahmias' study. This might be explained by the difference in the severity of PD between the studies. This study was conducted in early PD patients with distinct inclusion criteria following an HY score limited to 2. Therefore, the loss of dopaminergic neurons in our patients may be less than the patients in the Wahl and Nahmias' study. Although the clinical rating scale of the patients had not been described in the Wahl and Nahmias' study, their results implicitly indicated that the patients might suffer from late stages of PD (HY stage 3 or 4).

The finding in this work indicated that in addition to k_3, K_1 was likely to be another sensitive parameter to differentiate PD and normal patients. The difference in the results compared with previous studies was possibly

Table 2. The estimated FDOPA model parameters in the contralateral and ipsilateral sides

	Contralateral side (PD)			Ipsilateral side (normal)		
	K_1 (mL/min/g)	k_2 (/min)	k_3 (/min)	K_1 (mL/min/g)	k_2 (/min)	k_3 (/min)
Striatum						
Patient 1	0.0221	0.0155	0.0064	0.0242	0.0159	0.0111
Patient 2	0.0254	0.0203	0.0165	0.0268	0.0125	0.0210
Patient 3	0.0357	0.0163	0.0079	0.0363	0.0168	0.0088
Patient 4	0.0170	0.0287	0.0105	0.0192	0.0283	0.0159
Patient 5	0.0154	0.0171	0.0146	0.0160	0.0154	0.0195
Mean (SD)	0.0231 (0.0081)	0.0196 (0.0054)	0.0112 (0.0043)	0.0245 (0.0078)	0.0178 (0.0061)	0.0152 (0.0053)
Caudate						
Patient 1	0.0095	0.0214	0.0129	0.0096	0.0228	0.0163
Patient 2	0.0104	0.0258	0.0315	0.0109	0.0251	0.0352
Patient 3	0.0137	0.0317	0.0246	0.0113	0.0201	0.0121
Patient 4	0.0071	0.0265	0.0144	0.0077	0.0264	0.0171
Patient 5	0.0061	0.0130	0.0183	0.0061	0.0193	0.0270
Mean (SD)	0.0094 (0.0030)	0.0237 (0.0070)	0.0203 (0.0077)	0.0091 (0.0022)	0.0228 (0.0031)	0.0215 (0.0094)
Putamen						
Patient 1	0.0109	0.0209	0.0098	0.0124	0.0211	0.0146
Patient 2	0.0128	0.0301	0.0148	0.0136	0.0203	0.0208
Patient 3	0.0173	0.0214	0.0081	0.0202	0.0286	0.0161
Patient 4	0.0087	0.0344	0.0094	0.0102	0.0366	0.0174
Patient 5	0.0084	0.0272	0.0142	0.0090	0.0204	0.0191
Mean (SD)	0.0116 (0.0037)	0.0268 (0.0057)	0.0113 (0.0030)	0.0131 (0.0044)	0.0254 (0.0072)	0.0176 (0.0025)

FDOPA: Fluoro-L-dopa, SD: Standard deviation, PD: Parkinson's disease

because of the data collection method. The simulation of the PK model fitted to the patient's data in this work was an image-based analysis acquired from radioactivity uptake in the striatal region, whereas previous reports collected the data based on a combination of arterialized venous blood sampling and image analysis. Although the biochemical assay method may be preferable, the image-based analysis could be better and more convenient in ^{18}F-FDOPA PET quantification. It is less invasive, has reduced occupational dose and complexity, and can provide retrospective data. It was noticeable that PD patients had stopped taking the FDOPA decarboxylase inhibitor 2 days before the imaging examination. The elimination half-life of carbidopa in plasma is approximately 107 min. Two days of drug discontinuation should be long enough to ensure that there was no visual interpretation bias due to the carbidopa effect on the physiological uptake in the striatum.

This study did not include healthy volunteers as the control group. The striatum contralateral side to the main symptoms that had a lower ^{18}F-FDOPA uptake was considered to be PD and the other side of the same patient

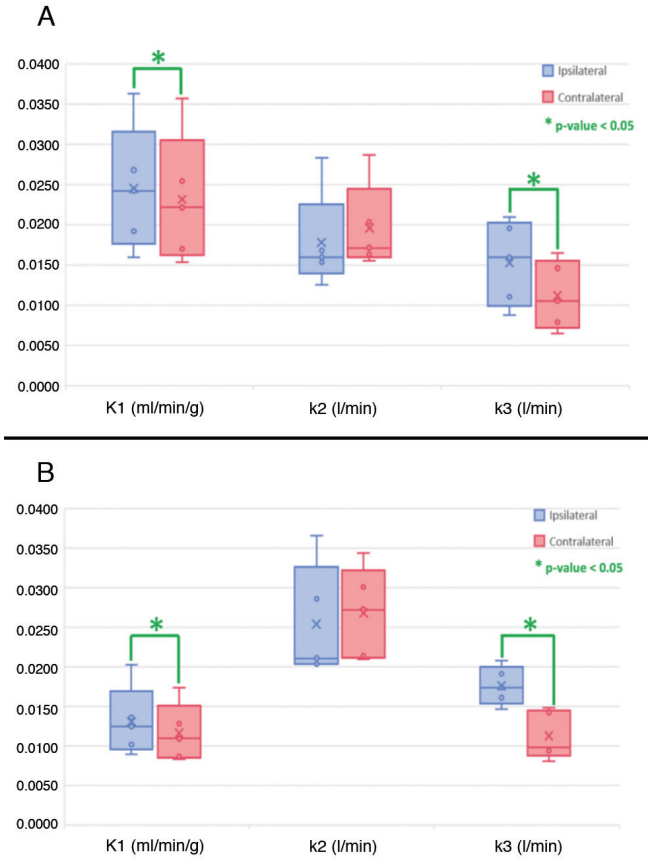

Figure 5. Box plots of the transfer rate constants in the contralateral (red) and ipsilateral (blue). (A) striatum and (B) putamen

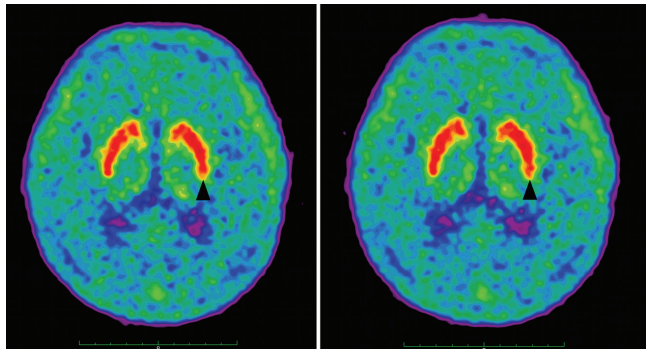

Figure 6. Example of static ^{18}F-FDOPA PET images in a case of the early PD with HY rate stage II. The arrows indicate the relatively mild decreased FDOPA uptake demonstrated by the red light shading at the dorsal part of left posterior putamen

^{18}F-FDOPA: ^{18}F-fluoro-L-dopa, PET: Positron emission tomography, PD: Parkinson's disease, HY: Hoehn and Yahr

Table 3. Comparison of transfer rate constants between earlier reports and this study			
Study	Huang et al. (21)	Wahl and Nahmias (22)	This study
Overall demographic			
Subjects	Normal: 10	Normal: 4, PD: 2	PD: 5
HY stage	N/A	Late	Early
Average (SD) transfer rate constants in the ipsilateral striatum (normal)			
K_1 (mL/min/g)	0.0283 (0.0051)	0.0403 (0.0177)	0.0245 (0.0078)
k_2 (/min)	0.0228 (0.0048)	0.0342 (0.0185)	0.0178 (0.0061)
k_3 (/min)	0.0124 (0.0041)	0.0124 (0.0058)	0.0152 (0.0053)
Average (SD) transfer rate constants in the contralateral striatum (PD)			
K_1 (mL/min/g)	N/A	0.0494 (0.0072)	0.0231 (0.0081)
k_2 (/min)		0.0281 (0.0072)	0.0196 (0.0054)
k_3 (/min)		0.0043 (0.0010)	0.0112 (0.0043)
HY: Hoehn and Yahr, PD: Parkinson's disease, SD: Standard deviation, N/A: Not applicable			

was non-PD. We elaborately recruited the typical type of early PD patients following the inclusion and exclusion criteria suggested by nuclear medicine experts and the joint EANM/SNMMI procedure guidelines (25). All patients were followed up and clinically diagnosed with early PD. Hence, the uniform uptake of FDOPA at the caudate and putamen on the ipsilateral side was assumed as a normal reference in the same patient. The comparison within the same patient would possibly eliminate the variables from cross-patient studies. However, the sensitivity of this asymmetry method depended on the degree of difference between each side. Moreover, the cases with symmetric involvement would be missed even if the abnormality is substantial. Further study on biokinetic data comparing healthy subjects or patients with non-neurodegenerative parkinsonism is required to confirm the results of this work.

The striatal delineation approach using SPM in this study was also performed to improve the reproducibility of striatal subregion segmentation. In the process of reorienting images, the patient's own MRI should be used to roughly align structural images with standard space for coregistration before automated subcortical structures segmentation using SPM. However, some patients in this study did not have their own MRI brain scans. To address this drawback, we used the standard MRI provided by the SPM to reorient the PET images before tissue class segmentation. Although this approach might not be perfect, the uncertainty was acceptable for keeping the consistency in the reorienting process. This approach provided the segmented subregions in every patient with the same volume (Figure 1) and might not yield a perfect coregistration and segmentation accordingly.

Study Limitations

This limitation may lead to variations in the ^{18}F-FDOPA quantification in brain tissues for generating the time-activity curve to simulate the kinetic model.

Conclusion

The two-tissue compartmental model with three-transfer rate constants was able to describe ^{18}F-FDOPA kinetics in the striatum, caudate, and putamen, which was consistent with earlier studies. The K_1 and k_3 transfer rate constants of ^{18}F-FDOPA in the striatum and putamen on the contralateral side to the patient's symptom were significantly lower than the control. The K_1 and k_3 could be potential indicators for quantitative detection to improve early PD diagnosis. These findings provided more insight of the FDOPA PKs for PD patients and could be useful in clinical practice.

Acknowledgements

The authors would like to thank Mr. Natakorn Siritranont for his help on imaging data collection. The authors would also like to thank the nuclear medicine technologists, medical physicists, and nuclear medicine physicians at the Division of Nuclear Medicine, KCMH, and Chulalongkorn University for their kind support in this study. We deeply thank Associate Professor Dr. Shuichi Shiratori for his valuable advice in the FDOPA mechanism. We also thank Professor Dr. Roongroj Bhidayasiri from Chulalongkorn Center of Excellence for PD and Related Disorders for the valuable PD patient information. This work was funded by Chulalongkorn University, government budget (GB-A_61_006_30_02), and the Thailand Research Fund (MRG6180141). Miss Wirunpatch Buratachwatanasiri was supported by a Graduate School Scholarship, the Faculty of Medicine, Chulalongkorn University, Thailand.

Ethics

Ethics Committee Approval: This study was approved by the Institutional Review Board (IRB) of the Faculty of Medicine, Chulalongkorn University (IRB no. 361/61).

Informed Consent: The use of already collected, anonymized, imaging data for the purposes of this study was deemed exempt from the formal informed consent by the IRB of our institution.

Peer-review: Externally and internally peer-reviewed.

Authorship Contributions

Concept: K.K., W.B., M.C., Design: K.K., W.B., Data Collection or Processing: W.B., Y.R., J.O., Analysis or Interpretation: W.B., K.K., M.C., Y.C., Literature Search: K.K., W.B., Writing: K.K., W.B.

Conflict of Interest: No conflict of interest was declared by the authors.

Financial Disclosure: This work was funded by the government budget (GB-A_61_006_30_02) Chulalongkorn University, and the Thailand Research Fund (MRG6180141).

References

1. DeMaagd G, Philip A. Parkinson's Disease and Its Management: Part 1: Disease Entity, Risk Factors, Pathophysiology, Clinical Presentation, and Diagnosis. P T 2015;40:504-532.
2. Antić S, Lisak M, Trkanjec Z, Demarin V. Parkinsonova bolest. Acta Clin Croat 2009;48:377-380.
3. Lang AE, Lozano AM. Parkinson's disease. New England Journal of Medicine. 1998;339:1130-1143.
4. Brooks DJ. Neuroimaging in Parkinson's disease. NeuroRx 2004;1:243-254.

5. Sawle GV. The detection of preclinical Parkinson's disease: What is the role of positron emission tomography? Movement disorders: official journal of the Movement Disorder Society 1993;8:271-277.
6. Hughes AJ, Daniel SE, Kilford L, Lees AJ. Accuracy of clinical diagnosis of idiopathic Parkinson's disease: a clinico-pathological study of 100 cases. J Neurol Neurosurg Psychiatry 1992;55:181-184.
7. Kumakura Y, Gjedde A, Danielsen EH, Christensen S, Cumming P. Dopamine storage capacity in caudate and putamen of patients with early Parkinson's disease: correlation with asymmetry of motor symptoms. J Cereb Blood Flow Metab 2006;26:358-370.
8. Leung K. L-3, 4-Dihydroxy-6-[18F] fluorophenylalanine. In: Molecular Imaging and Contrast Agent Database (MICAD)[Internet]. National Center for Biotechnology Information (US); 2011.
9. Nanni C, Fanti S, Rubello D. 18F-DOPA PET and PET/CT. J Nucl Med 2007;48:1577-1579.
10. Kish SJ, Shannak K, Hornykiewicz O. Uneven pattern of dopamine loss in the striatum of patients with idiopathic Parkinson's disease. Pathophysiologic and clinical implications. N Engl J Med 1988;318:876-880.
11. Brück A, Aalto S, Nurmi E, Vahlberg T, Bergman J, Rinne JO. Striatal subregional 6-[18F] fluoro-L-dopa uptake in early Parkinson's disease: a two-year follow-up study. Mov Disord 2006;21:958-963.
12. Lotankar S, Prabhavalkar KS, Bhatt LK. Biomarkers for Parkinson's Disease: Recent Advancement. Neurosci Bull 2017;33:585-597.
13. Sung YH, Lee J, Nam Y, Shin HG, Noh Y, Shin DH, Kim EY. Differential involvement of nigral subregions in idiopathic parkinson's disease. Hum Brain Mapp 2018;39:542-553.
14. Morrish PK, Sawle GV, Brooks DJ. Clinical and [18F] dopa PET findings in early Parkinson's disease. J Neurol Neurosurg Psychiatry 1995;59:597-600.
15. Yagi S, Yoshikawa E, Futatsubashi M, Yokokura M, Yoshihara Y, Torizuka T, Ouchi Y. Progression from unilateral to bilateral parkinsonism in early Parkinson disease: implication of mesocortical dopamine dysfunction by PET. J Nucl Med 2010;51:1250-1257.
16. Chang IC, Lue KH, Hsieh HJ, Liu SH, Kao CH. Automated striatal uptake analysis of ^{18}F-FDOPA PET images applied to Parkinson's disease patients. Ann Nucl Med 2011;25:796-803.
17. Morris ED, Endres CJ, Schmidt KC, Christian BT, Muzic RF, Fisher RE. Kinetic modeling in positron emission tomography. Emission Tomography: The Fundamentals of PET and SPECT Academic, San Diego. 2004.
18. Nelissen N, Warwick J, Dupont P. Kinetic modelling in human brain imaging. Positron Emission Tomography. Current Clinical and Research Aspects 2012:978-953.
19. Seo Y, Teo BK, Hadi M, Schreck C, Bacharach SL, Hasegawa BH. Quantitative accuracy of PET/CT for image-based kinetic analysis. Med Phys 2008;35:3086-3089.
20. Watabe H, Ikoma Y, Kimura Y, Naganawa M, Shidahara M. PET kinetic analysis—compartmental model. Ann Nucl Med 2006;20:583-588.
21. Huang SC, Yu DC, Barrio JR, Grafton S, Melega WP, Hoffman JM, Satyamurthy N, Mazziotta JC, Phelps ME. Kinetics and modeling of L-6-[18F]fluoro-dopa in human positron emission tomographic studies. J Cereb Blood Flow Metab 1991;11:898-913.
22. Wahl L, Nahmias C. Modeling of fluorine-18-6-fluoro-L-Dopa in humans. J Nucl Med 1996;37:432-437.
23. Bhidayasiri R, Tarsy D. Parkinson's disease: hoehn and yahr scale. In: Movement Disorders: A Video Atlas. Springer; 2012:4-5.
24. Hughes A, Ben-Shlomo Y, Daniel S, Lees A. UK Parkinson's disease society brain bank clinical diagnostic criteria. J Neurol Neurosurg Psychiatr 1992;55:e4.
25. Darcourt J, Booij J, Tatsch K, Varrone A, Vander Borght T, Kapucu OL, Någren K, Nobili F, Walker Z, Van Laere K. EANM procedure guidelines for brain neurotransmission SPECT using (123)I-labelled dopamine transporter ligands, version 2. Eur J Nucl Med Mol Imaging 2010;37:443-450.
26. Morbelli S, Esposito G, Arbizu J, Barthel H, Boellaard R, Bohnen NI, Brooks DJ, Darcourt J, Dickson JC, Douglas D, Drzezga A, Dubroff J, Ekmekcioglu O, Garibotto V, Herscovitch P, Kuo P, Lammertsma A, Pappata S, Peñuelas I, Seibyl J, Semah F, Tossici-Bolt L, Van de Giessen E, Van Laere K, Varrone A, Wanner M, Zubal G, Law I. EANM practice guideline/SNMMI procedure standard for dopaminergic imaging in Parkinsonian syndromes 1.0. Eur J Nucl Med Mol Imaging 2020;47:1885-1912.
27. Ashburner J, Barnes G, Chen CC, Daunizeau J, Flandin G, Friston K, Jafarian A, Kiebel S, Kilner J, Litvak V, Moran R, Penny W, Razi A, Stephan K, Tak S, Zeidman P, Gitelman D, Henson R, Hutton C, Glauche V, Mattout J, Phillips C. SPM12 manual. Wellcome Trust Centre for Neuroimaging, London, UK. 2014:2464.
28. Barrett PH, Bell BM, Cobelli C, Golde H, Schumitzky A, Vicini P, Foster DM. SAAM II: Simulation, Analysis, and Modeling Software for tracer and pharmacokinetic studies. Metabolism 1998;47:484-492.
29. Tavola F, Janzen T, Giussani A, Facchinetti D, Veronese I, Uusijärvi-Lizana H, Mattsson S, Hoeschen C, Cantone MC. Nonlinear compartmental model of 18F-choline. Nucl Med Biol 2012;39:261-268.
30. Bozdogan H. Model selection and Akaike's information criterion (AIC): The general theory and its analytical extensions. Psychometrika 1987;52:345-370.
31. Schwarz G. Estimating the dimension of a model. The Annals of Statistics 1978;6:461-464.

Original Article
Mol Imaging Radionucl Ther 2021;30:79-85 DOI:10.4274/mirt.galenos.2021.92053

^{68}Ga-PSMA PET/CT Versus ^{18}F-FDG PET/CT for Imaging of Hepatocellular Carcinoma

Hepatoselüler Karsinomun Görüntülenmesinde ^{18}F-FDG PET/BT'ye Karşı ^{68}Ga-PSMA PET/BT

Cihan Gündoğan[1], Nurhan Ergül[2], Mehmet Semih Çakır[3], Özgür Kılıçkesmez[3], Rıza Umar Gürsu[4], Tamer Aksoy[2], Tevfik Fikret Çermik[2]

[1]University of Health Sciences Turkey, Gazi Yaşargil Training and Research Hospital, Clinic of Nuclear Medicine, Diyarbakır, Turkey
[2]University of Health Sciences Turkey, İstanbul Training and Research Hospital, Clinic of Nuclear Medicine, İstanbul, Turkey
[3]University of Health Sciences Turkey, İstanbul Training and Research Hospital, Clinic of Radiology, İstanbul, Turkey
[4]University of Health Sciences Turkey, İstanbul Training and Research Hospital, Clinic of Medical Oncology, İstanbul, Turkey

Abstract

Objectives: This study aimed to compare the metabolic parameters obtained from ^{18}fluorine-fluorodeoxyglucose (^{18}F-FDG) positron emission tomography/computed tomography (PET/CT) and gallium-68 (^{68}Ga)-prostate-specific membrane antigen (PSMA) PET/CT and investigate the relationship between serum alpha-fetoprotein and PET scan parameters in patients with hepatocellular carcinoma.

Methods: Fourteen patients were recruited after dynamic magnetic resonance imaging (MRI) of the upper abdomen, and ^{18}F-FDG and ^{68}Ga-PSMA PET/CT imaging studies were conducted. Regions of interest (ROIs) were drawn from lesion-free liver tissue, abdominal aorta (A), and right medial gluteal muscle (G) for the background activity. Maximum standard uptake value (SUV_{max}) of these regions were compared with the SUV_{max} of primary tumor (T).

Results: On visual assessment, five patients (36%) experienced low ^{18}F-FDG uptake in the primary lesion, three patients (21%) experienced moderate uptake, and six patients (43%) experienced high uptake. However, only one patient (7%) showed low ^{68}Ga-PSMA uptake, two patients (14%) showed moderate uptake, and 11 patients (79%) showed high uptake. Four patients with a low ^{18}F-FDG uptake showed high ^{68}Ga-PSMA uptake, while one patient exhibited low uptake with both ^{18}F-FDG and ^{68}Ga-PSMA. The number of lesions on ^{68}Ga-PSMA PET/CT and MRI was significantly higher than ^{18}F-FDG PET/CT (p=0.042 and 0.026, respectively). T/A and T/G values were significantly higher in ^{68}Ga-PSMA than ^{18}F-FDG (p=0.002 and 0.002, respectively).

Conclusion: ^{68}Ga-PSMA PET/CT is superior to ^{18}F-FDG PET/CT in the staging of hepatocellular carcinoma. High ^{68}Ga-PSMA uptake could be promising for PSMA-targeted radionuclide treatments.

Keywords: Hepatocellular cancer, ^{68}Ga-PSMA, ^{18}F-FDG, PET/CT, AFP

Address for Correspondence: Cihan Gündoğan MD, University of Health Sciences Turkey, Gazi Yaşargil Training and Research Hospital, Clinic of Nuclear Medicine, Diyarbakır, Turkey
Phone: +90 412 258 01 01 **E-mail:** cihangd@hotmail.com ORCID ID: orcid.org/0000-0001-5700-6292
Received: 11.01.2021 **Accepted:** 13.02.2021

Öz

Amaç: Bu çalışmanın amacı, ^{18}flor-florodeoksiglukoz (^{18}F-FDG) pozitron emisyon tomografisi/bilgisayarlı tomografi (PET/BT) ve galyum-68 (^{68}Ga)-prostat spesifik membran antijen (PSMA) PET/BT'den elde edilen metabolik parametreleri karşılaştırmak ve hepatosellüler karsinomlu hastalarda serum alfa-fetoprotein ve PET parametreleri arasındaki ilişkiyi araştırmaktı.

Yöntem: Çalışmaya üst karın bölgesinden dinamik manyetik rezonans görüntüleme (MRG) görüntülemesi olan 14 hasta alındı ve ^{18}F-FDG ve ^{68}Ga-PSMA PET/BT görüntülemeleri yapıldı. Arka plan aktivitesi için lezyonsuz karaciğer dokusundan, abdominal aortadan (A) ve sağ medial gluteal kastan (G) ilgi alanları (ROI) çizildi ve bu bölgelerin maksimum standardize uptake değerini (SUV_{maks}) primer tümörün (T) SUV_{maks}'ı ile karşılaştırıldı.

Bulgular: Görsel değerlendirmede, ^{18}F-FDG PET/BT'de 5 hastada (%36) primer lezyonda düşük ^{18}F-FDG tutulumu, 3 hastada (%21) orta düzeyde ve 6 hastada (%43) yüksek düzeyde tutulum vardı. Öte yandan, ^{68}Ga-PSMA PET/BT'de sadece 1 hastada (%7) düşük PSMA tutulumu varken, 2 hastada (%14) orta düzeyde ve 11 hastada (%79) yüksek düzeyde tutulum vardı. Düşük FDG tutulumu gösteren dört hasta yüksek PSMA tutulumu gösterirken, 1 hasta hem düşük ^{18}F-FDG, hem de düşük PSMA tutulumu göstermiştir. ^{68}Ga-PSMA PET/BT ve MRG'deki lezyon sayısı ^{18}F-FDG PET/BT'den anlamlı derecede yüksekti (sırasıyla p=0,042 ve 0,026). ^{68}Ga-PSMA'da T/A ve T/G değerleri ^{18}F-FDG'den anlamlı olarak yüksekti (sırasıyla p=0,002 ve 0,002).

Sonuç: ^{68}Ga-PSMA PET/BT, hepatoselüler karsinomun evrelendirilmesinde ^{18}F-FDG PET/BT'den üstün bulunmuştur. Yüksek ^{68}Ga-PSMA tutulumu, PSMA hedefli radyonüklid tedavileri için umut verici olabilir.

Anahtar kelimeler: Hepatosellüler kanser, ^{68}Ga-PSMA, ^{18}F-FDG, PET/BT, AFP

Introduction

Liver cancer is the 6th most frequent malignancy and the 4th most common cause of cancer-related deaths worldwide. Hepatocellular carcinoma (HCC), which develops due to major risk factors such as hepatitis B virus, hepatitis C virus, aflatoxin-containing foods, and non-alcoholic steatohepatitis, accounts for 75%-85% of primary liver cancers (1). Conventional dynamic contrast-enhanced imaging methods, including computed tomography (CT) and magnetic resonance imaging (MRI), are routinely used in the diagnosis of HCC, with 62%-82% sensitivity and over 90% specificity. Nodules larger than 1 cm show high contrast enhancement in the arterial phase of CT and MRI and wash out in venous and late phases (2). Alpha-fetoprotein (AFP), a serum biomarker, is one of the most commonly used markers in HCC screening and diagnosis. However, its sensitivity and specificity are unsatisfactory, especially in early-stage HCCs (3). The histopathological examination of the tumor tissue is the gold standard in the definitive diagnosis of HCC, but it may cause tissue damage and seeding along the biopsy tract (4).

^{18}Flourine-fluorodeoxyglucose (^{18}F-FDG) positron emission tomography(PET)/CT is associated with the aggressiveness of HCC; moderately and well-differentiated HCCs exhibit a low ^{18}F-FDG uptake, while poorly differentiated HCCs show high uptake (5,6). ^{18}F-FDG PET/CT shows a high sensitivity in detecting lymph nodes and extrahepatic metastases, which are poor prognostic factors for HCC, but show a low sensitivity in detecting primary HCC lesions (7,8).

Prostate-specific membrane antigen (PSMA) is a type 2 transmembrane protein and is overexpressed in prostate cancer (PCa). ^{68}Ga-PSMA PET/CT is widely used in staging, evaluating the treatment response, and assessing relapse in PCa (9). However, in many solid tumors, including HCCs, high PSMA uptake indicates neoangiogenesis (10,11).

In this prospective study, we compared the metabolic parameters obtained from ^{18}F-FDG PET/CT and ^{68}Ga-PSMA-11 PET/CT and investigated the association between PET parameters and serum AFP in patients with HCC.

Material and Methods

Patient Characteristics

Fourteen patients [13 males; 1 female; mean age: 63.8±6.0 years (58-76)] were included in this study. Twelve patients had a Child-Pugh (CP) score "A" cirrhosis, and two patients had a CP-B cirrhosis. Twelve patients had a newly diagnosed HCC, one patient had a history of transarterial chemoembolization (TACE), and one had radiofrequency ablation + TACE for HCC. While six patients had a histopathological confirmation, eight patients were diagnosed with HCC based on radiological findings and serum AFP levels. Patients were recruited after dynamic MRI of the upper abdomen, and ^{18}F-FDG and ^{68}Ga-PSMA-11 PET/CT imaging studies were conducted in the same week. AFP and routine laboratory tests and ^{18}F-FDG PET/CT were performed for all patients on the same day. Patients who previously received chemotherapy or had a history of hepatic tumor surgery were excluded from the study. This study was conducted in concordance with the local good clinical practice guidelines and current laws. The Local Ethics Committee of İstanbul Training and Research Hospital approved this study under the decision number: 2018/1297. Written informed consent was obtained from all patients.

PET/CT Scan and Evaluation

Whole-body PET/CT imaging was performed 60 min after intravenous injection of ^{18}F-FDG (3.5-5.5 MBq/kg) and ^{68}Ga-PSMA-11 (2-2.5 MBq/kg) in a PET/CT scanner [mCT 20 ultra HD LSO PET/CT (Siemens molecular imaging, Hoffmann Estates, Illinois, USA)] on different days. CT imaging was performed in the craniocaudal direction with a 5 mm slice thickness and rotation time of 0.5 sec [80-140 kV, 20-266 mAs, 0.8 pitch, and 512x512 matrix (personalized settings determined by the automatic exposure control system; automatically defined by the software used by the manufacturer, depending on the patient)]. Then, PET imaging was performed in the same range through the craniocaudal direction for 2 min for each PET bed; ultra HD images were acquired using the time of flight + true X algorithm at iteration two and subset 16 values for reconstruction.

^{18}F-FDG and ^{68}Ga-PSMA-11 PET/CT images were both evaluated by two nuclear medicine physicians with at least 10 years of experience in PET/CT, and decisions were made with consensus. Both PET/CT studies were scored visually. 1: Low uptake (equal or less than liver), 2: Moderate uptake (slightly higher than liver), 3: High uptake (markedly higher than liver). SUV_{max} of primary lesions were acquired by drawing a volume of interest to include the lesion in all three planes in ^{18}F-FDG and ^{68}Ga-PSMA-11 PET/CT. Moreover, regions of interest of 1 cm diameter were drawn from lesion-free liver tissue (L), abdominal aorta (A), and right medial gluteal muscle (M) for background maximum standard uptake value (SUV_{max}). Using these three background SUV_{max}, tumor to normal liver parenchyma (T/L), tumor to abdominal aorta (T/A), and tumor to gluteal muscle (T/G) parameters were calculated separately.

Statistical Analysis

SPSS version 21.0 software (IBM Corporation, Armonk, New York, USA) was used for statistical analyses of the variables. The normality of one-variable data was tested with the Shapiro-Francia test, while variance homogeneity was evaluated using Levene's test. Mann-Whitney U test was used to compare independent and non-normally distributed variables, while the Wilcoxon signed-rank test was used to compare dependent and normally distributed variables. Pearson and Spearman's rho tests were used to analyze the correlation of variables. The variables had a 95% confidence interval, and a p value less than 0.05 was considered significant.

Results

Six patients exhibited a bilobar involvement, while eight patients had a lobar involvement. On MRI, nine patients showed a mosaic enhancement pattern, and five patients showed a homogeneous enhancement pattern. The median size of primary tumors on MRI is 80.5 mm (20 mm-140 mm). The smallest lesion detected on ^{68}Ga-PSMA PET had a diameter of 8 mm, and the lesion had been described on MRI.

On the visual evaluation, five patients (36%) showed a low ^{18}F-FDG uptake in the primary lesion, three patients (21%) showed a moderate ^{18}F-FDG uptake, and six patients (43%) showed a high ^{18}F-FDG uptake. In contrast, one patient (7%) showed low ^{68}Ga-PSMA uptake, two patients (14%) showed moderate ^{68}Ga-PSMA uptake, and 11 patients (79%) showed high ^{68}Ga-PSMA uptake. Four patients with low ^{18}F-FDG uptake showed high ^{68}Ga-PSMA uptake (Figure 1), while one patient exhibited low uptake with both ^{18}F-FDG and ^{68}Ga-PSMA (Figure 2). Two patients with moderate ^{18}F-FDG uptake showed higher ^{68}Ga-PSMA uptake (Figure 3). In contrast, one patient with moderate ^{68}Ga-PSMA uptake showed higher ^{18}F-FDG uptake (Table 1).

The total number of liver lesions on ^{68}Ga-PSMA PET/CT, MRI, and ^{18}F-FDG PET/CT are 61, 57, and 30, respectively. The number of liver lesions on ^{68}Ga-PSMA PET/CT and MRI were significantly higher than ^{18}F-FDG PET/CT (p=0.042 and 0.026, respectively). There was no statistically significant difference between the number of liver lesions on MRI and ^{68}Ga-PSMA PET/CT (p=0.593) (Table 2).

^{68}Ga-PSMA PET/CT revealed a pathologically increased radiotracer uptake in the abdominal lymph nodes of four patients. Of these four patients, one patient had no ^{18}F-FDG uptake. Two patients had ^{18}F-FDG and ^{68}Ga-PSMA-

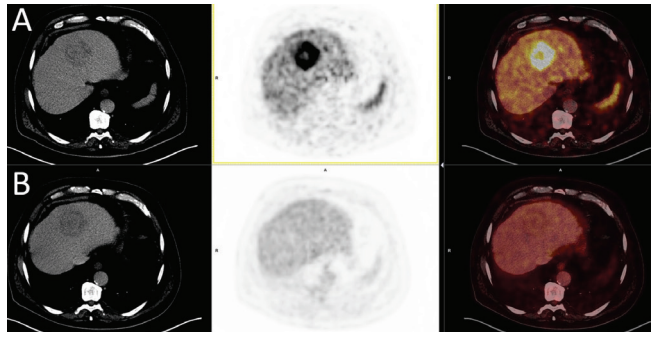

Figure 1. A 69-year-old male diagnosed with hepatocellular carcinoma (AFP: 4.5 ng/mL) by magnetic resonance imaging. The left lobe mass showed (A) an intense ^{68}Ga-PSMA (T/L: 4.49), while it showed no significant ^{18}F-FDG (B) uptake (T/L: 1.01)

AFP: Alpha-fetoprotein, ^{68}Ga: Gallium-68, ^{18}F-FDG: ^{18}Fluorine-fluorodeoxyglucose, T: Tumor uptake, L: Normal liver parenchyma uptake, PSMA: Prostate-specific membrane antigen

positive mediastinal lymph nodes, while the remaining patient, who was later histopathologically diagnosed with anthracosis, had only ^{18}F-FDG uptake. One patient had focally increased radiotracer accumulation in the prostate gland on both ^{18}F-FDG and ^{68}Ga-PSMA PET/CT, consistent with a synchronous tumor in the prostate.

The median SUV_{max} of primary lesions in ^{18}F-FDG and ^{68}Ga-PSMA PET/CT were 6.45 (range: 3.7-21.3) and 16.7 (range: 9.3-48.9), respectively. When median T/L, T/A, and T/G ratios were compared, T/L ratio had no statistically significant difference between ^{18}F-FDG and ^{68}Ga-PSMA (p=0.331), whereas T/A and T/G were significantly higher in ^{68}Ga-PSMA than ^{18}F-FDG (p=0.002 and 0.002, respectively).

Of our six patients with histopathology results, one was reported as having poorly differentiated HCC, two, as well-

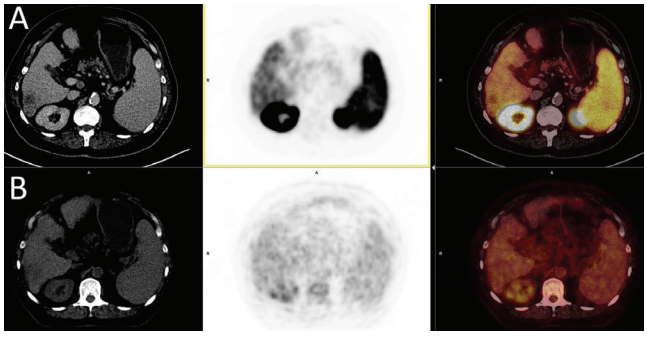

Figure 2. A 62-year-old male with alcohol-induced cirrhosis. Magnetic resonance imaging revealed a mass compatible with hepatocellular carcinoma, showing a typical contrast enhancement pattern (not shown). AFP: 1.648 ng/mL. ^{68}Ga-PSMA: (A) SUV_{max}: 9.3; T/L 0.93. ^{18}F-FDG: (B) SUV_{max}: 4.5; T/L 0.85

AFP: Alpha-fetoprotein, ^{18}F-FDG: ^{18}Fluorine-fluorodeoxyglucose, SUV_{max}: Maximum standard uptake value, PSMA: Prostate-specific membrane antigen, T: Tumor uptake, L: Normal liver parenchyma uptake

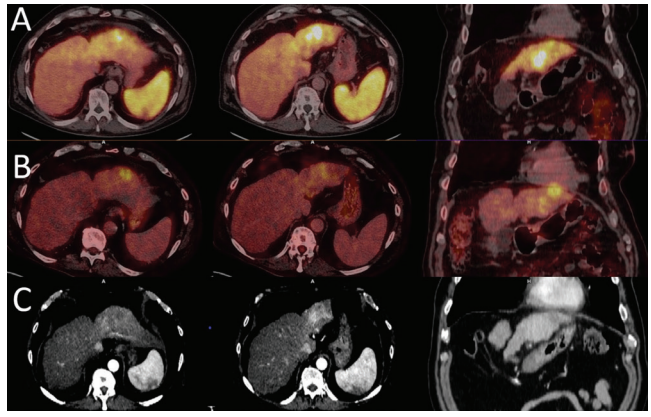

Figure 3. A 67-year-old cirrhotic male with hepatocellular carcinoma in the left lobe of the liver. ^{68}Ga-PSMA: (A) SUV_{max}: 28.1; T/L: 3.95; T/G: 31.2. ^{18}F-FDG: (B) SUV_{max}: 10.1; T/L: 2.76; T/G: 7. In arterial phase CT images (C), it is seen that PSMA uptake is higher in the hyperenhancement areas and ^{18}F-FDG uptake is higher in the non-enhancing areas of the tumor

T: Tumor uptake, L: Normal liver parenchyma uptake, G: Gluteus medius muscle uptake, ^{68}Ga: Gallium-68, ^{18}F-FDG: ^{18}Fluorine-fluorodeoxyglucose, PSMA: Prostate-specific membrane antigen, SUV_{max}: Maximum standard uptake value, CT: Computed tomography

Table 1. ^{18}F-FDG and ^{68}Ga-PSMA PET/CT findings of patients

Patient no	AFP (µg/L)	^{18}F-FDG LN	PSMA LN	^{18}F-FDG uptake	PSMA uptake	^{18}F-FDG T/L	PSMA T/L	^{18}F-FDG T/A	PSMA T/A	^{18}F-FDG T/G	PSMA T/G
1	351	1	6	Moderate	High	1.36	3.84	1.33	8.75	3.42	21.65
2	1643	2	2	Moderate	High	1.39	2.16	1.78	4.62	3.88	12.64
3	4.7	1	1	High	High	5.54	1.88	4.5	6.06	10.38	5.73
4	7.8	1	1	Low	High	0.86	2.11	0.93	7.27	1.63	20.75
5	4.5	1	1	Low	High	1.01	4.49	1.19	10.4	2.69	22.23
6	1648	1	1	Low	Low	0.85	0.93	1.4	4.94	4.44	11.33
7	17.3	1	1	Moderate	Moderate	1.48	1.44	1.84	4.86	5	9.47
8	60473	1	2	High	Moderate	4.62	1.37	6.01	3.31	15.22	16.71
9	205	4	>20	High	High	4.36	1.87	4.36	4.45	9.21	17.09
10	1042	12	>20	High	High	3.86	10.1	4.47	16.82	11.22	47.89
11	15195	1	2	High	High	2.91	2.81	3.73	5.07	7.68	20.63
12	10	1	1	Low	High	1.11	2.74	1.39	8.31	4.84	21.55
13	91	2	2	High	High	2.76	3.95	2.4	8.74	6.99	31.16
14	24.7	1	1	Low	High	1.11	3.98	2.4	7.33	3.28	41.22

AFP: Alpha-fetoprotein, A: Aorta, LN: Lesion number, L: Liver, T: Tumor, G: Medial gluteal muscle, ^{18}F-FDG: ^{18}Fluorine-fluorodeoxyglucose, ^{68}Ga: Gallium-68, PSMA: Prostate-specific membrane antigen, PET/CT: Positron emission tomography/computed tomography

Table 2. Comparison of ^{18}F-FDG and ^{68}Ga-PSMA PET/CT uptake ratios (SUV_{max})

	Mean	Median	SD	Minimum	Maximum	p
^{18}F-FDG SUV_{max}	8.99	6.45	5.30	3.72	21.3	**0.006^{w}**
PSMA SUV_{max}	20.88	16.69	11.76	9.29	48.9	
T/L ^{18}F-FDG	2.36	1.42	1.63	0.850	5.54	0.331^{w}
T/L PSMA	3.12	2.45	2.30	0.930	10.1	
T/G ^{18}F-FDG	6.42	4.92	3.89	1.63	5.73	**0.002^{w}**
T/G PSMA	21.43	20.69	11.76	15.2	47.9	
T/A ^{18}F-FDG	2.62	1.81	1.65	0.932	6.01	**0.002^{w}**
T/A PSMA	7.21	6.67	3.45	3.31	16.8	

^{w}Wilcoxon signed-rank, T: Tumor; L: Liver, A: Aorta, G: Medial gluteal muscle, ^{18}Fluorine-fluorodeoxyglucose, ^{68}Ga: Gallium-68, PSMA: Prostate-specific membrane antigen, PET/CT: Positron emission tomography/computed tomography, SUV_{max}: Maximum standard uptake value

differentiated HCC, and three, as HCC without specifying differentiation levels. ^{18}F-FDG (T/B: 1.48) and PSMA (T/B: 1.44) uptake in the patient with poorly differentiated HCC were similar, and a moderate radiopharmaceutical uptake was observed in both studies. The primary tumors in the two patients with well-differentiated HCC showed a low level of radiopharmaceutical uptake (T/B: 1.11 and 1.12) in ^{18}F-FDG PET/CT and intense radiopharmaceutical uptake (T/B: 2.74 and 3.96) in PSMA PET/CT. Two of the three patients whose differentiation level was not specified showed intense ^{18}F-FDG (T/B: 3.86 to 2.76) and PSMA (T/B:10.1 to 3.98) uptake, while one patient showed low ^{18}F-FDG (T/B: 0.86) and intense PSMA (T/B: 2.1) uptake.

When the relationship between the laboratory results and PET parameters was examined, serum AFP levels showed a statistically significant positive correlation with ^{18}F-FDG T/A ratio only (r=0.641 p=0.007). However, there was no correlation between ^{68}Ga-PSMA parameters and serum AFP (p>0.05).

Discussion

In this prospective study, we investigated the contribution of ^{68}Ga-PSMA PET/CT to the evaluation of HCCs. The most important findings in this study were primary tumors showing higher ^{68}Ga-PSMA uptake on visual assessment and the ability of ^{68}Ga-PSMA to detect more primary and metastatic lesions compared with ^{18}F-FDG. Conventional imaging methods, such as MRI, are routinely used as the first choice in the diagnosis of HCC due to the typical enhancement pattern with hyperenhancement in the arterial phase and wash out in the portal and late venous phases (12). Although MRI is generally sufficient for diagnosis, it cannot provide information about the biological behavior of HCC. PET radiopharmaceuticals, especially ^{18}F-FDG, are helpful in this context. ^{18}F-FDG PET/CT appears as an important non-invasive diagnostic tool, especially in terms of detecting metastatic lesions in HCC. It is known that ^{18}F-FDG PET/CT findings constitute a stronger prognostic factor than the nodule's size and number, as described in Milan criteria. Because ^{18}F-FDG avidity may predict the risk of relapse in patients who are planned to undergo liver transplantation, resection, or ablation, it may have a direct effect on the transplantation and ablation outcome (13,14). However, ^{18}F-FDG PET/CT has a low sensitivity in HCC due to overexpression of multidrug resistance protein and increased glucose-6-phosphatase activity in HCC cells, and its use in routine clinical practice is limited (15,16). Therefore, different radiopharmaceuticals have been investigated for the evaluation of primary and extrahepatic metastases of HCCs. Agents with high sensitivity, including ^{18}F-fluorocholine and ^{11}C-acetate, have a relatively poorer availability and, therefore, a limited use (17,18).

Non-prostate solid tumors may exhibit a wide endothelial PSMA expression, associated with neoangiogenesis and vascular growth factor regulation (19,20,21). Recent studies have shown that HCC shows a higher ^{68}Ga-PSMA uptake compared with ^{18}F-FDG (11,22). In our study, ^{68}Ga-PSMA PET/CT revealed more lesions than ^{18}F-FDG PET/CT, and the lesions showed a higher PSMA uptake compared with ^{18}F-FDG.

A recent study has reported that peritumoral/vascular expression of PSMA is greatly associated with grade 3 HCC (5/6, 83.3%) but can also be observed in grade 2 HCC (10/15, 66.7%). This was associated with the clinicopathological characteristics of HCC. Fibrolamellar HCC, normal hepatic tissue, and non-neoplastic cirrhotic tissue are reported to not overexpress PSMA. HCCs, arising in the setting of cirrhosis (9/10, 90.0%), show a significantly increased peritumoral/vascular PSMA

expression compared with non-cirrhotic HCCs (6/12, 50%) ($p<0.05$) (23).

In a study that evaluates seven patients and 37 lesions, Kesler et al. (11) demonstrated ^{68}Ga-PSMA uptake to be much higher than the background hepatic activity in 36/37 lesions. Twenty-eight lesions with no ^{18}F-FDG uptake showed high ^{68}Ga-PSMA uptake, while eight lesions showed both ^{18}F-FDG and ^{68}Ga-PSMA uptake. In their study involving 19 patients, Kuyumcu et al. (22) reported that ^{68}Ga-PSMA uptake was higher than ^{18}F-FDG uptake in nine patients. Four patients had a higher ^{18}F-FDG uptake compared with ^{68}Ga-PSMA, while two patients showed no uptake (22). In our study, 13 patients had an increased ^{68}Ga-PSMA uptake, while nine patients had an increased ^{18}F-FDG uptake. Four patients with no ^{18}F-FDG uptake had a high ^{68}Ga-PSMA uptake, however, one patient showed neither ^{18}F-FDG nor ^{68}Ga-PSMA uptake. One patient with moderate ^{68}Ga-PSMA uptake exhibited a higher ^{18}F-FDG uptake. Because of these results, the staging and treatment strategy can be changed through using ^{68}Ga-PSMA PET/CT instead of ^{18}F-FDG PET/CT for metabolic imaging in patients with HCC.

Kesler et al. (11) reported extrahepatic involvement in two of seven patients, while Kuyumcu et al. (22) reported extrahepatic involvement in one patient. In our study, four patients had extrahepatic involvement on ^{68}Ga-PSMA PET/CT, whereas ^{18}F-FDG PET/CT failed to reveal the involvement in one of these patients. One patient with ^{68}Ga-PSMA-negative mediastinal lymph nodes, which was later evidenced to be anthracosis by histopathological examination, showed false positivity in ^{18}F-FDG PET/CT. This supports the deduction that ^{68}Ga-PSMA PET/CT may provide more accurate staging than ^{18}F-FDG PET/CT.

Kuyumcu et al. (22) found no statistically significant difference between the mean SUV_{max} of primary tumor in ^{18}F-FDG and ^{68}Ga-PSMA PET/CT and T/L ratios. The researchers only evaluated T/L ratio but did not analyze T/A and T/G ratios (22). Because it has recently been reported that T/A ratios have a prognostic significance in rectal cancer (24), we analyzed T/A and T/G ratios in our study as well. We observed no statistical significance in terms of T/L ratios between ^{18}F-FDG and ^{68}Ga-PSMA PET/CT, while we found significantly higher T/A and T/G ratios and SUV_{max} in ^{68}Ga-PSMA PET/CT.

Since patients with histopathology results are few in our study, it will be difficult to make a clear evaluation of the relationship between HCC differentiation and PSMA involvement. However, PSMA uptake was significantly higher than ^{18}F-FDG uptake in our patients with well-differentiated HCC. In our patient with less differentiated HCC, ^{18}F-FDG, and PSMA uptakes were found to be similar compared with the background activity. Low ^{18}F-FDG uptake is an expected finding in patients with well-differentiated and moderately differentiated HCC, and our findings on the relationship between HCC differentiation and ^{18}F-FDG involvement are consistent with the literature (25). Since there are no studies in the literature, no correlation could be made between PSMA PET/CT and HCC differentiation.

In this preliminary study, no relationship was found between ^{68}Ga-PSMA tumor uptake and serum AFP level, suggesting that tumor angiogenesis and AFP production are independent parameters in HCC.

Study Limitations

First limitation of the current study is the relatively small number of patients, although our population is similar to other prospective studies in the literature. Second, not all patients had a histopathologically confirmed diagnosis, and some patients were diagnosed according to typical radiological findings.

Conclusion

^{68}Ga-PSMA PET/CT is superior to ^{18}F-FDG PET/CT in the diagnosis and staging of HCC. These preliminary findings show that ^{68}Ga-PSMA PET/CT has a supportive role for MRI in T staging, especially in demonstrating multicentric tumors, and it can be superior to MRI in demonstrating extrahepatic involvement. High PSMA uptake is promising for PSMA-targeted radionuclide treatments in metastatic HCC, which responds poorly to standard chemotherapy regimens. ^{68}Ga-PSMA PET/CT may also be helpful in evaluating treatment response, warranting further prospective studies in this area.

Ethics

Ethics Committee Approval: The Local Ethics Committee of İstanbul Training and Research Hospital approved this study under the decision number: 2018/1297.

Informed Consent: Written informed consent was obtained from all patients.

Peer-review: Externally and internally peer-reviewed.

Authorship Contributions

Surgical and Medical Practices: C.G., Concept: N.E., C.G., Design: C.G., T.F.Ç., Ö.K., Data Collection or Processing: R.U.G., M.S.Ç., C.G., T.A., Analysis or Interpretation: C.G.,Ö.K., N.E., M.S.Ç., Literature Search: R.U.G., T.A., Writing: C.G., T.F.Ç.

Conflict of Interest: No conflict of interest was declared by the authors.

Financial Disclosure: The authors declared that this study has received no financial support.

References

1. Bray F, Ferlay J, Soerjomataram I, Siegel RL, Torre LA, Jemal A. Global cancer statistics 2018: GLOBOCAN estimates of incidence and mortality worldwide for 36 cancers in 185 countries. CA Cancer J Clin 2018;68:394-424. Erratum in: CA Cancer J Clin 2020;70:313.
2. Roberts LR, Sirlin CB, Zaiem F, Almasri J, Prokop LJ, Heimbach JK, Murad MH, Mohammed K. Imaging for the diagnosis of hepatocellular carcinoma: A systematic review and meta-analysis. Hepatology 2018;67:401-421.
3. De Stefano F, Chacon E, Turcios L, Marti F, Gedaly R. Novel biomarkers in hepatocellular carcinoma. Dig Liver Dis 2018;50:1115-1123.
4. Villanueva A. Hepatocellular Carcinoma. N Engl J Med 2019;380:1450-1462.
5. Sacks A, Peller PJ, Surasi DS, Chatburn L, Mercier G, Subramaniam RM. Value of PET/CT in the management of primary hepatobiliary tumors, part 2. AJR Am J Roentgenol 2011;197:W260-265.
6. Afshar-Oromieh A, Avtzi E, Giesel FL, Holland-Letz T, Linhart HG, Eder M, Eisenhut M, Boxler S, Hadaschik BA, Kratochwil C, Weichert W, Kopka K, Debus J, Haberkorn U. The diagnostic value of PET/CT imaging with the (68)Ga-labelled PSMA ligand HBED-CC in the diagnosis of recurrent prostate cancer. Eur J Nucl Med Mol Imaging 2015;42:197-209.
7. Anis M, Irshad A. Imaging of hepatocellular carcinoma: practical guide to differential diagnosis. Clin Liver Dis 2011;15:335-352, vii-x.
8. Jadvar H. Hepatocellular carcinoma and gastroenteropancreatic neuroendocrine tumors: potential role of other positron emission tomography radiotracers. Semin Nucl Med 2012;42:247-254.
9. Takada Y, Kaido T, Shirabe K, Nagano H, Egawa H, Sugawara Y, Taketomi A, Takahara T, Wakabayashi G, Nakanishi C, Kawagishi N, Kenjo A, Gotoh M, Toyoki Y, Hakamada K, Ohtsuka M, Akamatsu N, Kokudo N, Takeda K, Endo I, Takamura H, Okajima H, Wada H, Kubo S, Kuramitsu K, Ku Y, Ishiyama K, Ohdan H, Ito E, Maehara Y, Honda M, Inomata Y, Furukawa H, Uemoto S, Yamaue H, Miyazaki M, Takada T; LTx-PET study group of the Japanese Society of Hepato-Biliary-Pancreatic Surgery and the Japanese Liver Transplantation Society. Significance of preoperative fluorodeoxyglucose-positron emission tomography in prediction of tumor recurrence after liver transplantation for hepatocellular carcinoma patients: a Japanese multicenter study. J Hepatobiliary Pancreat Sci 2017;24:49-57.
10. Sheikhbahaei S, Werner RA, Solnes LB, Pienta KJ, Pomper MG, Gorin MA, Rowe SP. Prostate-Specific Membrane Antigen (PSMA)-Targeted PET Imaging of Prostate Cancer: An Update on Important Pitfalls. Semin Nucl Med 2019;49:255-270.
11. Kesler M, Levine C, Hershkovitz D, Mishani E, Menachem Y, Lerman H, Zohar Y, Shibolet O, Even-Sapir E. 68Ga-PSMA is a novel PET-CT tracer for imaging of hepatocellular carcinoma: A prospective pilot study. J Nucl Med 2019;60:185-191.
12. Wu JW, Yu YC, Qu XL, Zhang Y, Gao H. Optimization of hepatobiliary phase delay time of Gd-EOB-DTPA-enhanced magnetic resonance imaging for identification of hepatocellular carcinoma in patients with cirrhosis of different degrees of severity. World J Gastroenterol 2018;24:415-423.
13. Hayakawa N, Nakamoto Y, Nakatani K, Hatano E, Seo S, Higashi T, Saga T, Uemoto S, Togashi K. Clinical utility and limitations of FDG PET in detecting recurrent hepatocellular carcinoma in postoperative patients. Int J Clin Oncol 2014;19:1020-1028.
14. Asman Y, Evenson AR, Even-Sapir E, Shibolet O. [18F]fludeoxyglucose positron emission tomography and computed tomography as a prognostic tool before liver transplantation, resection, and loco-ablative therapies for hepatocellular carcinoma. Liver Transpl 2015;21:572-580.
15. Brito AF, Mendes M, Abrantes AM, Tralhão JG, Botelho MF. Positron emission tomography diagnostic imaging in multidrug-resistant hepatocellular carcinoma: focus on 2-deoxy-2-(18F)Fluoro-D-Glucose. Mol Diagn Ther 2014;18:495-504.
16. Izuishi K, Yamamoto Y, Mori H, Kameyama R, Fujihara S, Masaki T, Suzuki Y. Molecular mechanisms of [18F]fluorodeoxyglucose accumulation in liver cancer. Oncol Rep 2014;31:701-706.
17. Talbot JN, Fartoux L, Balogova S, Nataf V, Kerrou K, Gutman F, Huchet V, Ancel D, Grange JD, Rosmorduc O. Detection of hepatocellular carcinoma with PET/CT: a prospective comparison of 18F-fluorocholine and 18F-FDG in patients with cirrhosis or chronic liver disease. J Nucl Med 2010;51:1699-1706.
18. Song WS, Nielson BR, Banks KP, Bradley YC. Normal organ standard uptake values in carbon-11 acetate PET imaging. Nucl Med Commun 2009;30:462-465.
19. O'Keefe DS, Bacich DJ, Huang SS, Heston WDW. A Perspective on the Evolving Story of PSMA Biology, PSMA-Based Imaging, and Endoradiotherapeutic Strategies. J Nucl Med 2018;59:1007-1013.
20. Carter RE, Feldman AR, Coyle JT. Prostate-specific membrane antigen is a hydrolase with substrate and pharmacologic characteristics of a neuropeptidase. Proc Natl Acad Sci U S A 1996;93:749-753.
21. Mhawech-Fauceglia P, Zhang S, Terracciano L, Sauter G, Chadhuri A, Herrmann FR, Penetrante R. Prostate-specific membrane antigen (PSMA) protein expression in normal and neoplastic tissues and its sensitivity and specificity in prostate adenocarcinoma: an immunohistochemical study using mutiple tumour tissue microarray technique. Histopathology 2007;50:472-483.
22. Kuyumcu S, Has-Simsek D, Iliaz R, Sanli Y, Buyukkaya F, Akyuz F, Turkmen C. Evidence of Prostate-Specific Membrane Antigen Expression in Hepatocellular Carcinoma Using 68Ga-PSMA PET/CT. Clin Nucl Med 2019;44:702-706.
23. Chen W, Lee Z, Awadallah A, Zhou L, Xin W. Peritumoral/vascular expression of PSMA as a diagnostic marker in hepatic lesions. Diagn Pathol 2020;15:92.
24. Belge G, Bilgin C, Ozkaya G, Kandemirli SG, Alper E. Prognostic value of pretreatment tumor-to-blood standardized uptake ratio (SUR) in rectal cancer. Ann Nucl Med 2020;34:432-440.
25. Dubash SR, Idowu OA, Sharma R. The emerging role of positron emission tomography in hepatocellular carcinoma. Hepat Oncol 2015;2:191-200.

Original Article
Mol Imaging Radionucl Ther 2021;30:86-92 DOI:10.4274/mirt.galenos.2021.75983

The Role of Metabolic Volumetric Parameters in Predicting Malignancy in Incidental Thyroid Nodules Detected in ^{18}F-FDG PET/CT Scans

^{18}F-FDG PET/BT Taramalarında Tespit Edilen Tesadüfi Tiroid Nodüllerinde Maligniteyi Öngörmede Metabolik Volumetrik Parametrelerin Rolü

Mehmet Erdoğan[1], Hakan Korkmaz[2], Bora Torus[2], Mustafa Avcı[1], Şerife Mehtap Boylubay[2], Metin Çiriş[3], Mustafa Yıldız[1], Sevim Süreyya Şengül[1]

[1]*Süleyman Demirel University Faculty of Medicine, Department of Nuclear Medicine, Isparta, Turkey*
[2]*Süleyman Demirel University Faculty of Medicine, Department of Endocrinology and Metabolism, Isparta, Turkey*
[3]*Süleyman Demirel University Faculty of Medicine, Department of Pathology, Isparta, Turkey*

Abstract

Objectives: The metabolic activities of tumors can be calculated volumetrically during positron emission tomography/computed tomography (PET/CT) imaging using metabolic tumor volume (MTV) and total lesion glycolysis (TLG). This study aimed to evaluate the roles of MTV and TLG in predicting the malignancy risk of incidental thyroid nodules detected by PET/CT imaging.

Methods: Active metabolic areas of each section were manually drawn by region of interest to calculate the MTV of nodules, and all obtained values were then summed. TLG, the product of mean standardized uptake value and MTV, was calculated by multiplying two values. All participants underwent thyroid ultrasonography imaging. All nodules were divided into risk classes according to the European Thyroid Image Reporting and Data System (EU-TIRADS) that was developed by the European Thyroid Association. The American Thyroid Association Guidelines were used to determine which thyroid nodules would undergo thyroid fine-needle biopsy (FNAB). Results were classified according to the Bethesda scoring system.

Results: TLG levels were significantly higher in malignant or malignant-suspicious nodules than in benign nodules (p=0.013). Although MTV levels were high in malignant or malignant-suspicious nodules than in benign and non-diagnostic nodules, it was statistically insignificant at limit values (p=0.079). Areas under curve (AUC) were 0.726 (p=0.005) and AUC: 0.668 (p=0.039) for TLG and MTV, respectively. The 2.3 g cut-off value of TLG has a sensitivity of 85.7% and specificity of 59.0%. The 1.7 mL cut-off value of MTV has a sensitivity of 78.6% and specificity of 60.4%.

Conclusion: We believe that TLG evaluation will be useful in predicting high-risk malignancy or malignancy suspicion based on EU-TIRADS risk classification of incidental thyroid nodules detected in PET/CT images. We believe that unnecessary thyroid FNABs can be avoided for thyroid incidental nodules if such relation and cut-off values are determined and that it will be useful in hastening the operation of the necessary patients.

Keywords: Metabolic tumor volume, total lesion glycolysis, incidental thyroid nodules, ^{18}F-FDG PET/CT scans

Address for Correspondence: Asst. Prof. Mehmet Erdoğan MD, Süleyman Demirel University Faculty of Medicine, Department of Nuclear Medicine, Isparta, Turkey
Phone: +90 211 246 28 10 **E-mail:** mdr_erdogan@yahoo.com ORCID ID: orcid.org/0000-0001-7724-778X
Received: 30.10.2020 **Accepted:** 15.02.2021

Öz

Amaç: Tümörlerin metabolik aktivitesi pozitron emisyon tomografi/bilgisayarlı tomografinin (PET/BT) görüntüleme sırasında hacimsel olarak hesaplanabilir. Bunlar metabolik tümör hacmi (MTV) ve toplam lezyon glikolizidir (TLG). Bu çalışmanın amacı, PET/BT görüntüleme ile saptanan tesadüfi tiroid nodüllerinde malignite riskini tahmin etmede hacimsel olarak metabolik aktivite gösteren MTV ve TLG'nin rollerini değerlendirmektir.

Yöntem: Nodülün MTV'sini hesaplamak için, her bölümün aktif metabolik aktif lezyonlara ilgi alanları ile manuel olarak çizildi; daha sonra elde edilen tüm değerler toplandı. Ortalama standardize uptake değeri ve MTV'nin ürünü olan TLG, iki değer çarpılarak hesaplandı. Tüm katılımcıların tiroid ultrasonografileri yapıldı. Tüm nodüller, Avrupa Tiroid Birliği (ETA) tarafından geliştirilen "EU-TIRAD"a göre risk sınıflarına ayrıldı. ATA Kılavuzu'na göre hangi tiroid nodüllerinin tiroid İİAB geçireceğine karar verildi. Sonuçlar Bethesda puanlama sistemine göre verildi

Bulgular: TLG düzeyleri, benign nodüllere göre malign veya malign-şüpheli nodüllerde anlamlı olarak yüksekti (p=0,013). MTV düzeyleri malign veya malign-şüpheli nodüllerde benign ve tanısal olmayan nodüllere göre yüksek olmasına rağmen sınır değerlerde istatistiksel olarak anlamlı değildi (p=0,079). Eğri altındaki alan (AUC) TLG için 0,726 (p=0,005) olarak hesaplandı. TLG için 2,3 g kesme değeri için duyarlılık %85,7 ve özgüllük %59,0 olarak bulundu. MTV için AUC 0,668 olarak hesaplandı (p=0,039). MTV için 1,7 mL cut-off için duyarlılık %78,6, özgüllük ise %60,4 idi.

Sonuç: PET/BT ile saptanan tesadüfi tiroid nodüllerinde, yüksek riskli malignite veya malignite şüphesine sahip olma açısından TLG değerlendirmesinin, EU-TIRADS'ye göre yüksek ve çok yüksek riskinin tahmin edilmesinde faydalı olacağına inanıyoruz. Böyle bir ilişki ve kesim değerlerinin kesin olarak tespit edilmesi durumunda, tiroid tesadüfi nodüller için gereksiz tiroid İİAB'lerinden kaçınılabileceğini ve gerekli hastaların ameliyatının geciktirilmemesi açısından faydalı olacağını düşünüyoruz.

Anahtar kelimeler: Metabolik tümör hacmi, toplam lezyon glikoliz, tesadüfi tiroid nodülleri, ^{18}F-FDG PET/BT taramaları

Introduction

Thyroid cancers account for 3.0% of all new cancer cases and 0.4% of all cancer deaths, and its prevalence is increasing worldwide (1). Positron emission tomography/computed tomography (PET/CT) imaging is recently being used for various diseases, especially in malignancies. Thyroid nodules, called thyroid incidentalomas, are detected by chance in approximately 1-4% of cases during these tomographies (2). ^{18}Flor-fluorodeoxyglucose (^{18}F-FDG) PET/CT is an examination that determines the metabolic activity of tumors. The highest metabolic activity point of tumors is referred as the maximum standardized uptake value (SUV_{max}) (3). There is no sufficient evidence in previous studies to support that SUV_{max} is beneficial in determining the malignancy risk in thyroid incidentalomas (4,5,6). The metabolic activity of tumors can be calculated volumetrically during PET/CT imaging using metabolic tumor volume (MTV) and total lesion glycolysis (TLG). MTV is a semi-quantitative parameter that has prognostic clinical value in many malignancies, whereas TLG is also a semi-quantitative parameter that corresponds to the cell mass of the target lesion associated with ^{18}F-FDG involvement (7). It is unknown whether MTV and TLG have roles in determining the malignancy risk in thyroid incidentalomas.

All thyroid incidentalomas detected with other imaging methods must be evaluated using thyroid ultrasonography imaging (USI) (8). This determines the localization, size, echo structure, nodule shape, and image characteristics (echogenicity, calcifications, edge layout, halo presence, blood flow, and extrathyroidal spread presence) of the nodule and the presence of lymphadenopathy (9). Malignancy risk is classified based on the USI findings, and it is decided whether or not to conduct thyroid fine-needle biopsy (FNAB) according to the European Thyroid Image Reporting and Data System (EU-TIRADS) developed by the European Thyroid Association (ETA) (10).

The contribution of PET/CT images to thyroid USI in determining the malignancy risk will enable more accurate decisions to be made in determining patients who will undergo thyroid FNAB or surgical intervention in cases with thyroid incidentaloma. This study aimed to evaluate the roles of MTV and TLG, which determine metabolic activity volumetrically, in predicting the malignancy risk of incidental thyroid nodules detected by PET/CT imaging.

Materials and Methods

The study was approved by Süleyman Demirel University Ethics Board (date: 13.02.2020, approval number: 37). After screening the archives, written and verbal information about the study was given to the participants. Consent was obtained from the patients before they were included in the study. Data of 6.480 patients who underwent ^{18}F-FDG PET/CT screening for non-thyroid malignancy or other reasons at our clinic between 2017 and 2020 were evaluated retrospectively. The hypometabolic and hypermetabolic thyroid nodules detected during this screening were described as thyroid incidentaloma. Thyroid incidentalomas were detected in 190 (2.93%) patients who underwent PET/CT scans. A total of 101 of these patients (63 women and 38 men) and 153 nodules were included in the study. The inclusion criteria were as follows: (a) No previous thyroid disease (no history of benign or malignant thyroid nodules), (b) no history of thyroidectomy, (c) no diffuse involvement in the thyroid during PET/CT, (d) thyroid FNAB and thyroid USIs performed in our hospital, and (e) consent

to participate in the study. The design of the study is shown in Figure 1. The primary cancers and cancer rates of the patients included in the study are given in Table 1.

Thyroid USI Evaluation: An experienced endocrinologist (H.K.) performed the thyroid USIs for all participants using the Philips EPIQ 5 Device (Germany). The largest sizes of all thyroid nodules, their structures (cystic, solid, dominant cystic, or dominant solid), echogenicity (hypoechoic, isoechoic, or hyperechoic), halo (thin, thick, or irregular), border layout (regular or irregular), vascularity evaluation with Doppler (intranodular blood build-up, perinodular blood build-up, or no blood build-up), and calcifications (micro-macro or nucleus qualifications) were evaluated. All nodules were divided into risk classes according to EU-TIRADS that was developed by the ETA.

Implementation of Thyroid FNAB: The American Thyroid Association Guidelines were used to determine which thyroid nodules would undergo thyroid FNAB (2). The procedure was performed by a single endocrinologist (H.K.) using a 10 cc injector and 22 G needle tip as stated in the USI guide. At least two slides that were air dried were sent to the pathology laboratory on the same day in a closed container with liquid-based cytology solution and the remaining material.

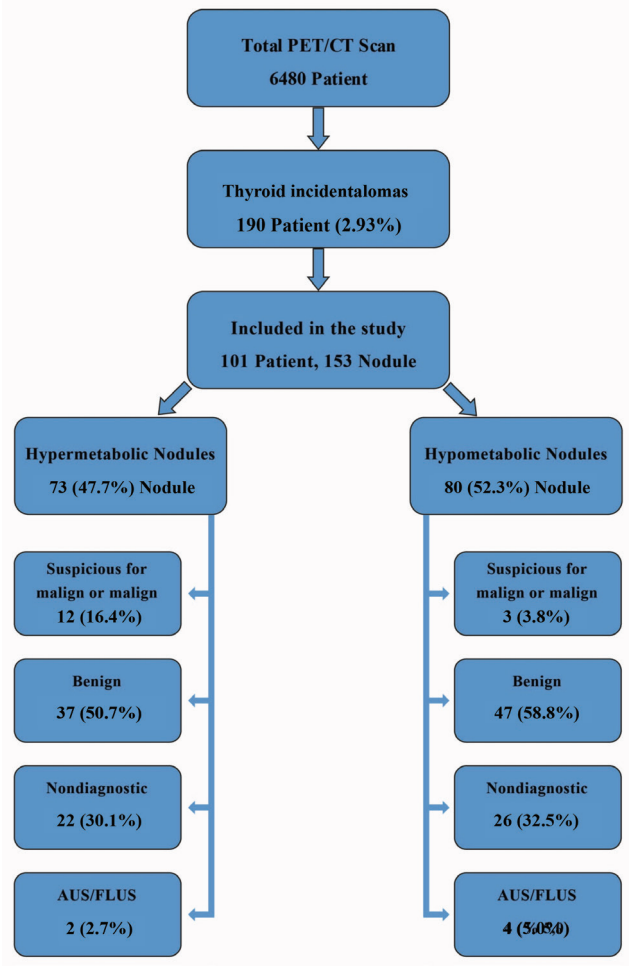

Figure 1. The design of the study

AUS/FLUS: Cytological atypia/follicular lesion of undetermined significance, PET/CT: Positron emission tomography/computed tomography

Table 1. Characteristics of patients included in the study

Variables	
Age (years)	63.72±12.22
Gender (male/female)	63/38
TSH (mIU/L)	1.04±1.7
Thyroid nodule diameter (mm)	19±12
Hypermetabolic/hypometabolic (n)	73/80
Bethesda scoring	
NDS Benign AUS/FLUS Suspicious for malign/malign	48 (31.4%) 84 (54.9%) 6 (3.9%) 15 (9.8%)
Primary cancer	
Breast cancer	19 (18.8%)
Laryngeal cancer	2 (2.0%)
Endometrial cancer	7 (6.9%)
Lung cancer	2 (2.0%)
Bladder cancer	1 (1.0%)
Lymphoma	8 (7.9%)
Rectal cancer	3 (3.0%)
Ovarian cancer	3 (3.0%)
Nasopharyngeal cancer	3 (3.0%)
Colon cancer	8 (7.9%)
Renal cell cancer	2 (2.0%)
Squamous cell carcinoma (skin)	1 (1.0%)
Malignant melanoma	2 (2.0%)
Gastric cancer	3 (3.0%)
Mediastinal mass	3 (3.0%)
Adrenal mass	1 (1.0%)
Breast mass	2 (2.0%)
Pancreatic mass	2 (2.0%)
Vertebral mass	1 (1.0%)
Small intestine mass	1 (1.0%)
Solitary pulmonary nodule	13 (12.9%)
Lung mass	14 (13.9%)
Fever of unknown cause	1 (1.0%)

TSH: Thyroid-stimulating hormone, NDS: Non-diagnostic, AUS/FLUS: Cytological atypia/follicular lesion of undetermined significance

Histopathological Evaluation: An experienced pathologist (M.Ç.) evaluated all the test samples. Samples sent on air-dried glasses were stained with Giemsa stain, whereas those sent in liquid were stained with hematoxylin-eosin, Giemsa, and Papanicolaou stains. At least four slides were prepared, and cytopathological evaluation was performed. Results were classified as non-diagnostic, benign, cytological atypia/follicular lesion of undetermined significance (AUS/FLUS), follicle neoplasia suspicion, malignancy-suspicious, and malignant according to the Bethesda scoring system (11). Nodules that were suspected to be malignant were considered malignant. The malignant and benign nodules were statistically evaluated.

PET/CT Protocol and Image Analysis: All PET/CT examinations were conducted using the Philips GEMINI TF PET/CT scanner (Philips Medical Systems, Cleveland, Ohio, USA) with time-of-flight imaging and a 64-slice CT scanner. Patients were prohibited from consuming caffeine, alcohol, and nicotine 24 h before the procedure. The blood sugar concentrations of all patients after 6 h of fasting were measured using a glucometer device (120 and 200 mg/dL for non-diabetic and diabetic patients, respectively). Then, intravenous 3.7 MBq/kg (0.1 mCi/kg) ^{18}F-FDG injection was given. All patients were orally hydrated with 1.5 L contrast during the 60-min waiting period. CT scan was performed first, followed by a PET scan (Figure 2). Three experienced nuclear medicine specialists (S.S.Ş., M.Y., and M.E.) evaluated the PET and CT images (non-corrected and attenuation-corrected) in rotating maximum intensity projection and cross-sectional view (transverse-sagittal-coronal). The highest ^{18}F-FDG involvement value in the thyroid nodules was determined using the semi-quantitative SUV_{max} value, is the highest activity involvement area in the nodules. The SUV_{max} value was calculated using the following formula: SUV_{max}: maximum activity in the range of interest (MBq/mL)/[injected dose (MBq)/body weight (g)] To calculate the MTV of nodules, active metabolic areas of each section were manually drawn by region of interest, and all obtained values were then summed. Meanwhile, TLG is the product of SUV_{mean} and MTV values.

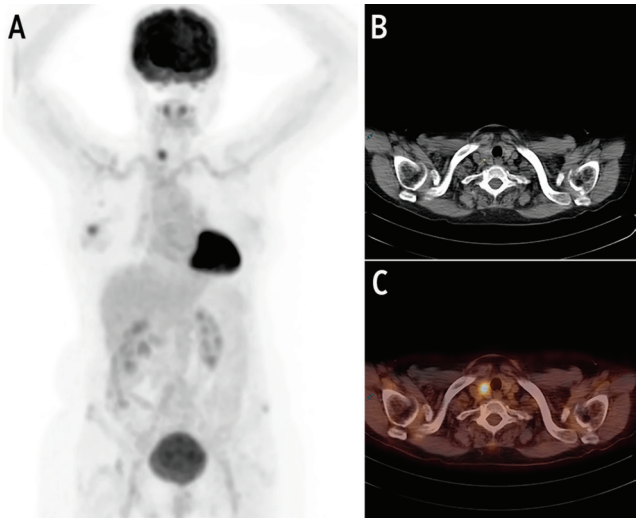

Figure 2. PET/CT findings of a breast cancer-diagnosed patient. Primary tumor in the right breast and hypermetabolic thyroid nodule in the right lobe of the thyroid gland were seen in the (A) total body PET maximum intensity projection image, (B) axial CT image, and (C) axial PET/CT fusion image

PET/CT: Positron emission tomography/computed tomography

Statistical Analysis

The Shapiro-Wilk test was used to evaluate the fitness of continuous variables to the normal distribution. The Kruskal-Wallis test was used to compare groups for variables that were not normally distributed. The Bonferroni-corrected Mann-Whitney U test was used to determine differences in variables between the groups. The comparison of categorical data was performed using the chi-square test. The diagnostic power of the possibility of malignant or premalignant results in incidental thyroid nodules using PET/CT imaging was evaluated with the receiver operating characteristic (ROC) curve analysis. The highest cutoff value for the sensitivity and specificity of these parameters in determining the malignancy risk was also calculated. Statistical Package for Social Sciences for Windows version 22.0 was used for statistical analyses, and $p<0.05$ was considered statistically significant.

Results

Of the 153 thyroid incidentalomas (9.8%) included in the study, 15 had malignant or malignant-suspicious histopathology. Of the thyroid nodules examined, 73 (47.7%) were hypermetabolic and 80 (52.3%) hypometabolic. Results of the thyroid FNABs for hypermetabolic nodules found that 12 (16.4%) were malignant or malignant-suspicious, 37 (50.7%) benign, 22 (30.1%) non-diagnostic, and 2 (2.7%) AUS/FLUS. Of the hypometabolic nodules, 3 (3.8%) were malignant or malignant-suspicious, 47 (58.8%) benign, 26 (32.5%) non-diagnostic, and 4 (5.0%) AUS/FLUS. The median level of thyroid-stimulating hormone was 1.04±1.7, and all of the cases included in the study were euthyroid.

The largest dimensions of the nodules were between 8 and 80 mm, and the median size was 19±12 mm in the thyroid USI evaluations.

No significant differences were detected in nodule size in PET/CT incidental thyroid nodules between the groups as a result of thyroid FNAB according to the Bethesda classification (p=0.063).

According to USI risk scoring, 6 (3.9%) of the nodules were EU-TIRADS 3, 44 (28.8%) EU-TIRADS 4, and 103 (67.3%) EU-TIRADS 5. No significant differences were detected in EU-TIRADS scores among the groups as a result of thyroid FNAB according to the Bethesda scoring system (p=0.488).

The PET/CT and USI findings of the PET/CT incidental thyroid nodules according to the Bethesda score are given in Table 2. SUV_{max} levels were significantly higher in malignant or malignant-suspicious nodules than in benign and non-diagnostic nodules (p<0.001 and p=0.002, respectively). SUV_{mean} levels were significantly higher in malignant or malignant-suspicious nodules than in benign and non-diagnostic nodules (p<0.001 and p=0.001, respectively). TLG levels were significantly higher in malignant or malignant-suspicious nodules than in benign nodules (p=0.013). Although MTV levels were high in malignant or malignant-suspicious nodules than in benign and non-diagnostic nodules, it was statistically insignificant at limit values (p=0.079).

The diagnostic power of the variables in predicting the risk of being malignant or malignant-suspicious in the incidental thyroid nodules detected in PET/CT scan were evaluated using ROC analysis. As shown in the ROC, the area under curve (AUC) was 0.827 (p<0.001) for SUV_{max}. The 2.4 cut-off value of SUV_{max} has a sensitivity of 85.7% and specificity of 71.2. AUC was 0.812 (p<0.001) for SUV_{mean}. The 1.8 cut-off value of SUV_{mean} has a sensitivity of 78.6% and specificity of 69.1%. AUC was 0.726 (p=0.005) for TLG. For the 2.3 g cut-off value of TLG, the sensitivity and specificity were 85.7% and 59.0%, respectively. AUC for MTV was 0.668 (p=0.039). For the 1.7 mL cut-off value of MTV, the sensitivity was 78.6% and specificity 60.4% (Figure 3).

Discussion

In this study, SUV_{max} and TLG were found useful in determining the risk of malignant and malignant-suspicious nodules with TFNB indication based on EU-TIRADS risk classification in thyroid nodules detected in PET/CT images. To the best of our knowledge, this study is the first to show a TLG increase in thyroid incidentalomas detected with PET/CT in malignant and malignant-suspicious lesions in thyroid FNAB than in benign ones.

Thyroid incidentaloma is detected in approximately 1.6-2.46% of patients during PET/CT imaging (12,13). Similar to the literature, in this study, thyroid incidentaloma was

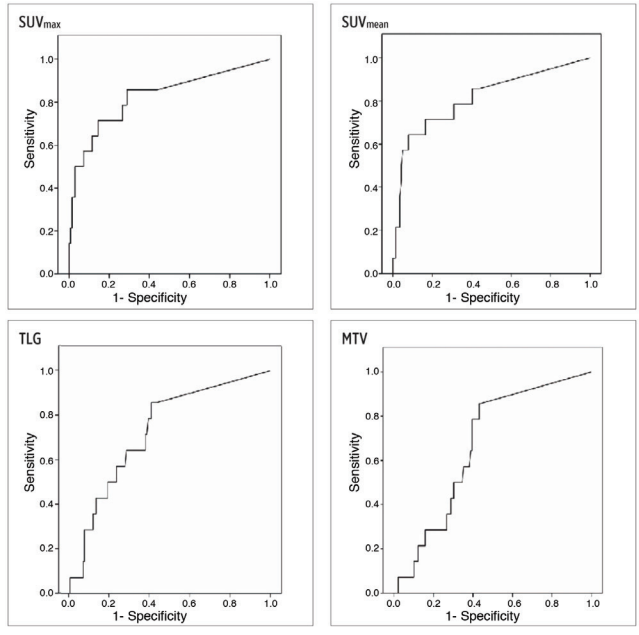

Figure 3. ROC analysis of PET parameters in predicting the risk of malignancy of thyroid incidentalomas

ROC: Receiver operating characteristic, PET: Positron emission tomography, SUV: Standardized uptake value, TLG: Total lesion glycolysis, MTV: Metabolic tumor volume

Table 2. PET/CT and USG findings according to Bathesda scoring of thyroid FNAB results

	Benign	Suspicious for malign/malign	AUS/FLUS	NDS	p
SUV_{mean}	1.01±1.32	2.80±1.79[a, b]	0.97±1.52	1.06±1.28	**0.002**
SUV_{max}	1.60±2.18	5.33±2.93[a, b]	1.59±2.53	1.64±2.07	**0.001**
MTV (mL)	3.80±7.52	5.76±9.78	1.05±1.66	3.89±7.55	0.166
TLG (g)	10.46±24.34	21.14±37.51[a]	3.12±5.13	8.33±16.41	**0.042**
EU-TIRADS	5±1	5±0.0	5±1	5±1	0.488
Nodule diameter (mm)	22±15	18±14	15.5±5	17±9	0.063

[a]Significantly different from benign (p<0.013), [b]Significantly different from NDS (p<0.013), PET/CT: Positron emission tomography/computed tomography, FNAB: Fine-needle biopsy, SUV: Standardized uptake value, MTV: Metabolic tumor volume, TLG: Total lesion glycolysis, EU-TIRADS: European Thyroid Imaging and Reporting Data System, AUS/FLUS: Cytological atypia/follicular lesion of undetermined significance, NDS: Non-diagnostic

detected in 2.93% of cases. The malignancy rates of these thyroid incidentalomas detected with PET/CT vary between 10% and 64% (12). In this study, on the other hand, malignancy was detected in 9.8% of incidental thyroid nodules. Of the 153 nodules included in the study, 47.7% were hypermetabolic, and 16.4% of the thyroid FNAB results of hypermetabolic nodules were malignant. In the meta-analyses of Soelberg et al. (12) and Bertagna et al. (13), the malignancy rates of hypermetabolic nodules were 34.8% and 34.6%, respectively. It is possible that the low malignancy rate in all thyroid incidentalomas and hypermetabolic thyroid incidentalomas was due to the high proportion of patients with biopsy compared with the literature. In addition, the high rate (31.3%) of non-diagnostic cytology in the study may contribute to the low malignity rate. In our study, thyroid FNAB was performed in 101 (53.15%) of 190 patients with thyroid incidentaloma. In the meta-analyses of Soelberg et al. (12) and Bertagna et al. (13), this rate was 46% and 35%, respectively. The similar rates in both meta-analyses can be explained with the inclusion of the same articles in the study.

No consensus has yet been reached on using SUV_{max} to predict malignancy. In the thyroid incidentalomas detected using PET/CT scan, only half of the studies in the literature found that the relation of SUV_{max} with malignancy is at a statistically significant level. A significant cut-off SUV_{max} value for malignancy was given in very few studies (12,13). In this study, higher ^{18}F-FDG intake was detected in patients who had suspected malignancy or malignancy as a result of thyroid FNAB from among thyroid incidentalomas. The mean SUV_{max} values in benign and malignant/malignant-suspicious lesions were 1.60±2.18 and 5.33±2.93 (p=0.001), respectively. The coincidence rate in terms of SUV_{max} was low between the benign, malignant, and malignant-suspicious groups. The cutoff value of SUV_{max} was 2.4 for predicting malignant or malignant-suspicious lesions. In a meta-analysis that included 22 studies, Soelberg et al. (12) found a significant relation between SUV_{max} and malignancy in eight studies. They found that the SUV_{max} values of benign and malignant lesions were 4.8±3.1 and 6.9±4.7, respectively (p<0.001) (11). The median SUV_{max} was higher in the benign and malignant groups than in our study.

Makis and Ciarallo (14) found a statistically significant difference in SUV_{max} between benign (mean SUV_{max} 4.8) and malignant thyroid incidentalomas (mean SUV_{max} 6.3); however, since there was a wide overlap of SUV_{max} values between the two, a significant SUV_{max} cut-off value was not determined. Kumar et al. (15) detected increased ^{18}F-FDG involvement in 55 of 1.016 patients for non-thyroid reasons (prevalence 2.26%). No significant difference was detected in their study between the mean SUV_{max} of benign and malignant thyroid incidentalomas (p=0.386). Although the incidence of thyroid incidentaloma is similar to that in our study, no significant differences were detected in SUV_{max} values between benign and malignant and malignant-suspicious lesions in our study. The reason for this might be that glucose transporter 1 expression, which plays an important role in the cell intake of ^{18}F-FDG, varies according to the differentiation in thyroid cancers (16). Barrio et al. (17) detected malignancies in 21 (21.4%) of 98 thyroid incidentalomas, which had focal ^{18}F-FDG involvement in 6.216 PET/CT scans. Similar to our study, they detected a statistically significant difference between benign and malignant thyroid incidentalomas in terms of SUV_{max}. To predict malignancy, the cut-off value of SUV_{max} was >2.

The number of studies conducted on volume-based metabolic parameters is quite limited in thyroid incidentalomas detected with ^{18}F-FDG PET/CT. Kim et al. (18) evaluated the predictive value of volume-based metabolic parameters (MTV and TLG) for pathological lateral lymph node metastasis (LNM) and its aggressiveness in differentiated thyroid cancers detected by chance with ^{18}F-FDG PET/CT and found that high MTV and TLG values were associated with LNM (18). In the present study, the TLG values were significantly higher in malignant or malignant-suspicious nodules than in benign and non-diagnostic nodules. Although the MTV values of malignant or malignant-suspicious nodules were high than in benign and non-diagnostic nodules, it was statistically insignificant at limit values. In this study, 96.1% of the thyroid incidentalomas that underwent thyroid FNAB were in the high or very high-risk group than using the EU-TIRADS risk scoring. Furthermore, 67.3% of the nodules were in the very high-risk group. The significance of TLG results in this study may be related to this.

Kim and Chang (19) compared intratumoral heterogeneity with thyroid FNAB results in thyroid nodules that were evaluated with PET/CT, and unlike this study, they reported a statistically significant difference between SUV_{max}, TLG, and MTV values between the malignant and malignant-suspicious groups according to the Bethesda classification. However, they detected no significant differences between the malignant and benign groups (19). In our study, 96.1% of the thyroid incidentalomas that underwent thyroid FNAB might be associated with being in a high or very high-risk group based on EU-TIRADS risk scoring.

Study Limitations

This study had several limitations. First, the study had a retrospective design. Second, pathologies after thyroidectomy were excluded because a limited number of

patients underwent thyroidectomy. In addition, the number of incidental thyroid nodules detected to be malignant after thyroid FNAB was relatively small.

Conclusion

As a result, we believe that evaluating SUV_{max} and TLG will be useful in predicting the high and very high risk of EU-TIRADS for having high-risk malignancy or malignancy suspicion from the incidental thyroid nodules detected by PET/CT. However, this must be supported with prospective studies, and more patients should be included. We believe that unnecessary thyroid FNABs for thyroid incidental nodules can be avoided if such relation and cutoff values are determined and that it will be useful in hastening the operation of the necessary patients.

Ethics

Ethics Committee Approval: The study was approved by Süleyman Demirel University Ethics Board (date: 13.02.2020, approval number: 37).

Informed Consent: Retrospective cross sectional study.

Peer-review: Externally peer-reviewed.

Authorship Contributions

Surgical and Medical Practices: M.E., H.K., S.S.Ş. Concept: M.E., H.K., S.S.Ş. Design: M.A., M.Y. Data Collection or Processing: B.T., H.K. Analysis or Interpretation: M.E., B.T., H.K., Literature Search: Ş.M.B., M.A. Writing: M.E., H.K., M.Ç.

Conflict of Interest: No conflict of interest was declared by the authors.

Financial Disclosure: The authors declared that this study has received no financial support.

References

1. SEER Cancer Statistics Review (CSR) 1975-2016 Updated February 14, 2020, https://seer.cancer.gov/statfacts/html/corp.html
2. Haugen BR, Alexander EK, Bible KC, Doherty GM, Mandel SJ, Nikiforov YE, Pacini F, Randolph GW, Sawka AM, Schlumberger M, Schuff KG, Sherman SI, Sosa JA, Steward DL, Tuttle RM, Wartofsky L. 2015 American Thyroid Association Management Guidelines for Adult Patients with Thyroid Nodules and Differentiated Thyroid Cancer: The American Thyroid Association Guidelines Task Force on Thyroid Nodules and Differentiated Thyroid Cancer. Thyroid 2016;26:1-133.
3. Larson SM, Erdi Y, Akhurst T, Mazumdar M, Macapinlac HA, Finn RD, Casilla C, Fazzari M, Srivastava N, Yeung HW, Humm JL, Guillem J, Downey R, Karpeh M, Cohen AE, Ginsberg R. Tumor Treatment Response Based on Visual and Quantitative Changes in Global Tumor Glycolysis Using PET-FDG Imaging. The Visual Response Score and the Change in Total Lesion Glycolysis. Clin Positron Imaging 1999;2:159-171.
4. Shie P, Cardarelli R, Sprawls K, Fulda KG, Taur A. Systematic review: prevalence of malignant incidental thyroid nodules identified on fluorine-18 fluorodeoxyglucose positron emission tomography. Nucl Med Commun 2009;30:742-748.
5. Hsiao YC, Wu PS, Chiu NT, Yao WJ, Lee BF, Peng SL. The use of dual-phase 18F-FDG PET in characterizing thyroid incidentalomas. Clin Radiol 2011;66:1197-1202.
6. Sager S, Vatankulu B, Sahin OE, Cınaral F, Uslu L, Baran A, Ozturk T, Sönmezoglu K. Clinical significance of standardized uptake values in thyroid incidentaloma discovered by F-18 fluorodeoxyglucose positron emission tomography/computed tomography. J Cancer Res Ther 2018;14:989-993.
7. Moon SH, Hyun SH, Choi JY. Prognostic significance of volume-based PET parameters in cancer patients. Korean J Radiol 2013;14:1-12.
8. Paschou SA, Vryonidou A, Goulis DG. Thyroid nodules: A guide to assessment, treatment and follow-up. Maturitas 2017;96:1-9.
9. Floridi C, Cellina M, Buccimazza G, Arrichiello A, Sacrini A, Arrigoni F, Pompili G, Barile A, Carrafiello G. Ultrasound imaging classifications of thyroid nodules for malignancy risk stratification and clinical management: state of the art. Gland Surg 2019;8(Suppl 3):S233-S244.
10. Russ G, Bonnema SJ, Erdogan MF, Durante C, Ngu R, Leenhardt L. European Thyroid Association Guidelines for Ultrasound Malignancy Risk Stratification of Thyroid Nodules in Adults: The EU-TIRADS. Eur Thyroid J 2017;6:225-237.
11. Alshaikh S, Harb Z, Aljufairi E, Almahari SA. Classification of thyroid fine-needle aspiration cytology into Bethesda categories: An institutional experience and review of the literature. Cytojournal 2018;15:4.
12. Soelberg KK, Bonnema SJ, Brix TH, Hegedüs L. Risk of malignancy in thyroid incidentalomas detected by 18F-fluorodeoxyglucose positron emission tomography: a systematic review. Thyroid 2012;22:918-925.
13. Bertagna F, Treglia G, Piccardo A, Giubbini R. Diagnostic and clinical significance of F-18-FDG-PET/CT thyroid incidentalomas. J Clin Endocrinol Metab 2012;97:3866-3875.
14. Makis W, Ciarallo A. Thyroid Incidentalomas on 18F-FDG PET/CT: Clinical Significance and Controversies. Mol Imaging Radionucl Ther 2017;26:93-100.
15. Kumar AA, Datta G, Singh H, Mukherjee PB, Vangal S. Clinical significance of thyroid incidentalomas detected on fluorodeoxyglucose positron emission tomography scan (PETomas): An Indian experience. World J Nucl Med 2019;18:273-282.
16. Schönberger J, Rüschoff J, Grimm D, Marienhagen J, Rümmele P, Meyringer R, Kossmehl P, Hofstaedter F, Eilles C. Glucose transporter 1 gene expression is related to thyroid neoplasms with an unfavorable prognosis: an immunohistochemical study. Thyroid 2002;12:747-754.
17. Barrio M, Czernin J, Yeh MW, Palma Diaz MF, Gupta P, Allen-Auerbach M, Schiepers C, Herrmann K. The incidence of thyroid cancer in focal hypermetabolic thyroid lesions: an 18F-FDG PET/CT study in more than 6000 patients. Nucl Med Commun 2016;37:1290-1296.
18. Kim BH, Kim SJ, Kim K, Kim H, Kim SJ, Kim WJ, Jeon YK, Kim SS, Kim YK, Kim IJ. High metabolic tumor volume and total lesion glycolysis are associated with lateral lymph node metastasis in patients with incidentally detected thyroid carcinoma. Ann Nucl Med 2015;29:721-729.
19. Kim SJ, Chang S. Predictive value of intratumoral heterogeneity of F-18 FDG uptake for characterization of thyroid nodules according to Bethesda categories of fine needle aspiration biopsy results. Endocrine 2015;50:681-688.

Original Article
Mol Imaging Radionucl Ther 2021;30:93-100 DOI:10.4274/mirt.galenos.2021.04934

Correlation of ^{18}F-FDG/PET SUV_{max}, SUV_{mean}, MTV, and TLG with HIF-1α in Patients with Colorectal Cancer

Kolorektal Kanserli Hastalarda ^{18}F-FDG/PET SUV_{maks}, $SUV_{ortalama}$, MTV, TLG ile HIF-1α'nın Korelasyonu

Zümrüt Arda Kaymak[1], Nermin Karahan[2], Mehmet Erdoğan[3], Evrim Erdemoğlu[4], İsmail Zihni[5], Sevim Süreyya Şengül[3]

[1]*Süleyman Demirel University Faculty of Medicine, Department of Radiaiton Oncology, Isparta, Turkey*
[2]*Süleyman Demirel University Faculty of Medicine, Department of Pathology, Isparta, Turkey*
[3]*Süleyman Demirel University Faculty of Medicine, Department of Nuclear Medicine, Isparta, Turkey*
[4]*Süleyman Demirel University Faculty of Medicine, Department of Gynecologic Oncology, Isparta, Turkey*
[5]*Süleyman Demirel University Faculty of Medicine, Department of Surgical Oncology, Isparta, Turkey*

Abstract

Objectives: Post-hypoxia hypoxia-inducible factor (HIF)-1α activation plays a vital role in colorectal cancer (CRC) angiogenesis. Although glucose metabolism is induced in some cancer types via HIF-1α, the prognostic significance of HIF-1α in CRC and its correlation with ^{18}fluorine-fluorodeoxyglucose (^{18}F-FDG) uptake in positron emission tomography (PET) remain controversial. This study aims to investigate the association between ^{18}F-FDG/PET parameters and HIF-1α expression in CRC.

Methods: Thirty-six histopathologically confirmed patients with CRC who had ^{18}F-FDG/PET scans before surgery were enrolled in the study. The correlations between the maximum standardized uptake value (SUV_{max}), SUV_{mean}, metabolic tumor volume (MTV), total lesion glycolysis, HIF-1α overexpression, and histopathological features were evaluated.

Results: The tumor location, tumor diameter, perineural invasion, lymphovascular invasion, T and N stage were not significantly correlated with HIF-1α overexpression. In contrast, the tumor differentiation was negatively correlated with HIF-1α expression (r=-0.332, p=0.048). None of the ^{18}F-FDG/PET parameters was significantly correlated with HIF-1α overexpression. A significant relationship was found between tumor differentiation, tumor necrosis percentage, and MTV (p=0.030, p=0.020).

Conclusion: The expected association between HIF-1α overexpression and ^{18}F-FDG/PET parameters was not found in this study. However, there was a relationship between MTV, tumor differentiation, and tumor necrosis percentage. Hence, further studies are required to predict the pathological and prognostic courses of CRC using a diagnostic ^{18}F-FDG/PET evaluation.

Keywords: Hypoxia-inducible factor-1α, colorectal cancer, ^{18}F-FDG/PET/CT, MTV, TLG

Address for Correspondence: Asst. Prof. Zümrüt Arda Kaymak, MD, Süleyman Demirel University Faculty of Medicine, Department of Radiaiton Oncology, Isparta, Turkey
Phone: +90 246 211 95 61 **E-mail:** ardakaymak84@yahoo.com ORCID ID: orcid.org/0000-0002-7284-008X
Received: 10.11.2020 **Accepted:** 24.03.2021

Öz

Amaç: Dokuda hipoksi sonrası hipoksi ile indüklenebilir faktör (HIF)-1α aktivasyonu, kolorektal kanser (KRK) anjiyogenezinde önemli bir rol oynar. Glikoz metabolizmasının bazı kanser türlerinde HIF-1α yoluyla indüklendiği bilinmesine rağmen; KRK'de HIF-1α'nın prognostik önemi ve pozitron emisyon tomografisinde (PET) ^{18}flor-florodeoksiglukoz (^{18}F-FDG) tutulumu ile korelasyonu önceki çalışmalarda tartışmalı konulardır. KRK olgularında ^{18}F-FDG/PET parametreleri ile HIF-1α ekspresyonu arasındaki ilişkiyi araştırmaktır.

Yöntem: Cerrahi öncesi ^{18}F-FDG/PET taramaları mevcut olan histopatolojik olarak tanı almış 36 KRK hastası çalışmaya alındı. Maksimum standardize uptake değeri (SUV_{maks}), $SUV_{ortalama}$, metabolik tümör hacmi (MTV), total lezyon glikolizis ve HIF-1α aşırı ekspresyonu ile histopatolojik özellikler arasındaki korelasyonlar değerlendirildi.

Bulgular: Tümör lokasyonu, tümör çapı, perinöral invazyon, lenfovasküler invazyon, T ve N evresi, HIF-1α aşırı ekspresyonu ile istatistiksel olarak anlamlı korelasyon göstermezken, tümör derecesi HIF-1α ekspresyonu ile negatif korelasyon gösterdi (r=-0,332, p=0,048). ^{18}F-FDG/PET parametrelerinin hiçbiri, HIF-1α aşırı ekspresyonu il e istatistiksel olarak anlamlı korele bulunmadı. Tümör derecesi ve tümör nekroz oranı ile MTV arasında anlamlı bir ilişki bulundu (p=0,030, 0,020).

Sonuç: HIF-1α aşırı ekspresyonu ile ^{18}F-FDG/PET parametreleri arasında beklenen ilişki bu çalışmada ortaya konamamıştır, ancak MTV ile tümör farklılaşması ve tümör nekroz oranı arasında bir ilişki mevcuttur. Bu nedenle, tanısal ^{18}F-FDG/PET değerlendirmesi ile KRK'nin patolojik ve prognostik seyrini tahmin etmek için daha fazla çalışmaya ihtiyaç vardır.

Anahtar kelimeler: Hipoksi ile indüklenebilir faktör-1α, kolorektal kanser, ^{18}F-FDG/PET/BT, MTV, TLG

Introduction

Colorectal cancer (CRC) is the third most common cancer in men and the second most common cancer in women worldwide (1). In all types of carcinoma, including CRC, the formation of new blood vessels is essential for tumor growth and distant metastasis (2,3). Many angiogenic growth factors have been described in the literature. The hypoxia-inducible factor (HIF)-1α gene family is one of these growth factors. In addition, HIFs are considered the main factors that initiate gene expression required for angiogenesis. HIF, a heterodimer, is a helix-loop-helix Per-ARNT-Sim transcription factor. It has three homologs identified as HIF-1α, HIF-2α, and HIF-3α. HIF-1α and HIF-2α play an essential role in tumor vascularization (4). In parallel with this, HIF-1α and HIF-2 HIF-2α are expressed in many types of cancer and can be used as prognostic factors in some cancers (5,6,7,8,9). HIF-1α expression is not affected by the hypoxic state of the cells and is already constitutively expressed. The accumulation of the subunit of HIF-1α in the cell in a short time occurs by preventing the naturally existing proteasomal degradation due to hypoxia. In hypoxia, the subunit that accumulates in the cell is HIF-1α (10,11,12). It is claimed that the expression of HIF-1α and HIF-2α in neoplastic cells has a predictive value on the survival of patients with CRC (13).

Positron emission tomography (PET), which is based on the high glucose uptake of neoplastic tissues, traces ^{18}fluorine-fluorodeoxyglucose (^{18}F-FDG) and enables the detection of tumoral activities in the whole body and thereby facilitates staging of the disease. By making a semiquantitative glucose measurement with ^{18}F-FDG/PET, the standardized uptake value (SUV) of the tumoral tissue is calculated (14). PET/computed tomography (CT) has been widely used in clinical practice to characterize and stage tumors non-invasively. The SUV, a semiquantitative index in PET/CT, has been popularly accepted by nuclear physicians in daily use to demonstrate the uptake of glucose in tumors/normal tissues. However, it remains questionable because of several reasons. First, the semiquantitative SUV_{max} is a sensitive indicator of metabolic activity and tumor proliferation; however, it is the SUV on the highest image pixel, reflecting a single-pixel value of the maximum intensity of ^{18}F-FDG activity in the tumor, ignoring the extent of metabolic abnormality and changes in the distribution of a tracer within the whole tumor mass (15,16). Second, SUV is calculated based on the whole-body weight metric (17). Third, studies have reported that many factors might influence SUV, and SUV_{max} is unreliable and recommendable because of its poor reproducibility (3%±11%). Researchers recommended volume-based variables such as metabolic tumor volume (MTV) and total lesion glycolysis (TLG) to reflect the metabolic activities within the whole tumor mass to overcome these controversies. Instead of whole-body weight, the administered dose should be based on volume-based parameters corrected by lean body mass (18).

By examining the correlation between HIF-1α expression and ^{18}F-FDG/PET parameters (SUV_{max}, SUV_{mean}, MTV, and TLG) in patients with CRC, the possibility of predicting the pathological and prognostic course of CRC by diagnostic ^{18}F-FDG/PET is investigated in the present study. In addition, the link between microscopic tumor diameter, lymphovascular invasion (LVI), perineural invasion (PNI), tumor necrosis percentage, tumor differentiation, and ^{18}F-FDG uptake was also evaluated.

Materials and Methods

Patients

The electronic database of patients diagnosed with colorectal adenocarcinoma by endoscopic biopsy between January 2018 and July 2019 in the department of surgical oncology of our institute was retrospectively reviewed. The ones scanned by ^{18}F-FDG/PET/CT for staging before surgery and undergoing curative surgical intent were included in the study. The patients who did not have a PET scan before primary surgery or had a PET scan but did not undergo primary surgery at our center were excluded. In addition, the patients who received neoadjuvant therapy for rectal cancer were not considered suitable for the pathological re-analysis and were excluded. The data of 36 patients who met the criteria were enrolled in the current study. ^{18}F-FDG/PET scans were performed on all patients between January 2018 and August 2019, at least 15 days after the endoscopic biopsy. If no distant metastases were defined on ^{18}F-FDG/PET images, patients were considered suitable for curative surgery.

The study was approved by the Scientific Research Ethics Committee of the Medical Faculty of University Süleyman Demirel (protocol code, 13.02.2020/51). All procedures applied were performed in accordance with the ethical standards of the institutional research committee in alliance with the 1964 Helsinki declaration and its later amendments. Informed consent was waived owing to the retrospective nature of the study.

Pathological Evaluation and Immunohistochemistry

The surgical materials were prepared for hematoxylin and eosin staining by paraffin blocking after slicing the primary tumor and resecting the lymph nodes. The slides were evaluated by an experienced pathologist from the department of pathology of our institute. Microscopic tumor diameter, LVI, PNI, tumor necrosis percentage, and differentiation were documented in the pathological evaluation. A tumor-node-metastasis (TNM) stage was defined for each patient according to the American Joint Committee on Cancer TNM staging classification (8th edition). The pathologist identified the most convenient paraffin-embedded block in the surgical specimen to perform the immunohistochemistry. Monoclonal rabbit anti-human HIF-1α antibodies (clone, EP1215Y; dilution, 1:100; Abcam, Cambridge, MA, USA) were used to evaluate the HIF-1α expression. A biotinylated goat anti-polyvalent secondary antibody (TP-125-BN; Thermo Fisher Scientific, Inc., Waltham, MA, USA) experiment was performed in parallel as a negative control, and human ovarian carcinoma was used as a positive control. The avidin-biotin-peroxidase complex accomplished the immunostaining process. The grade of staining was defined via a light microscope. Cytoplasmic and nuclear immunoreactivity in tumor cells was considered positive when evaluating immunostaining (Figure 1). The cut-off value to differentiate positive and negative immunoreactivity was determined as at least 10% (19).

^{18}F-FDG/PET Imaging Procedure

Whole-body ^{18}F-FDG/PET scans of patients diagnosed with CRC were performed with a Philips Gemini TF PET/CT scanner (Philips Medical Systems B. V., Eindhoven, Holland) in the nuclear medicine department of our institute. The procedure was initiated by checking that the patient's serum glucose level was under 150 mg/dL after six hours of fasting. Patients were administered ^{18}F-FDG intravenously (Monrol Eczacibasi, Istanbul, Turkey) calculated as 3.7 MBq (0.1 mCi/kg) per kilogram, and 60 minutes after injection, PET/CT scans were performed. Post-CT, a three-dimensional emission scan was recorded for two minutes per location.

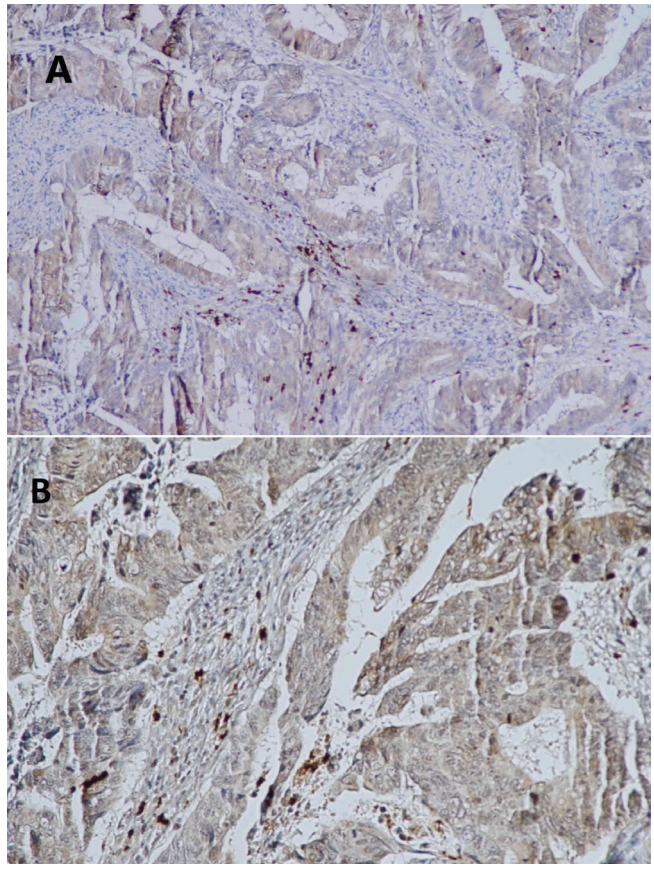

Figure 1. (A) Diffuse cytoplasmic and mild nuclear staining of HIF-1α in tumor cells (x100). (B) Diffuse-moderate cytoplasmic and mild nuclear staining of HIF-1α in tumor cells (x200)

HIF-1α: Hypoxia-inducible factor-1α

Images obtained from the PET and CT were examined in cross-sectional planes and rotational maximum intensity projection. The ^{18}F-FDG uptake in the primary tumor was measured semi-quantified by the SUV_{max} and the SUV_{mean}. The volume-based parameter MTV (mL) was determined using PET VCAR, the semiquantitative software embedded in the Philips workstation (the estimated threshold for discrimination of tumors was decided to be equal to or more than 42% of SUV_{max}. TLG was calculated based on the formula: $TLG=MTV\times SUV_{mean}$ (Figure 2).

Statistical Analysis

All values presented in the tables are expressed as medians (minimum-maximum) due to the non-parametric distribution of the variables. The clinicopathological features of the HIF-1α positive and negative groups were compared using the chi-square test. The medians of PET/CT parameters and tumor diameters of the HIF-1α groups were compared with the Mann-Whitney U test. Correlations between pathological findings, HIF-1α overexpression, and PET/CT parameters were analyzed by the Spearman correlation test. All analyses were two-sided, and $p<0.05$ was considered statistically significant. Statistical analyses were conducted via SPSS, version 21.0 (SPSS Inc. Chicago, IL, USA).

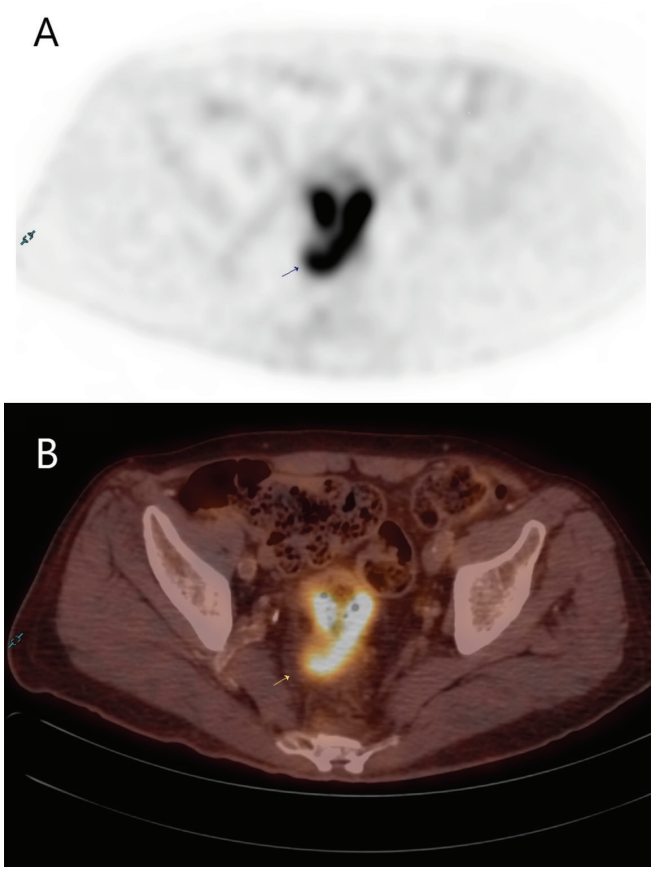

Figure 2. (A) ^{18}F-FDG/PET and (B) hybrid PET/computed axial tomography images demonstrating a rectosigmoid colorectal adenocarcinoma with conspicuously increased ^{18}F-FDG uptake (maximum standardized uptake value: 20.36, metabolic tumor volume: 98.05, total lesion glycolysis: 684:37) in a 74-year-old man. Histopathological features of the tumor were as follows: pT3 (5.7 cm), N0, well-differentiated, and HIF-1α overexpressed

^{18}F-FDG: ^{18}Fluorine-fluorodeoxyglucose, PET: Positron emission tomography, HIF-1α: Hypoxia-inducible factor-1α

Results

Patient Characteristics

Thirteen (36.1%) female and 23 (63.9%) male patients were enrolled in the study. The median age was 64 (37-88) years. The primary tumor locations were the colon in seven (19.4%) patients, the sigmoid colon in four (11.1%) patients, the rectosigmoid in five (13.9%) patients, and the rectum in 20 (55.6%) patients. Seventeen (47.22%) patients were HIF-1α negative, and 19 (52.78%) were positive. The difference between HIF-1α positive and negative groups regarding gender, age, tumor location, TN stage, PNI, LVI, tumor differentiation, tumor necrosis percentage, or tumor diameter (p=0.083-0.879) were not statistically significant. Moreover, SUV_{max}, SUV_{mean}, MTV (mL), and TLG were also not significantly different in the HIF-1α groups (p=0.090-0.318). Table 1 shows all the clinicopathological features and PET/CT parameters of HIF-1α groups and patients.

HIF-1α, Pathological, and PET/CT Parameters

The correlations between HIF-1α expression, pathological features, and FDG-PET parameters were evaluated by Spearman's rank test. As a result, only tumor differentiation was weakly negatively correlated with HIF-1α expression (r=-0.332, p=0.048) (Table 2). There were no statistically significant correlations between HIF-1α expression and ^{18}F-FDG/PET parameters. Tumor diameter was positively correlated with MTV (mL) and TLG as predicted from the calculation formulas of MTV (mL) and TLG ($p<0.001$). The only significant correlations were between tumor differentiation, tumor necrosis percentage, and MTV (mL) (p=0.030 and p=0.020, respectively) in the correlation tests of pathological features with ^{18}F-FDG/PET parameters (Table 3).

Discussion

Hypoxia is known as a factor that adversely affects the treatment response in solid cancers. Hypoxia is associated with poor survival in many types of cancer, such as breast, bladder, gynecological, and pancreatic

cancers (5,6,7,8,20,21). HIFS occurs as a transcriptional response to hypoxic stress. Post-hypoxia HIF-1α activation plays a vital role in CRC angiogenesis. HIF binds to the vascular endothelial growth factor (VEGF) promoter region, allowing VEGF transcription to form new blood vessels. Therefore, HIF-1α is used as a poor prognostic marker (22). The overexpression of both HIF-1α and HIF-2α is associated with a poor prognosis in colorectal cancer. In addition, a correlation was found between HIF-1α overexpression and clinicopathological features, such as stage, depth of invasion, lymph node involvement, and metastasis (23). In the present study, HIF-1α positive and negative group patients were compared for T and N stages, LVI, PNI, tumor differentiation, tumor necrosis percentage, and tumor size., However, no significant difference was found between them (p=0.879-0.083).

Clavo et al. (24) researched ^{18}F-FDG uptake status changes under different oxygen levels in various tumor cells *in vitro*. It was considered that hypoxia regulates the ^{18}F-FDG uptake according to the increased ^{18}F-FDG levels after mild hypoxic treatment (24,25). Toba et al. (26) investigated the relation of HIF-1α, GLUT-1, VEGF, and ^{18}F-FDG uptake in thymic epithelial tumors. Tumor size was the most significant parameter that correlated with SUV_{max} (r=0.60,

Table 1. The clinicopathological features and ^{18}F-FDG/PET parameters of HIF-1α negative and positive groups and all patients

	Total (n=36)	HIF-1α negative (n=17)	HIF-1α positive (n=19)	p
Gender				
Female	13 (36.1%)	8 (47.1%)	5 (26.3%)	0.172
Male	23 (63.9%)	9 (52.9%)	14 (73.7%)	
Age				
<65	22 (61.1%)	10 (58.8%)	12 (63.2%)	0.530
≥65	14 (36.8%)	7 (41.2%)	7 (36.8%)	
Tumor location				
Colon	7 (19.4%)	4 (23.5%)	3 (15.8%)	0.385
Sigmoid	4 (11.1%)	3 (17.6%)	1 (5.3%)	
Rectosigmoid	5 (13.9%)	1 (5.9%)	4 (21.1%)	
Rectum	20 (55.6%)	9 (52.9%)	11 (57.9%)	
T stage				
T1	3 (8.3%)	1 (5.9%)	2 (10.5%)	0.879
T2	4 (11.1%)	2 (11.8%)	2 (10.5%)	
T3	29 (80.6%)	14 (82.4%)	15 (78.9%)	
N stage				
N0	19 (52.8%)	10 (58.8%)	9 (47.4%)	0.683
N1	11 (30.6%)	4 (23.5%)	7 (36.8%)	
N2	6 (16.7%)	3 (17.6%)	3 (15.8%)	
PNI				
Yes	17 (47.2%)	9 (52.9%)	8 (42.1%)	0.376
No	19 (52.8%)	8 (47.1%)	11 (57.9%)	
LVI				
Yes	16 (44.4%)	7 (41.2%)	9 (47.4%)	0.485
No	20 (55.6%)	10 (58.8%)	10 (52.6%)	
Tumor differentiation				
Well-differentiated	18 (50%)	6 (35.3%)	12 (63.2%)	0.083
Moderately differentiated	15 (41.7%)	8 (47.1%)	7 (36.8%)	
Poorly differentiated	3 (8.3%)	3 (17.6%)	0	
Tumor necrosis percentage*	10% (0%-45%)	15% (0%-45%)	8% (0%-35%)	0.232
Tumor diameter (cm)*	5.5 (1-12.5)	6 (3-12.5)	5.5 (1-7)	0.193
SUV_{max}*	17.31 (7.9-36.79)	19.29 (8.07-35.09)	17.21 (7.9-36.79)	0.159
SUV_{mean}*	7.56 (4.23-13.86)	7.63 (4.23-13.86)	7.51 (4.31-12.65)	0.318
MTV (mL)*	83.5 (6.27-435.84)	119.29 (10.49-341.25)	46.59 (6.27-435.84)	0.117
TLG*	596.32 (27.03-3756.94)	1030.18 (68.01-2639.73)	363.41 (27.03-3756.94)	0.090

*The median values and minimum-maximum ranges are denoted for the numerical data. ^{18}F-FDG: ^{18}Fluorine-fluorodeoxyglucose, PET: Positron emission tomography, HIF-1α: Hypoxia-inducible factor-1α, PNI: Perineural invasion, LVI: Lymphovascular invasion, SUV_{max}: Maximum standardized uptake value, MTV: Metabolic tumor volume, TLG: Total lesion glycolysis

p<0.001), and the expression of HIF-1α showed a moderate association, but the expression of GLUT-1 showed no correlation with SUV_{max}. Moreover, Rajendran et al. (27) studied the association between hypoxia proportional to ^{18}F-fluoromisonidazole (FMISO) uptake and glycolysis evaluated by ^{18}F-FDG uptake on PET images in soft-tissue sarcomas, glioblastoma multiforme, breast cancers, and patients with head and neck cancer. When the four tumor types were analyzed separately, a correlation between ^{18}F-FDG and FMISO was significant in only head and neck tumors (27).

CRC presenting with large necrotic and hypoxic lesions tend to be resistant to chemoradiotherapy. Although CRC with HIF-1α overexpression has been indicated to have a worse prognosis (23,28,29,30), there are conflicting opinions in the literature regarding the prognostic importance of HIF-1α for CRC. In the present study, the prognostic value of HIF-1α was not investigated because the study population was heterogeneous for tumor localization (seven colon, four sigmoid colon, five rectosigmoid, and 20 rectum), which have different treatment modalities and different prognoses.

The primary aim of the present study was to evaluate the link between HIF-1α overexpression and the PET/CT parameters in CRC. No statistically significant correlation was found between HIF-1α, SUV_{max}, SUV_{mean}, MTV, or TLG. Glucose uptake, a hallmark of cancers, increases with malignancy through the up-regulation of membrane glucose transporters and improves hexokinase activity. It is usually evaluated on ^{18}F-FDG/PET by calculating SUV in the tumor. In addition, SUV_{max} is the most commonly used parameter in clinical trials.

Nevertheless, the tumor metabolic burden regarding MTV and TLG can comprehensively reflect glucose uptake within the whole tumor rather than a single-pixel value of ^{18}F-FDG activity (SUV_{max}). They were adopted as the optimal parameters for the therapeutic evaluation by PET Response Criteria in Solid Tumors (31). Also, MTV and TLG are more accurate biomarkers for T and M stage predictions than SUV_{max} (32). The significant correlation found in the present study between MTV, TLG, and tumor diameter was due to the calculation methods of MTV and TLG. Besides, the statistically significant correlations between MTV, TLG, tumor differentiation, and tumor necrosis percentage are

Table 2. Correlation results of HIF-1α overexpression and clinicopathological features of patients

	Correlation coefficient	p value
Tumor location	0.171	0.319
T stage	-0.050	0.770
N stage	0.083	0.631
PNI	-0.108	0.529
LVI	0.062	0.719
Tumor differentiation	**-0.332**	**0.048**
Tumor necrosis percentage	-0.204	0.233
Tumor diameter	-0.220	0.197

The statistically significant results are in bold. HIF-1α: Hypoxia-inducible factor-1α, PNI: Perineural invasion, LVI: Lymphovascular invasion

Table 3. Correlation results of HIF-1α, pathological findings, and TN stage with ^{18}F-FDG/PET parameters

		SUV_{max}	SUV_{mean}	MTV	TLG
HIF-1α	Correlation coefficient p value	-0.238 0.162	-0.169 0.325	-0.265 0.118	-0.287 0.090
Tumor diameter	Correlation coefficient p value	0.136 0.429	0.145 0.398	**0.672** **<0.001**	**0.616** **<0.001**
Tumor differentiation	Correlation coefficient p value	-0.126 0.465	-0.163 0.342	**0.362** **0.030**	0.281 0.097
Tumor necrosis percentage	Correlation coefficient p value	-0.152 0.376	-0.223 0.191	**0.386** **0.020**	0.300 0.076
PNI	Correlation coefficient p value	0.185 0.281	-0.040 0.816	0.032 0.852	-0.008 0.963
LVI	Correlation coefficient p value	-0.156 0.363	-0.108 0.532	0.110 0.522	0.065 0.708
T stage	Correlation coefficient p value	-0.077 0.654	-0.105 0.541	0.328 0.051	0.237 0.164
N stage	Correlation coefficient p value	-0.176 0.305	-0.115 0.506	0.052 0.763	0.003 0.988

The statistically significant results are in bold. HIF-1α: Hypoxia-inducible factor-1α, TN: Tumor-node, ^{8}F-FDG: ^{18}Fluorine-fluorodeoxyglucose, PET: Positron emission tomography, PNI: Perineural invasion, LVI: Lymphovascular invasion, MTV: Metabolic tumor volume, TLG: Total lesion glycolysis, SUV_{max}: Maximum standardized uptake value

remarkable. Poor tumor differentiation is related to a worse prognosis in CRC (33).

Study Limitations

This study has some limitations because of its retrospective design and small sample size. The sample size was limited because ^{18}F-FDG/PET is not routinely indicated in the staging of CRC. Therefore, a heterogeneous group of tumor locations was enrolled in the study to compose the sample size.

Conclusion

The prognostic significance of HIF-1α in CRC and its correlation with PET/CT parameters were controversial issues in previous studies. We found no significant relationship between HIF-1α and clinicopathological features or PET/CT parameters. However, there was a relationship between MTV, TLG, and tumor differentiation, and tumor necrosis percentage. Hence, further studies are required to predict the pathological and prognostic courses of CRC using a diagnostic ^{18}F-FDG/PET evaluation.

Ethics

Ethics Committee Approval: The study was approved by the Scientific Research Ethics Committee of the Medical Faculty of University Süleyman Demirel (protocol code, 13.02.2020/51).

Informed Consent: Informed consent was waived owing to the retrospective nature of the study.

Peer-review: Externally and internally peer-reviewed.

Authorship Contributions

Surgical and Medical Practices: S.S.Ş., N.K., M.E., İ.Z., Concept: S.S.Ş., Z.A.K., E.E., Design: S.S.Ş., Z.A.K., Data Collection or Processing: S.S.Ş., N.K., Z.A.K., M.E., Analysis or Interpretation: Z.A.K., Literature Search: Z.A.K., E.E., S.S.Ş., Writing: Z.A.K.

Conflict of Interest: No conflict of interest was declared by the authors.

Financial Disclosure: The authors declared that this study has received no financial support.

References

1. Torre LA, Bray F, Siegel RL, Ferlay J, Lortet-Tieulent J, Jemal A. Global cancer statistics, 2012. CA Cancer J Clin 2015;65:87-108.
2. Tanigawa N, Amaya H, Matsumura M, Lu C, Kitaoka A, Matsuyama K, Muraoka R. Tumor angiogenesis and mode of metastasis in patients with colorectal cancer. Cancer Res 1997;57:1043-1046.
3. Choi HJ, Hyun MS, Jung GJ, Kim SS, Hong SH. Tumor angiogenesis as a prognostic predictor in colorectal carcinoma with special reference to mode of metastasis and recurrence. Oncology 1998;55:575-581.
4. Semenza GL. Expression of hypoxia-inducible factor 1: mechanisms and consequences. Biochem Pharmacol 2000;59:47-53.
5. Sivridis E, Giatromanolaki A, Gatter KC, Harris AL, Koukourakis MI; Tumor and Angiogenesis Research Group. Association of hypoxia-inducible factors 1alpha and 2alpha with activated angiogenic pathways and prognosis in patients with endometrial carcinoma. Cancer 2002;95:1055-1063.
6. Birner P, Schindl M, Obermair A, Plank C, Breitenecker G, Oberhuber G. Overexpression of hypoxia-inducible factor 1alpha is a marker for an unfavorable prognosis in early-stage invasive cervical cancer. Cancer Res 2000;60:4693-4696.
7. Birner P, Gatterbauer B, Oberhuber G, Schindl M, Rössler K, Prodinger A, Budka H, Hainfellner JA. Expression of hypoxia-inducible factor-1 alpha in oligodendrogliomas: its impact on prognosis and on neoangiogenesis. Cancer 2001;92:165-171.
8. Giatromanolaki A, Koukourakis MI, Sivridis E, Turley H, Talks K, Pezzella F, Gatter KC, Harris AL. Relation of hypoxia inducible factor 1 alpha and 2 alpha in operable non-small cell lung cancer to angiogenic/molecular profile of tumours and survival. Br J Cancer 2001;85:881-890.
9. Bos R, van der Groep P, Greijer AE, Shvarts A, Meijer S, Pinedo HM, Semenza GL, van Diest PJ, van der Wall E. Levels of hypoxia-inducible factor-1alpha independently predict prognosis in patients with lymph node negative breast carcinoma. Cancer 2003;97:1573-1581.
10. Wang GL, Jiang BH, Rue EA, Semenza GL. Hypoxia-inducible factor 1 is a basic-helix-loop-helix-PAS heterodimer regulated by cellular O2 tension. Proc Natl Acad Sci U S A 1995;92:5510-5514.
11. Yu AY, Frid MG, Shimoda LA, Wiener CM, Stenmark K, Semenza GL. Temporal, spatial, and oxygen-regulated expression of hypoxia-inducible factor-1 in the lung. Am J Physiol 1998;275:L818-826.
12. Huang LE, Arany Z, Livingston DM, Bunn HF. Activation of hypoxia-inducible transcription factor depends primarily upon redox-sensitive stabilization of its alpha subunit. J Biol Chem 1996;271:32253-32259.
13. Yoshimura H, Dhar DK, Kohno H, Kubota H, Fujii T, Ueda S, Kinugasa S, Tachibana M, Nagasue N. Prognostic impact of hypoxia-inducible factors 1alpha and 2alpha in colorectal cancer patients: correlation with tumor angiogenesis and cyclooxygenase-2 expression. Clin Cancer Res 2004;10:8554-8560.
14. Czernin J, Phelps ME. Positron emission tomography scanning: current and future applications. Annu Rev Med 2002;53:89-112.
15. Burger IA, Huser DM, Burger C, von Schulthess GK, Buck A. Repeatability of FDG quantification in tumor imaging: averaged SUVs are superior to SUVmax. Nucl Med Biol 2012;39:666-670.
16. Lodge MA, Chaudhry MA, Wahl RL. Noise considerations for PET quantification using maximum and peak standardized value. J Nucl Med 2012;53:1041-1047.
17. Keramida G, Peters AM. Scaling of Glomerular Filtration Rate and SUV for Body Size: The Curious Conflict of Whole-Body Metric Preferences. J Nucl Med 2016;57:2028.
18. Erselcan T, Turgut B, Dogan D, Ozdemir S. Lean body mass-based standardized uptake value, derived from a predictive equation, might be misleading in PET studies. Eur J Nucl Med Mol Imaging 2002;29:1630-1638.
19. Dales JP, Garcia S, Meunier-Carpentier S, Andrac-Meyer L, Haddad O, Lavaut MN, Allasia C, Bonnier P, Charpin C. Overexpression of hypoxia-inducible factor HIF-1alpha predicts early relapse in breast cancer: retrospective study in a series of 745 patients. Int J Cancer 2005;116:734-739.
20. Shibaji T, Nagao M, Ikeda N, Kanehiro H, Hisanaga M, Ko S, Fukumoto A, Nakajima Y. Prognostic significance of HIF-1 alpha overexpression in human pancreatic cancer. Anticancer Res 2003;23:4721-4727.
21. Theodoropoulos VE, Lazaris ACh, Sofras F, Gerzelis I, Tsoukala V, Ghikonti I, Manikas K, Kastriotis I. Hypoxia-inducible factor 1 alpha expression

correlates with angiogenesis and unfavorable prognosis in bladder cancer. Eur Urol 2004;46:200-208.

22. Sutter CH, Laughner E, Semenza GL. Hypoxia-inducible factor 1alpha protein expression is controlled by oxygen-regulated ubiquitination that is disrupted by deletions and missense mutations. Proc Natl Acad Sci U S A 2000;97:4748-4753.
23. Chen Z, He X, Xia W, Huang Q, Zhang Z, Ye J, Ni C, Wu P, Wu D, Xu J, Qiu F, Huang J. Prognostic value and clinicopathological differences of HIFs in colorectal cancer: evidence from meta-analysis. PLoS One 2013;8:e80337.
24. Clavo AC, Brown RS and Wahl RL. Fluorodeoxyglucose uptake in human cancer cell lines is increased by hypoxia. J Nucl Med 1995;36:1625-1632.
25. Higashi K, Clavo AC and Wahl RL. Does FDG uptake measure proliferative activity of human cancer cells? In vitro comparison with DNA flow cytometry and tritiated thymidine uptake. J Nucl Med 1993;34:414-419.
26. Toba H, Kondo K, Sadohara Y, Otsuka H, Morimoto M, Kajiura K, Nakagawa Y, Yoshida M, Kawakami Y, Takizawa H, Kenzaki K, Sakiyama S, Bando Y, Tangoku A. 18F-fluorodeoxyglucose positron emission tomography/computed tomography and the relationship between fluoro-deoxyglucose uptake and the expression of hypoxia-inducible factor-1α, glucose transporter-1 and vascular endothelial growth factor in thymic epithelial tumours. Eur J Cardiothorac Surg 2013;44:105-112.
27. Rajendran JG, Mankoff DA, O'Sullivan F, Peterson LM, Schwartz DL, Conrad EU, Spence AM, Muzi M, Farwell DG, Krohn KA. Hypoxia and glucose metabolism in malignant tumors: evaluation by [18F] fluoromisonidazole and [18F] fluorodeoxyglucose positron emission tomography imaging. Clin Cancer Res 2004;10:2245-2252.
28. Baba Y, Nosho K, Shima K, Irahara N, Chan AT, Meyerhardt JA, Chung DC, Giovannucci EL, Fuchs CS, Ogino S. HIF1A overexpression is associated with poor prognosis in a cohort of 731 colorectal cancers. Am J Pathol 2010;176:2292-2301.
29. Ioannou M, Paraskeva E, Baxevanidou K, Simos G, Papamichali R, Papacharalambous C, Samara M, Koukoulis G. HIF-1α in colorectal carcinoma: review of the literature. J BUON 2015;20:680-689.
30. Lee-Kong SA, Ruby JA, Chessin DB, Pucciarelli S, Shia J, Riedel ER, Nitti D, Guillem JG. Hypoxia-related pro-teins in patients with rectal cancer undergoing neoadjuvant combined modalitytherapy. Dis Colon Rectum 2012;55:990-995.
31. Joo Hyun O, Lodge MA, Wahl RL. Practical PERCIST: a simplified guide to PET response criteria in solid tumors 1.0. Radiology 2016;280:576-584.
32. Suzuki Y, Okabayashi K, Hasegawa H, Tsuruta M, Shigeta K, Murakami K, Kitagawa Y. Metabolic Tumor Volume and Total Lesion Glycolysis in PET/CT Correlate With the Pathological Findings of Colorectal Cancer and Allow Its Accurate Staging. Clin Nucl Med 2016;41:761-765.
33. Purdie CA, Piris J. Histopathological grade, mucinous differentiation and DNA ploidy in relation to prognosis in colorectal carcinoma. Histopathology 2000;36:121-126.

Original Article
Mol Imaging Radionucl Ther 2021;30:101-106 DOI:10.4274/mirt.galenos.2021.20633

Contribution of ^{18}F-FDG PET/CT in the Differential Diagnosis of Pulmonary Hamartomas and Pulmonary Carcinoids

^{18}F-FDG PET/BT'nin Pulmoner Hamartomların ve Pulmoner Karsinoidlerin Ayırıcı Tanısına Katkısı

Ebru Tatcı[1], Özlem Özmen[1], Ayperi Öztürk[2], Funda Demirağ[3]

[1]University of Health Sciences Turkey, Atatürk Chest Diseases and Thoracic Surgery Training and Research Hospital, Clinic of Nuclear Medicine, Ankara, Turkey
[2]University of Health Sciences Turkey, Atatürk Chest Diseases and Thoracic Surgery Training and Research Hospital, Clinic of Interventional Pulmonology, Ankara, Turkey
[3]University of Health Sciences Turkey, Atatürk Chest Diseases and Thoracic Surgery Training and Research Hospital, Clinic of Pathology, Ankara, Turkey

Abstract

Objectives: This study aimed to evaluate ^{18}fluorine-fluorodeoxyglucose (^{18}F-FDG) positron emission tomography/computed tomography (PET/CT) findings in the differential diagnosis of pulmonary carcinoids and pulmonary hamartomas.

Methods: ^{18}F-FDG PET/CT findings of 34 patients with pulmonary carcinoids (12 atypical, 22 typical) and 32 patients with pulmonary hamartomas were retrospectively evaluated. Both mean diameter and mean maximum standardized uptake value (SUV_{max}) of hamartomas and carcinoids were compared by Mann-Whitney U and Kruskall-Wallis H tests.

Results: The mean longest diameter of atypical carcinoids (3.5±1.7 cm) was higher than that of hamartomas (2.1±1 cm) (p=0.038). No significant difference was found between the mean diameter of typical carcinoids and mean diameter of hamartomas (p=0.128). The mean SUV_{max} of atypical carcinoids (5.97±3.7) and typical carcinoids (4.22±1.7) were higher than those of hamartomas (1.65±0.9) (p=0.002 and p=0.003, respectively). There were collapse/consolidation in 55.8%, bronchiectasis or mucoid impaction in 47%, and air trapping in 14.7% in the peripheral parenchyma of the 34 carcinoids. Collapse/consolidation was detected in a patient with endobronchial hamartoma, and other finding was not found in the parenchyma around hamartomas.

Conclusion: The ^{18}F-FDG uptake of pulmonary carcinoids can vary from minimal to intense. ^{18}F-FDG uptake can be seen in pulmonary hamartomas. However, the mean SUV_{max} of atypical carcinoids and typical carcinoids were higher compared to hamartomas. Pulmonary carcinoid must be suspected in cases with accompanying bronchial obstruction findings in the periphery of the mass.

Keywords: Pulmonary hamartoma, pulmonary carcinoid tumor, atypical pulmonary carcinoid tumor, ^{18}F-FDG PET/CT

Address for Correspondence: Ebru Tatcı MD, University of Health Sciences Turkey, Atatürk Chest Diseases and Thoracic Surgery Training and Research Hospital, Clinic of Nuclear Medicine, Ankara, Turkey
Phone: +90 505 914 53 61 **E-mail:** ebrualkandr@yahoo.com ORCID ID: orcid.org/0000-0002-9216-658X
Received: 24.09.2020 **Accepted:** 12.01.2021

Öz

Amaç: Bu çalışmanın amacı pulmoner karsinoid tümörlerin ve pulmoner hamartomların ayırıcı tanısında ^{18}flor-florodeoksiglukoz (^{18}F-FDG) pozitron emisyon tomografi/bilgisayarlı tomografinin (PET/BT) bulgularını değerlendirmektir.

Yöntem: Pulmoner karsinoidli 34 hastanın (12 atipik, 22 tipik) ve pulmoner hamartomlu 32 hastanın ^{18}F-FDG PET/BT bulguları geriye dönük olarak değerlendirildi. Hamartomların ve karsinoidlerin hem ortalama çapı hem de ortalama maksimum standardize uptake değeri (SUV_{maks}) değeri Mann-Whitney U ve Kruskall-Wallis H testleri ile karşılaştırıldı.

Bulgular: Atipik karsinoid tümörlerin ortalama en uzun çapı (3,5±1,7 cm), hamartomlardan (2,1±1 cm) daha fazlaydı (p=0,038). Tipik karsinoid tümörün ortalama çapı (2,7±1,7 cm) ile hamartomların ortalama çapları arasında anlamlı bir fark yoktu (p=0,128). Atipik karsinoidlerin (5,97±3,7) ve tipik karsinoidlerin (4,22±1,7) ortalama SUV_{maks} değerleri hamartomlara (1,65±0,9) göre daha yüksekti (sırasıyla; p=0,002 ve p=0,003). Otuz dört karsinoidin periferik parankiminde %55.8'inde kollaps konsolidasyon, %47'sinde bronşektazi veya mukoid impaksiyon ve %14.7'sinde hava hapsi vardı. Endobronşiyal hamartomlu bir hastada kollaps konsolidasyon tespit edildi. Bunun dışında hamartomların etrafındaki parankimde ek bulguya rastlanmadı.

Sonuç: Pulmoner karsinoidlerde ^{18}F-FDG tutulumu minimalden yoğuna kadar değişebilir. Ayrıca pulmoner hamartomlarda ^{18}F-FDG tutulumu görülebilir. Ancak, çalışmamıza göre atipik karsinoidlerin ve tipik karsinoidlerin ortalama SUV_{maks}'ı hamartomlara göre daha yüksekti. Ayrıca kitle çevresinde bronşiyal obstrüksiyon bulgularının eşlik etmesi durumunda pulmoner karsinoidden şüphelenilmelidir.

Anahtar kelimeler: Pulmoner hamartom, pulmoner karsinoid tümör, atipik pulmoner karsinoid tümör, ^{18}F-FDG PET/BT

Introduction

Hamartoma is a benign neoplasm consisting of an abnormal mixture of cells and tissues of the organ from which it originates and may contain cartilage, muscle, fat, connective tissue, and respiratory epithelium. Pulmonary hamartoma is the most common benign tumor of the lung in adults. They constitute 77% of benign lung lesions (1,2).

Pulmonary carcinoids are well-differentiated neuroendocrine carcinomas, originating from neuroendocrine cells called Kulchitzky, located in the bronchial or bronchiolar epithelium, comprising 1%-2% of all primary lung cancers (3,4). Pulmonary carcinoids and pulmonary hamartomas are often observed as well-circumscribed, lobulated, rounder oval lesions on computed tomography (CT) (1,5). ^{18}Fluorine-fluorodeoxyglucose (^{18}F-FDG) positron emission tomography (PET)/CT is a widely used method for the evaluation of suspected malignant lung nodules. It prevents unnecessary invasive procedures and enables detection of malignancy at an early stage (6). However, pulmonary carcinoids may not show significant ^{18}F-FDG uptake (7). In addition, false-positive ^{18}F-FDG uptake can be observed in infective and inflammatory processes (8). This retrospective study aimed to investigate the contribution of ^{18}F-FDG PET/CT findings in the differential diagnosis of pulmonary carcinoids and pulmonary hamartomas; thus, both CT and ^{18}F-FDG PET findings of these lesions were evaluated.

Materials and Methods

Medical records of patients who underwent ^{18}F-FDG PET/CT to evaluate pulmonary nodules, which were detected on CT between 2009 and 2019 at our hospital, were retrospectively reviewed. Patients with pulmonary carcinoid or pulmonary hamartoma, which was pathologically confirmed by biopsy or surgical resection, were included in the study. The exclusion criteria of the patients were as follows: (1) Nodule with diameter <10 mm and (2) presence of significant respiratory motion artifacts that affected the assessment of lesion on PET/CT. Thus, a total of 34 patients with pulmonary carcinoids (12 atypical, 22 typical) and a total of 32 patients with pulmonary hamartomas were included in this study. Age, sex, lesion location within the lung parenchyma, type of operation, and PET/CT findings were recorded.

PET/CT (Biograph LSO HI-REZ PET/CT; Siemens, Medical Solutions, Knoxville, TN) was performed within 45-60 min after intravenous injection of 0.15 mCi/kg ^{18}F-FDG. Blood glucose was confirmed to be <200 mg/dL before the injection of ^{18}F-FDG. Patients fasted for at least 6 h prior to the ^{18}F-FDG injection. After taking CT images from the vertex of the skull to the proximal femur, PET was performed in 6-8 bed positions (3 min per bed). CT data were used for attenuation correction. After the reconstruction of raw data with ordered subset expectation maximization algorithms, images were evaluated in axial, coronal, and sagittal formats. The maximum standardized uptake value (SUV_{max}), longest diameter values, and presence of intralesional calcification and fat were noted. In addition, accompanying findings in the peripheral parenchyma of the lesion, such as air trapping, bronchiectasis, mucoid impaction of the bronchi, and collapse/consolidation, were assessed. Density found similar to subcutaneous fatty tissue in the lesion was considered fat density. The SUV_{max} of the lesions were calculated automatically by drawing the relevant area around the lesions.

This study was approved by the Local Ethics Committee of University of Health Sciences Turkey, Ataturk Chest Diseases and Thoracic Surgery Training and Research Hospital (date: 16.07.2020, protocol number: 682).

Statistical Analysis

Data collected in this study were analyzed by the SPSS 21 statistical package software. As data were not normally distributed, the Mann-Whitney U test was used in two-group comparisons, and the Bonferroni-corrected Kruskall-Wallis H test was used in three-group comparisons. The Mann-Whitney U test was used for post-hoc comparisons. Significant difference was set at p value <0.05.

Results

A total of the 66 (42 male, 24 female) patients were included in the study. Of these patients, 34 had carcinoids and 32 had hamartomas. There were 12 atypical and 22 typical carcinoids. Clinicopathological features of the patients are given in Table 1.

The mean diameters of lesions and SUV_{max} value are shown in Table 2. The mean longest diameter of atypical carcinoids (3.5±1.7 cm) was higher than that of hamartomas (2.1±1 cm) (p=0.038). No significant difference was found between the mean diameter of typical carcinoids (2.7±1.7 cm) and the mean diameter of atypical carcinoids (p=0.325). In addition, no significant difference was noted between the mean diameter of typical carcinoids and the mean diameter of hamartomas (p=0.128).

The mean SUV_{max} was 4.22±1.7 (range, 1.2±7.1) in typical carcinoids, 5.97±3.7 (range, 2-13.25) in atypical carcinoids, and 1.65±0.9 (range, 0-3.3) in hamartomas. The SUV_{max} of hamartomas was substantially low in comparison with typical and atypical carcinoids (p=0.003 and p=0.002, respectively). No significant difference between SUV_{max} of typical and atypical carcinoids was determined (p=0.325).

The CT features of ^{18}F-FDG PET/CT images of lesions are shown in Table 3. Collapse/consolidation (n=19), bronchiectasis and/or mucoid impaction (n=16), and air trapping (n=5) were seen in the peripheral pulmonary parenchyma of 34 carcinoids (Figure 1). Pleural effusion on the side of the lesion was detected in two patients. Peripheral pulmonary collapse/consolidation was found in one patient with endobronchial hamartoma, and no other finding was found in the parenchyma around hamartomas.

Intralesional calcification was found in 52.9% of 34 carcinoids. Calcification was detected in 46.8% of 32 hamartomas (Figure 2). Intralesional fat density was observed in 4 of 32 (12.5%) patients with hamartoma (Figure 3).

Table 1. Clinicopathological features

Histopathologic diagnosis	Carcinoids	Hamartomas
n	34	32
Sex (male/female)	11/23	13/19
Age, y (mean ± SD)	49±15.2	54.4±10.4
Location (central/peripheral) (n)	22/12	3/29
Location (right/lung) (n)	21/13	19/13
Type of biopsy or surgery		
Lobectomy or bilobectomy	24	1
Pneumonectomy	1	
Wedge resection or excision	8	18
TTNA or truncate biopsy		13
Bronchoscopic biopsy	1	

TTNA: Transthoracic needle aspiration SD: Standard deviation

Discussion

A meta-analysis revealed that ^{18}F-FDG PET/CT has high sensitivity (81.9%) but lower specificity (62.4%) in distinguishing benign from malign pulmonary nodules. The presence of ^{18}F-FDG uptake in inflammatory or infective diseases, other than malignant diseases, reduces the specificity of PET/CT (8). Low ^{18}F-FDG uptake can be observed in pulmonary hamartomas (Figure 2) (9,10). Ergonul et al. (9) reported ^{18}F-FDG PET/CT findings of 106 patients with benign lung lesions. Of 106 patients, 19 had hamartomas. The SUV_{max} of 19 hamartomas ranged from 0 to 4.5 (9). Jiang et al. (10) reported the ^{18}F-FDG PET/CT findings of 14 pulmonary hamartomas with a mean diameter of 1.7±0.8 cm (range, 0.7-3.1 cm), and the mean SUV_{max} of lesions was 1.5±0.6 (range, 0.7-2.6)

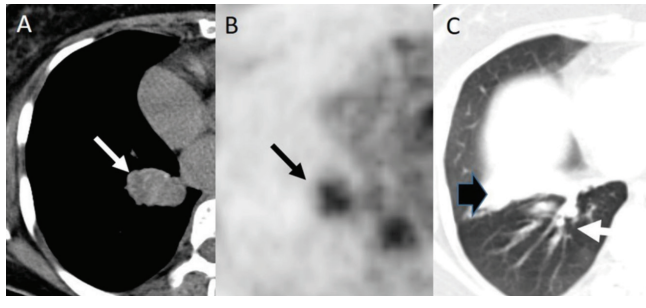

Figure 1. Atypical carcinoid. Axial CT (A) and PET (B) images of the PET/CT scan showing high ^{18}F-FDG uptake on a lobulated mass with eccentric calcifications (thin arrows). Adjacent atelectasis (black thick arrow) and air trapping (white thick arrow) are detected. The maximum standardized uptake value of carcinoid was 4.16

CT: Computed tomography, PET: Positron emission tomography, ^{18}F-FDG: ^{18}F-fluorodeoxyglucose

Table 2. SUV_{max} and diameter differences between atypical carcinoids, typical carcinoids, and hamartomas							
Diagnosis	**AC**	**TC**	**Hamartoma**	**p value$^{\mu}$**	**p value***	**p value"**	**p value$^{\pm}$**
n	12	22	32	-	-	-	-
Mean diameter ± SD range, (cm)	3.5±1.7 (1.2-7)	2.7±1.7 (0.7-8)	2.1±1 (0.7-5.5)	0.035	0.325	0.128	0.038
Mean SUV_{max} ± SD range	5.97±3.7 (2-13.2)	4.22±1.7 (1.2-7.1)	1.65±0.9 (0-3.3)	0.0001	0.325	0.003	0.002

$^{\mu}$p value for comparison among three groups (Kruskal-Wallis test), *p value for comparison between AC and TC, "p value for comparison between hamartoma and typical carcinoids, $^{\pm}$p value for comparison between hamartoma and AC. SUV_{max}: Maximum standardized uptake value, AC: Atypical carcinoid, TC: Typical carcinoid, SD: Standard deviation

Table 3. CT findings of ^{18}F-FDG PET/CT images of patients with pulmonary carcinoids and hamartomas		
Histopathologic diagnosis	**Carcinoids**	**Hamartomas**
n	34	32
Intralesional calcification (n)	18	15
Intralesional fat (n)	0	4
Bronchiectasis or mucoid impaction (n)	16	0
Collapse/consolidation (n)	19	1
Air trapping (n)	5	0
Pleural effusion (n)	2	0

PET/CT: Positron emission tomography/computed tomography, ^{18}F-FDG: ^{18}F-fluorodeoxyglucose

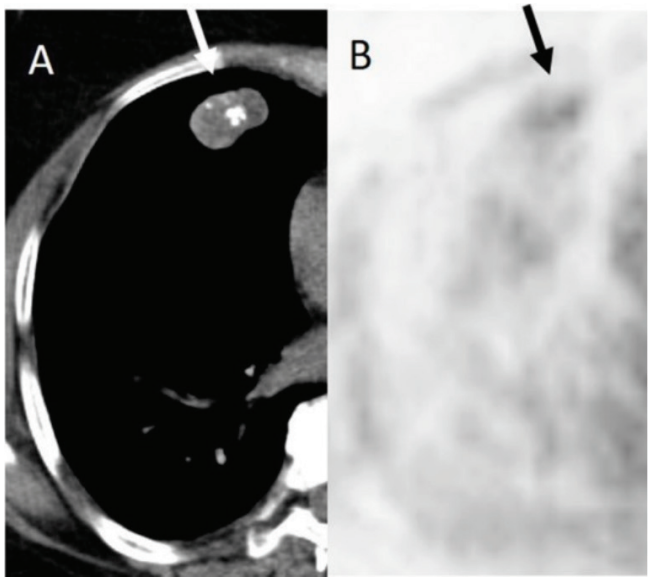

Figure 2. Pulmonary hamartoma. Axial CT (A) and PET (B) images of the PET/CT scan show low ^{18}F-FDG uptake on a nodule with popcorn calcifications (arrows). The maximum standardized uptake value was 2.34

CT: Computed tomography, PET: Positron emission tomography, ^{18}F-FDG: ^{18}F-fluorodeoxyglucose

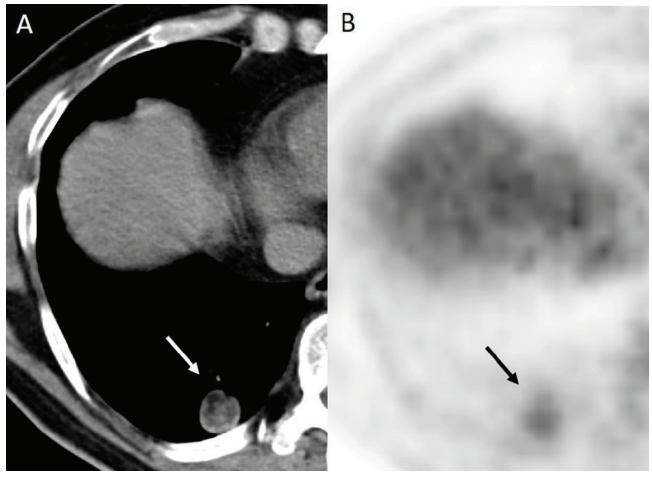

Figure 3. Pulmonary hamartoma. Axial CT (A) and PET (B) images of the PET/CT scan show low ^{18}F-FDG uptake on the slightly lobulated, well-defined, fat-containing nodule (arrows). The maximum standardized uptake value of carcinoid was 2.33

CT: Computed tomography, PET: Positron emission tomography, ^{18}F-FDG: ^{18}F-fluorodeoxyglucose

(10). Similarly, in the present study, the mean SUV_{max} was 1.65±0.9 (range, 0-3.38).

Although the sensitivity of ^{18}F-FDG PET/CT is high, false-negative ^{18}F-FDG results can occur in the determination of malignity. In malignant tumors with low glucose metabolic activity such as carcinoid, solid adenocarcinoma, minimally invasive carcinoma, and atypical adenomatous hyperplasia, a lack of ^{18}F-FDG uptake can be seen on PET images (8). ^{18}F-FDG PET/CT is the first choice in the evaluation of indeterminate pulmonary nodules. However, at present, Gallium-68 (^{68}Ga)- 1,4,7,10-tetraazacyclododecane-1,4,7,10-tetraacetic acid (DOTA)-conjugated peptides that show affinity for somatostatin receptors are used in the imaging of carcinoids through PET/CT (11). While the sensitivity of ^{68}Ga-DOTA-conjugated peptides in detecting pulmonary carcinoids ranged from 79% to 100%, the sensitivity of ^{18}F-FDG PET/CT in identifying pulmonary

carcinoids ranged from 52% to 100% (12). In our retrospective study in 2014, we evaluated ^{18}F-FDG PET/CT findings of 22 patients with pulmonary carcinoids (14 typical, 8 atypical). In that study, the sensitivity of ^{18}F-FDG PET/CT was 81.8% in detecting pulmonary carcinoids (13).

In the present study, the mean SUV_{max} was 4.22 for typical carcinoids and 5.97 for atypical carcinoids (Figure 1). No significant difference was found in the SUV_{max} between typical and atypical carcinoids (p=0.325). The mean SUV_{max} was significantly lower in hamartoma than in typical and atypical carcinoids (p=0.003 and p=0.002, respectively). Uhlén et al. (14) compared the ^{18}F-FDG PET/CT findings of 36 patients with pulmonary carcinoid and 51 patients with pulmonary hamartoma. They found that the SUV_{max} was lower in hamartomas (mean, 1.4) than in carcinoids (mean, 3.9) ($p \leq 0.00001$).

While approximately 80% of pulmonary carcinoids are located in central airways, 90% of pulmonary hamartomas are located peripherally (5,15). The central carcinoids may occur with associated pneumonia, atelectasis, air trapping, mucoid impaction, and bronchiectasis (5). In the present study, 64.7% of carcinoids were centrally located. Distal collapse/consolidation was detected in 55.8% of 34 carcinoids, mucoid impaction or bronchiectasis in 47%, and air trapping in 14.7%. Calcification was found in the 57.7% of 34 carcinoids. Moreover, 90.6% of the hamartomas were located peripherally. Accompanying collapse/consolidation was found in a patient with endobronchial located hamartoma, and no other finding was seen for hamartomas in the peripheral parenchyma.

Diffuse, punctate, or eccentric calcification can be observed in 30% of carcinoids on CT images (16). Moreover, 25%-30% of benign pulmonary hamartomas exhibit calcification/ossification. Especially, the presence of calcification in the form of popcorn or comma suggests hamartoma (1). We found intralesional calcification in 52.9% of the 34 carcinoids and also in 46.8 % of 32 hamartomas. Pulmonary hamartoma and carcinoid may have similar morphologic features on CT. Especially, peripheral carcinoids are generally asymptomatic and found incidentally. Peripheral carcinoids are slow-growing tumors. It may be difficult to distinguish peripheral carcinoids from benign pulmonary nodules. Thin-slice CT images can show the relationship between small airways and carcinoid nodules (16).

Study Limitations

This study has some limitations. In a previous study, intralesional fat was seen in approximately 60% of hamartomas (1). Approximately -40 to -120 Hounsfield units (HU) are compatible with intralesional fat density and are typical for hamartoma on thin-slice CT images (17). However, in the present study, fat density was found in 13.3% of 32 hamartomas. In addition, PET/CT images were taken while the patient was breathing freely. Respiratory motion during scanning causes artifacts in PET/CT images, particularly in cases of small nodules. Thus, we prefer to evaluate the presence of intranodular fat visually, instead of measuring the HU value. The rate of intrapulmonary fat content may be incorrectly low in our study. The contour, density, and size of pulmonary nodules, presence of intralesional calcification, and indirect findings of airway involvement, especially in peripheral and small nodules, can be evaluated more effectively by thin-slice CT (18).

Conclusion

The ^{18}F-FDG uptake in pulmonary carcinoids is higher than hamartomas. However, ^{18}F-FDG uptake can be seen in hamartomas. In the presence of calcifying central pulmonary lesions that are well circumscribed or lobulated, showing marked FDG uptake and bronchial obstruction findings in the peripheral parenchyma, carcinoids should be considered in the diagnosis. Differential diagnosis of peripheral carcinoids, particularly small ones, without a finding of bronchial obstruction in the adjacent parenchyma, is only possible by histopathological methods.

Ethics

Ethics Committee Approval: This study was approved by the Local Ethics Committee of University of Health Sciences Turkey, Atatürk Chest Diseases and Thoracic Surgery Training and Research Hospital (date: 16.07.2020, protocol number: 682).

Informed Consent: Informed consent was not required for such a retrospective study.

Peer-review: Externally peer-reviewed.

Authorship Contributions

Surgical and Medical Practices: A.Ö., Concept: E.T., Design: F.D., Data Collection or Processing: Ö.Ö., Literature Search: E.T., Writing: E.T.

Conflict of Interest: No conflict of interest was declared by the authors.

Financial Disclosure: The authors declared that this study has received no financial support.

References

1. Lundeen KS, Raj MS, Rajasurya V, Ludhwani D. Pulmonary Hamartoma. [Updated 2020 Jul 10]. In: StatPearls [Internet]. Treasure Island (FL): StatPearls Publishing; 2021.

2. Ahmed S, Arshad A, Mador MJ. Endobronchial hamartoma; a rare structural cause of chronic cough. Respir Med Case Rep 2017;22:224-227.
3. Rekhtman N. Neuroendocrine tumors of the lung: an update. Arch Pathol Lab Med 2010;134:1628-1638.
4. Li X, Hou Y, Shi T, He Y, Ren D, Song Z, Wei S, Chen G, Chen J, Xu S. Clinicopathological characteristics and genetic analysis of pulmonary carcinoid tumors: A single-center retrospective cohort study and literature review. Oncol Lett 2020;19:2446-2456.
5. Chong S, Lee KS, Chung MJ, Han J, Kwon OJ, Kim TS. Neuroendocrine tumors of the lung: clinical, pathologic, and imaging findings. Radiographics 2006;26:41-57; discussion 57-58.
6. Mosmann MP, Borba MA, de Macedo FP, Liguori Ade A, Villarim Neto A, de Lima KC. Solitary pulmonary nodule and (18)F-FDG PET/CT. Part 1: epidemiology, morphological evaluation and cancer probability. Radiol Bras 2016;49:35-42.
7. Liu Y. Lung Neoplasms with Low F18-Fluorodeoxyglucose Avidity. PET Clin 2018;13:11-18.
8. Divisi D, Barone M, Bertolaccini L, Zaccagna G, Gabriele F, Crisci R. Diagnostic performance of fluorine-18 fluorodeoxyglucose positron emission tomography in the management of solitary pulmonary nodule: a meta-analysis. J Thorac Dis 2018;10(Suppl 7):S779-S789.
9. Ergonul AG, Akcam TI, Özdil A, Turhan K, Cakan A, Cagirici U. Diagnostic value of 18F-FDG-PET/CT in benign lung diseases. Kardiochir Torakochirurgia Pol 2018;15:1-4.
10. Jiang L, Huang Y, Tang Q, Zhao Q, Li Y, Wu X, Wang H. 18F-FDG PET/CT characteristics of pulmonary sclerosing hemangioma vs. pulmonary hamartoma. Oncol Lett 2018;16:660-665.
11. Virgolini I, Ambrosini V, Bomanji JB, Baum RP, Fanti S, Gabriel M, Papathanasiou ND, Pepe G, Oyen W, De Cristoforo C, Chiti A. Procedure guidelines for PET/CT tumour imaging with 68Ga-DOTA-conjugated peptides: 68Ga-DOTA-TOC, 68Ga-DOTA-NOC, 68Ga-DOTA-TATE. Eur J Nucl Med Mol Imaging 2010;37:2004-2010.
12. Jiang Y, Hou G, Cheng W. The utility of 18F-FDG and 68Ga-DOTA-Peptide PET/CT in the evaluation of primary pulmonary carcinoid: A systematic review and meta-analysis. Medicine (Baltimore) 2019;98:e14769.
13. Tatci E, Ozmen O, Gokcek A, Biner IU, Ozaydin E, Kaya S, Arslan N. 18F-FDG PET/CT rarely provides additional information other than primary tumor detection in patients with pulmonary carcinoid tumors. Ann Thorac Med 2014;9:227-231.
14. Uhlén N, Grundberg O, Jacobsson H, Sundin A, Dobra K, Sánchez-Crespo A, Axelsson R, Kölbeck KG. 18F-FDG PET/CT Diagnosis of Bronchopulmonary Carcinoids Versus Pulmonary Hamartomas. Clin Nucl Med 2016;41:263-267.
15. Sodhi KS, Virmani V, Jindal SK, Khandelwal N. Pulmonary hamartoma. Ann Acad Med Singap 2009;38:1110.
16. Jeung MY, Gasser B, Gangi A, Charneau D, Ducroq X, Kessler R, Quoix E, Roy C. Bronchial carcinoid tumors of the thorax: spectrum of radiologic findings. Radiographics 2002;22:351-365.
17. Siegelman SS, Khouri NF, Scott WW Jr, Leo FP, Hamper UM, Fishman EK, Zerhouni EA. Pulmonary hamartoma: CT findings. Radiology 1986;160:313-317.
18. Meisinger QC, Klein JS, Butnor KJ, Gentchos G, Leavitt BJ. CT features of peripheral pulmonary carcinoid tumors. AJR Am J Roentgenol 2011;197:1073-1080.

Interesting Image
Mol Imaging Radionucl Ther 2021;30:107-109 DOI:10.4274/mirt.galenos.2020.69783

Peptide Receptor Radionuclide Therapy with ^{177}Lu-DOTATATE in a Case of Concurrent Neuroendocrine Tumors and Meningioma: Achieving Two Things in a Single Action

Eşzamanlı Nöroendokrin Tümör ve Menenjiyom Olgusunda ^{177}Lu-DOTATATE ile Peptid Reseptör Radyonüklid Tedavisi: Tek Bir Uygulama ile İki Hastalığın Tedavisi

Majid Assadi[1], Seyed Javad Rekabpour[2], Abdullatif Amini[3], Habibollah Dadgar[4], Reza Nemati[5], Ali Gholamrezanezhad[6], Iraj Nabipour[7], Esmail Jafari[1], Hojjat Ahmadzadehfar[8]

[1]*Bushehr University of Medical Sciences, Bushehr Medical University Hospital, The Persian Gulf Nuclear Medicine Research Center, Department of Molecular Imaging and Radionuclide Therapy, Bushehr, Iran*
[2]*Bushehr University of Medical Sciences, Bushehr Medical University Hospital, Department of Oncology, Bushehr, Iran*
[3]*Bushehr University of Medical Sciences, Bushehr Medical Heart Center, Department of Cardiology, Bushehr, Iran*
[4]*Cancer Research Center, RAZAVI Hospital, Imam Reza International University, Mashhad, Iran*
[5]*Bushehr University of Medical Sciences, Bushehr Medical University Hospital, Department of Neurology, Bushehr, Iran*
[6]*University of Southern California, Keck School of Medicine, Department of Radiology, Los Angeles, USA*
[7]*Bushehr University of Medical Sciences, Bushehr Medical University Hospital, Department of Internal Medicine, Division of Endocrinology, Bushehr, Iran*
[8]*Klinikum Westfalen, Department of Nuclear Medicine, Dortmund, Germany*

Abstract

We present a partial response of peptide receptor radionuclide therapy (PRRT) with ^{177}Lu-DOTATATE in a case of concurrent neuroendocrine tumors (NETs) and meningioma. In addition to the valuable role of PRRT in inoperable NETs, it has been demonstrated that this treatment can be a promising therapy for progressive meningioma, especially in patients with low grade and refractory to standard regime.

Keywords: ^{68}Ga-DOTATATE PET/MRI, PRRT, neuroendocrine tumor, ^{18}F-FDG-PET/CT

Öz

Bu olgu sunumunda eşzamanlı nöroendokrin tümör (NET) ve menenjiyom tanılı bir olgunun ^{177}Lu-DOTATATE ile peptid reseptör radyonüklid tedavisine (PRRT) kısmi yanıtı sunulmaktadır. İnoperabl NET'lerde PRRT'nin önemli rolüne ek olarak, bu tedavinin özellikle düşük dereceli ve standart rejime dirençli hastalarda ilerleyici menenjiyom için umut verici bir tedavi olabileceği gösterilmiştir.

Anahtar kelimeler: ^{68}Ga-DOTATATE PET/MRG, PRRT, nöroendokrin tümör, ^{18}F-FDG-PET/BT

Address for Correspondence: Majid Assadi MD, Bushehr University of Medical Sciences, Bushehr Medical University Hospital, The Persian Gulf Nuclear Medicine Research Center, Department of Molecular Imaging and Radionuclide Therapy, Bushehr, Iran
Phone: +0098-771-2580169 **E-mail:** assadipoya@yahoo.com ORCID ID: orcid.org/0000-0002-2166-3765
Received: 10.08.2019 **Accepted:** 14.04.2020

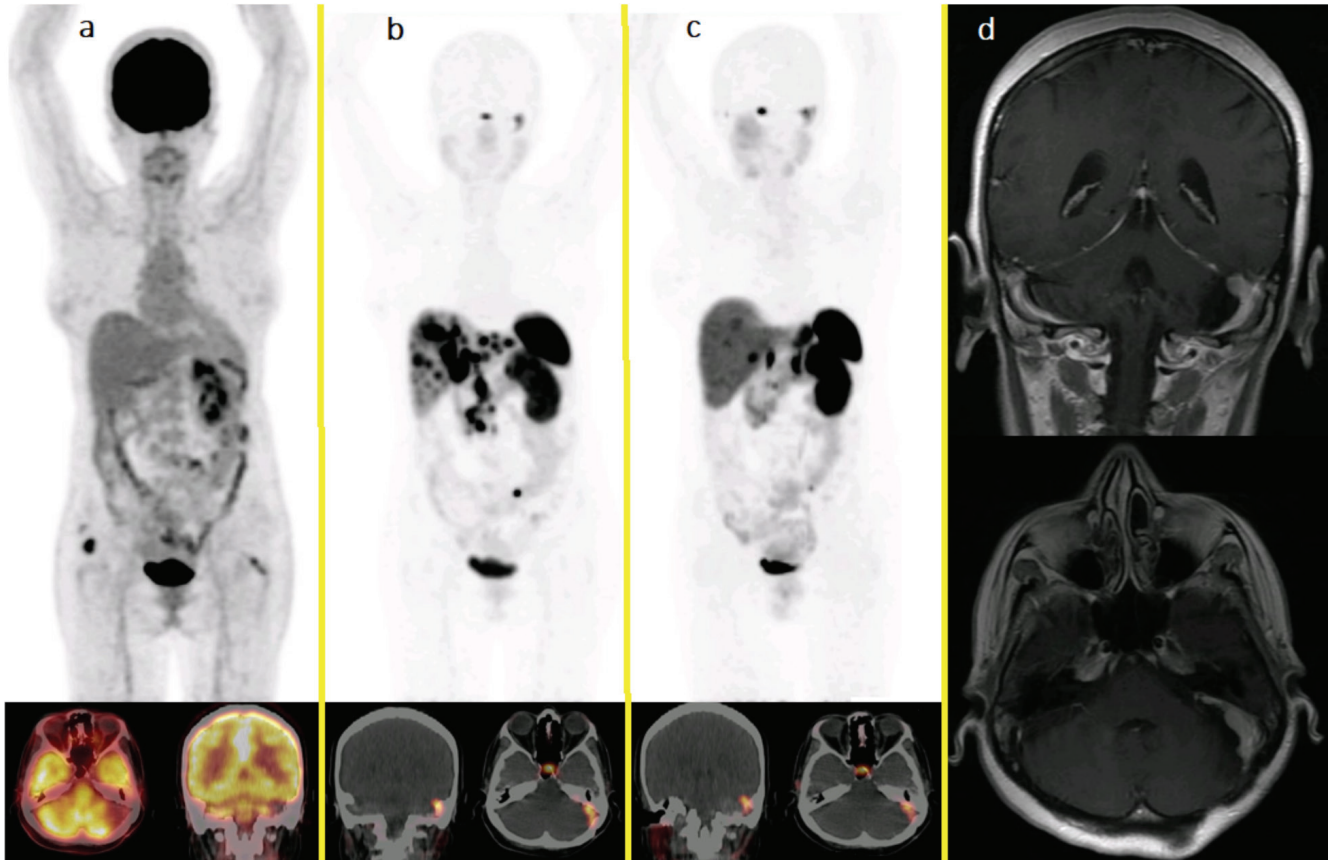

Figure 1. A 50-year-old female patient diagnosed as a case of metastatic neuroendocrine tumor (NET) with MiB1 index 5% and prior history of failure to several cycles of chemotherapy presented for probable peptide receptor radionuclide therapy (PRRT). (a) Pretreatment ^{18}flor-fluorodeoxyglucose (^{18}F-FDG) positron emission tomography/computed tomography (PET/CT) showed no ^{18}F-FDG uptake, while all lesions in the liver [maximum standardized uptake value (SUV_{max}): 26.26, size: 34 mm], around the inferior vena cava (IVC) in the right side (SUV_{max}: 20.03; size: 23 mm), the sacrum (SUV_{max}: 34.74), as well as a focus in the left side of vermis on pretreatment galium-68 (^{68}Ga)-DOTATATE PET/CT had significant expression of somatostatin receptor (SSTR), thus suggesting a good differentiation (b). The two hot foci in the pelvis observed on ^{18}F-FDG PET/CT were due to contamination. She showed a significant decrease in abdominal pain and frequency of diarrhea after two cycles of PRRT with ^{177}Lu-DOTATATE. (c) On follow-up ^{68}Ga-DOTATATE PET/CT, four months after the fourth cycle of PRRT, there was excellent partial response with residual viable disease in the liver (SUV_{max}: 12.23; size: 20 mm), large-sized IVC metastases (SUV_{max}: 4.51; size: 16 mm), and sacrum (SUV_{max}: 7.94). The patient also had meningioma grade I/III of WHO classification, which measures about 2.3x1.1x2.0 cm in the left side of vermis, thus suggesting a residual/remnant left posterior fossa meningioma. She had a prior history of surgery of this lesion (d). The SUV_{max} of such meningioma on ^{68}Ga-DOTATATE PET/CT before (b) and after PPRT (c) was 11.76 and 9.02, respectively, and no significant change in size on magnetic resonance imaging also represents a stable disease. This may be related to the point that functional imaging usually precedes anatomical imaging and may take longer time to occur on anatomical imaging. In addition to the approved role of PRRT in inoperable NETs, it has been demonstrated that this technique can be a promising therapy for progressive meningioma, especially in patients with low grade and refractory to standard regime (1,2,3). Molecular imaging of SSTR with ^{68}Ga-DOTATATE/-TOC in NET and meningioma can assist the implementation of targeted radionuclide therapy with lesion-based therapy concept in the aggressive/refractory subtype of such cancers (4,5).

Ethics

Informed Consent: Written informed consent of the patient was obtained from the patient.

Peer-review: Externally peer-reviewed.

Authorship Contributions

Surgical and Medical Practices: M.A., S.J.R., A.A., H.D., R.N., I.N., E.J., H.A., Concept: M.A., A.G., H.A., Design: M.A., E.J., Data Collection or Processing: M.A., E.J., H.D., Analysis or Interpretation: M.A., E.J., H.D., R.N., Literature Search: M.A., E.J., Writing: M.A., E.J., H.A.

Conflict of Interest: No conflict of interest was declared by the authors.

Financial Disclosure: The authors declared that this study received no financial support.

References

1. Makis W, McCann K, McEwan AJ. Rhabdoid papillary meningioma treated with 177Lu DOTATATE PRRT. Clin Nucl Med 2015;40:237-240.
2. Bartolomei M, Bodei L, De Cicco C, Grana CM, Cremonesi M, Botteri E, Baio SM, Aricò D, Sansovini M, Paganelli G. Peptide receptor radionuclide therapy with (90)Y-DOTATOC in recurrent meningioma. Eur J Nucl Med Mol Imaging 2009;36:1407-1416.
3. Carlsen EA, Fazio N, Granberg D, Grozinsky-Glasberg S, Ahmadzadehfar H, Grana CM, Zandee WT, Cwikla J, Walter MA, Oturai PS, Rinke A, Weaver A, Frilling A, Gritti S, Arveschoug AK, Meirovitz A, Knigge U, Sorbye H. Peptide receptor radionuclide therapy in gastroenteropancreatic NEN G3: a multicenter cohort study. Endocr Relat Cancer 2019;26:227-239.
4. Sommerauer M, Burkhardt JK, Frontzek K, Rushing E, Buck A, Krayenbuehl N, Weller M, Schaefer N, Kuhn FP. 68Gallium-DOTATATE PET in meningioma: A reliable predictor of tumor growth rate? Neuro Oncol 2016;18:1021-1027.
5. Seystahl K, Stoecklein V, Schüller U, Rushing E, Nicolas G, Schäfer N, Ilhan H, Pangalu A, Weller M, Tonn JC, Sommerauer M, Albert NL. Somatostatin receptor-targeted radionuclide therapy for progressive meningioma: benefit linked to 68Ga-DOTATATE/-TOC uptake. Neuro Oncol 2016;18:1538-1547.

Interesting Image
Mol Imaging Radionucl Ther 2021;30:110-112 DOI:10.4274/mirt.galenos.2020.33255

Oncological Follow-up with 2-[^{18}F]-FDG PET/CT in Li-Fraumeni Syndrome

Li-Fraumeni Sendromunda 2-[^{18}F]-FDG PET/BT ile Onkolojik Takip

Marylin Acuña Hernandez[1], Iván Fabricio Vega Gonzalez[2], Lina López Vélez[2], Catalina Melo Arango[3]

[1]*Autonomous University of Bucaramanga (UNAB), Department of Nuclear Medicine, Bucaramanga, Santander, Colombia*
[2]*Las Américas Clinic Auna, Department of Nuclear Medicine, Medellin, Antioquia, Colombia*
[3]*Las Américas Clinic Auna, Department of Radiology, Medellin, Antioquia, Colombia*

Abstract

Li-Fraumeni syndrome is a rare disorder caused by abnormalities of the tumor-suppressor protein *P53* gene. We present the case of a 26-years-old female diagnosed with bilateral ductal carcinoma. The genetic panel for breast cancer gene 1 (BRCA1) and BRCA2 mutations was negative and positive heterozygous germline tumor protein *P53* gene mutations, considering Li-Fraumeni syndrome. A 2-[^{18}F]-fluorodeoxyglucose (FDG) positron emission tomography/computed tomography (PET/CT) was used for postsurgical staging to show the right lung hypermetabolic nodule. A lobectomy was accomplished, and histopathology reported pulmonary adenocarcinoma. A year later, oncological follow-up was conducted with 2-[^{18}F]-FDG PET/CT without evidence of abnormalities.

Keyword: Li-Fraumeni syndrome, positron emission tomography, fluorodeoxyglucose ^{18}F

Öz

Li-Fraumeni sendromu, tümör baskılayıcı protein *P53* genindeki anormalliklerin neden olduğu nadir bir hastalıktır. Burada, bilateral duktal karsinom tanısı almış 26 yaşında bir kadın olgu sunulmuştur. Meme kanseri geni 1 *(BRCA1)* ve *BRCA2* mutasyonları için genetik panelin negatif oluşu ve pozitif heterozigot germline tümör proteini *P53* gen mutasyonlarının varlığı, Li-Fraumeni sendromunu düşündürmüştür. Post-op evreleme için yapılan 2-[^{18}F]-florodeoksiglukoz (FDG) pozitron emisyon tomografisi/bilgisayarlı tomografide (PET/BT), sağ akciğerde hipermetabolik nodül saptanmıştır. Lobektomi yapılmış ve histopatolojisi pulmoner adenokarsinom olarak raporlanmıştır. Bir yıl sonra, herhangi bir anormallik kanıtı olmadığı görüldü ve 2-[^{18}F]-FDG PET/BT ile onkolojik takip yapıldı.

Anahtar kelimeler: Li-Fraumeni sendromu, pozitron emisyon tomografisi, florodeoksiglukoz ^{18}F

Address for Correspondence: Marylin Acuña Hernandez MD, Autonomous University of Bucaramanga (UNAB), Department of Nuclear Medicine, Bucaramanga, Santander, Colombia
Phone: (57) 3124234989 **E-mail:** macuna766@unab.edu.co ORCID ID: orcid.org/0000-0001-7381-1910
Received: 10.11.2019 **Accepted:** 24.04.2020

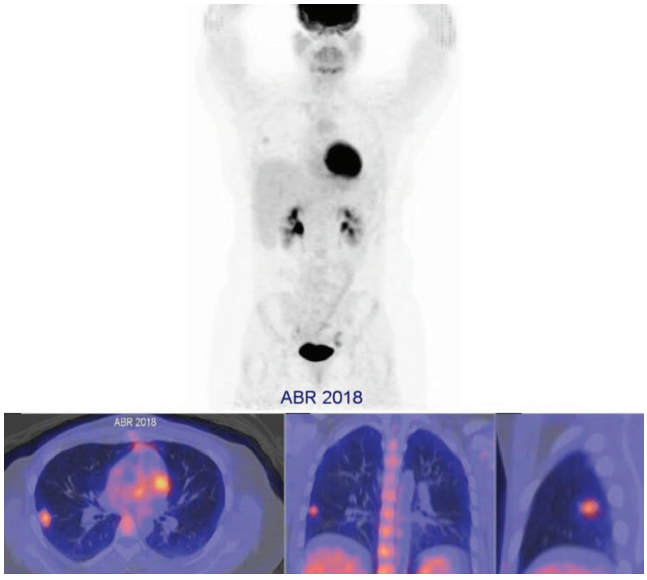

Figure 1. A 26-year-old female diagnosed with bilateral breast carcinoma (invasive ductal carcinoma), hormonal-receptor-negative, and Her-2-Neu-positive. The genetic panel for breast cancer gene 1 (BRCA1) and BRCA2 mutations was negative, with positive heterozygous germline mutations on TP53, considering Li-Fraumeni syndrome. Post-surgical staging with 2-[18F]-fluorodeoxyglucose (FDG) positron emission tomography/computed tomography (PET/CT) reported a hypermetabolic pulmonary module in the superior segment of The right lower lobe.

Li-Fraumeni syndrome is a rare disorder caused by abnormalities of the tumor suppressor protein *P53* gene (TP53) (1), and an autosomal dominant inheritance that affects approximately 400 families worldwide (1,2).

The importance of P53 as an anticancer filter lies in the activation of DNA repair proteins and induction of apoptosis (1,2). When altered, it represents a greater risk of developing neoplasms (90% in females and 73% in males) (1). The most frequent cases in children are adrenocortical carcinoma, osteosarcomas, and rhabdomyosarcomas (1), while those in adults less than 46 years old are sarcomas, brain tumors, breast cancer, leukemia, and bronchoalveolar carcinoma (2,3).

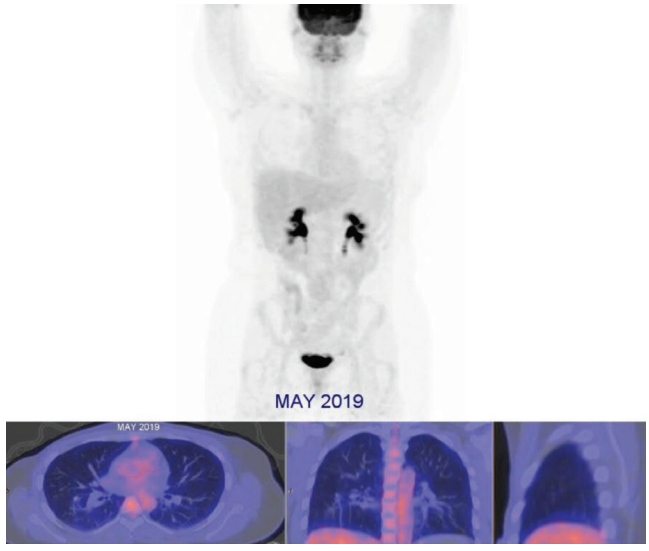

Figure 2. A lobectomy was accomplished with a histopathology report of pulmonary adenocarcinoma with lepidic pattern. A year later, oncological follow-up was indicated with 2-[18F]-FDG PET/CT without evidence of abnormalities.

The diagnostic images play a role in the follow-up. It is recommended to have an ultrasound of the abdomen and pelvis every 3 months in children and annually in adults (2) or an annual total body magnetic resonance (1,2) and annual images of the breasts for females aged 20 years old and above. Ionizing radiation is not recommended, given the hypothetical risk of developing another neoplasm (2).

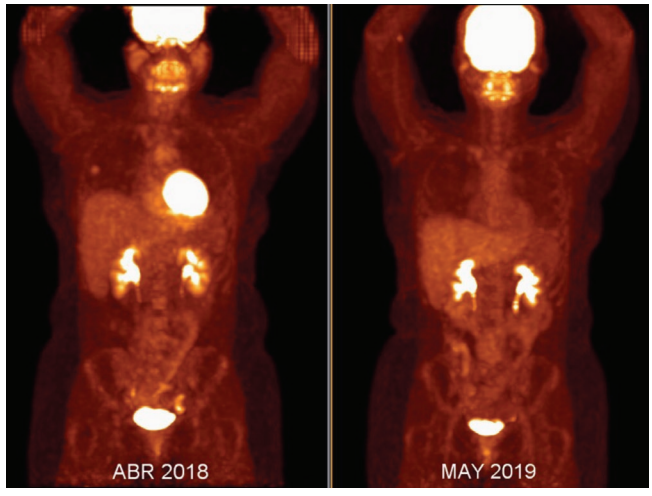

Figure 3. Comparison of 2-[18F]-FDG PET/CT used for cancer follow-up

According to the cohort of 30 patients from Nogueira et al. (3) in Brazil, although the detection of tumor lesions with 2-[18F]-FDG PET/CT in this syndrome can be as low as 20%, this type of diagnostic test helps confirm the presence of lesions, as is demonstrated in our case, and should be considered as a determining factor for the choice of this technique with respect to other modalities because a report of a metabolically lesion requires immediate histopathological confirmation.

Similarly, the replacement of other diagnostic imaging methods and tranquility of the patient and medical staff in charge of a suspected associated neoplasm contribute to a 2-[18F]-FDG PET/CT-negative result during the follow-up.

Ethics

Informed Consent: Informed consent was obtained from patient.

Peer-review: Externally peer-reviewed.

Authorship Contributions

Surgical and Medical Practices: M.A.H., I.F.V.G., L.L.V., C.M.A., Concept: M.A.H., I.F.V.G., Design: M.A.H., I.F.V.G., Data Collection or Processing: M.A.H., I.F.V.G., L.L.V., C.M.A., Analysis or Interpretation: M.A.H., I.F.V.G., L.L.V., C.M.A., Literature Search: M.A.H., Writing: M.A.H., I.F.V.G., L.L.V., C.M.A.

Conflict of Interest: No conflict of interest was declared by the authors.

Financial Disclosure: The authors declared that this study received no financial support.

References

1. Aedma SK, Kasi A. Li-Fraumeni Syndrome. 2020 Nov 24. In: StatPearls [Internet]. Treasure Island (FL): StatPearls Publishing; 2021.
2. McBride KA, Ballinger ML, Killick E, Kirk J, Tattersall MH, Eeles RA, Thomas DM, Mitchell G. Li-Fraumeni syndrome: cancer risk assessment and clinical management. Nat Rev Clin Oncol 2014;11:260-271.
3. Nogueira ST, Lima EN, Nóbrega AF, Torres Ido C, Cavicchioli M, Hainaut P, Achatz MI. (18)F-FDG PET-CT for Surveillance of Brazilian Patients with Li-Fraumeni Syndrome. Front Oncol 2015;19;5:38.

Interesting Image
Mol Imaging Radionucl Ther 2021;30:113-116 DOI:10.4274/mirt.galenos.2020.89266

Incidental Skeletal Findings on Sodium-fluoride Positron Emission Tomography: A Collection of Benign Tumors

Sodyum-florür Pozitron Emisyon Tomografisinde İnsidental İskelet Sistemi Bulguları: Benign Tümörlerden Bir Derleme

Nada Almenieir[1,2], Marc Hickeson[1], Javier Novales-Diaz[1], Vilma Derbekyan[1], Gad Abikhzer[3]

[1]*McGill University Health Center, Department of Nuclear Medicine, Montreal, Canada*
[2]*King Saud University, Department of Radiology and Medical Imaging, Riyadh, Saudi Arabia*
[3]*Jewish General Hospital, Departement of Nuclear Medicine, Montreal, Canada*

Abstract

Sodium-fluoride (NaF) positron emission tomography (PET) is a sensitive method to detect altered bone mineralization. Its increasing use in routine clinical practice for metastatic bone disease has also resulted in the detection or characterization of incidental benign bone lesions. A spectrum of NaF PET scan cases with benign bone tumors are presented in this article, including whole body PET bone scan and selected PET/computed tomography (CT), CT, or magnetic resonance imaging (MRI) of the region of interest. The reader will be able to improve their knowledge related to the clinical presentation of these entities, some are rare and recognize based on NaF PET and CT/MRI patterns by reviewing these cases.

Keywords: NaF, sodium-fluoride PET, benign bone lesions

Öz

Sodyum-florür (NaF) pozitron emisyon tomografisi (PET), kemik mineralizasyonu değişimini tespit etmek için hassas bir yöntemdir. Metastatik kemik hastalığı için rutin klinik uygulamada artan kullanımı aynı zamanda insidental iyi huylu kemik lezyonlarının saptanması veya karakterizasyonu ile de sonuçlanmıştır. Bu makalede, tüm vücut PET kemik taraması ve ilgili bölgenin seçilmiş PET/bilgisayarlı tomografisi (BT), BT veya manyetik rezonans görüntüleme (MRG) dahil, benign kemik tümörlerinin NaF PET ile tarandığı olguların bir spektrumu sunulmuştur. Okuyucu, bu olguların klinik prezentasyonuyla ilgili bilgilerini geliştirebilecek, bazıları nadir olan bu olguları gözden geçirerek, NaF PET ve BT/MRG modellerine dayanarak tanıyabilecektir.

Anahtar kelimeler: NaF, sodyum-florür PET, iyi huylu kemik lezyonları

Address for Correspondence: Nada Almenieir MD, McGill University Health Center, Department of Nuclear Medicine, Montreal, Canada
Phone: +8573526301 **E-mail:** n.almenieir@gmail.com ORCID ID: orcid.org/0000-0002-6377-0542
Received: 07.12.2019 **Accepted:** 26.04.2020

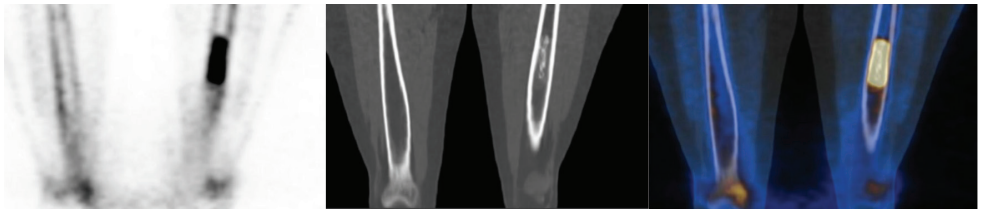

Figure 1. Enchondroma: A 29-year-old female patient with breast cancer. Sodium-fluoride (NaF) positron emission tomography/computed tomography (PET/CT) images demonstrated segmental intensely increased uptake in the mid diaphysis of the left femur, with classic "rings and arcs" calcifications in the CT.

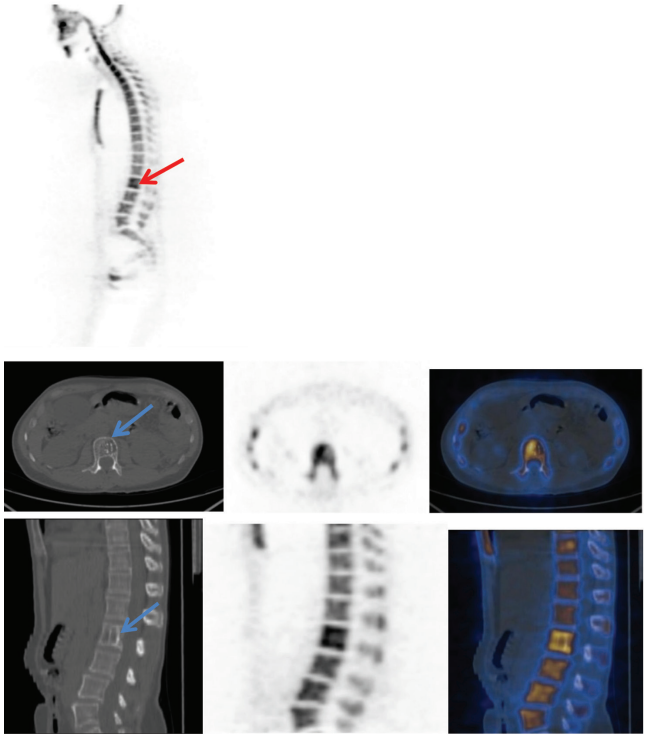

Figure 2. Hemangioma: A 50-year-old female patient with breast cancer. NaF PET images demonstrated mild heterogenous uptake in the L2 vertebral body, which upon closer inspection is actually decreased in the bone lesion. CT images demonstrated thickened vertebral trabeculae with axial images showing the typical "polka dot" sign of intraosseous hemangioma (1).

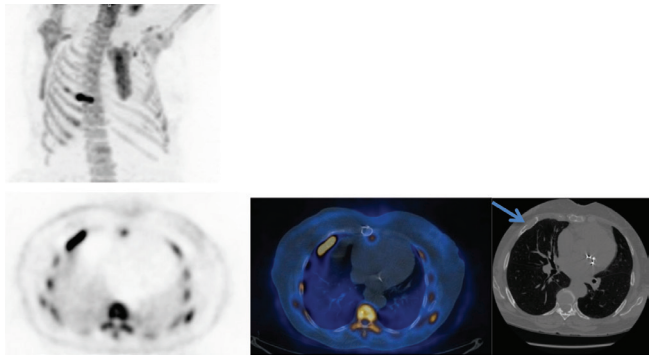

Figure 3. Fibrous dysplasia: A 77-year-old female patient with breast cancer. NaF PET images demonstrated segmental uptake in the right 5th rib. A misregistered activity was noted on hybrid fusion due to patient motion in the expansile lesion with cortical disruption on CT. Biopsy was performed, which demonstrated fibrous dysplasia. Fibrous dysplasia is the most common benign rib lesionn (2).

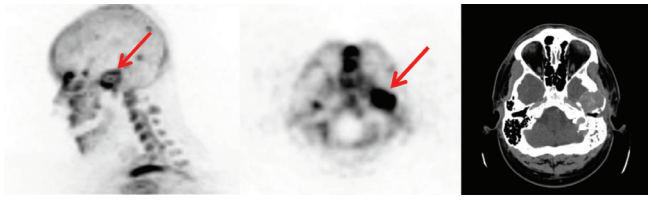

Figure 4. Chondroblastoma: A 42-year-old male patient with new onset hearing loss in the left ear. NaF PET images demonstrated an intensely increased activity in the region of the left temporal bone. CT images demonstrated an extra-axial mass in the left medial cranial fossa causing erosion of the temporal bone, mastoid bone, middle ear ossicles, and temporal side of the left temporomandibular joint. Biopsy of the lesion showed chondroblastoma. Chondroblastomas are rare primary bone tumors, occurring predominantly in young patients (<20 years of age), with an overall male predilection (3), which are usually three-phase positive on conventional bone scan using tc99m- methylene diphosphonate, and can demonstrate increased fluorodeoxyglucose uptake, thus differentiating these lesions from malignancy is important.

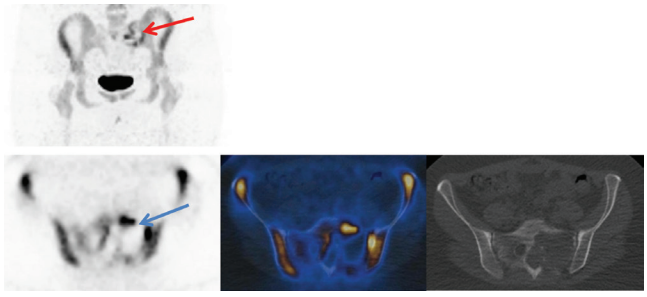

Figure 5. Giant cell tumor (GCT): A 32-year-old female patient with back pain. NaF PET images demonstrated a rim of mild to moderate heterogeneous increased activity with a photopenic center in an expansile radiolucent lesion in the left sacrum. Biopsy demonstrated a GCT. GCTs are usually solitary, involving 4%-9% of the sacrum (4).

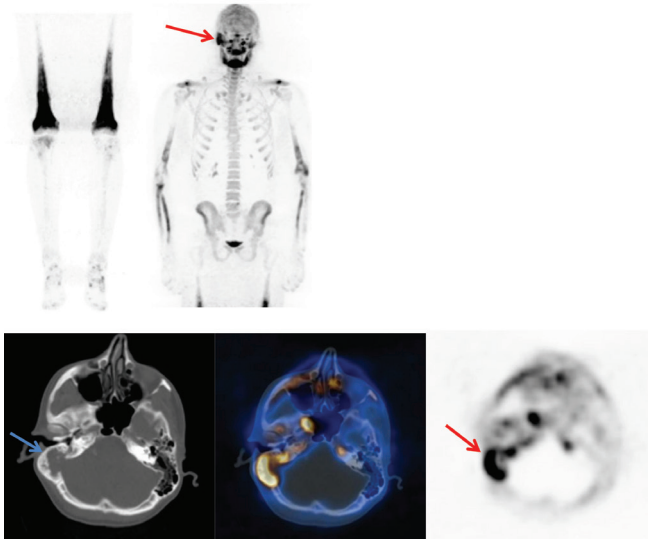

Figure 6. Langerhans' cell histiocytosis (LCH): A 31-year-old male patient with incidental lytic skull lesion on head imaging. NaF PET images demonstrated an increased uptake in the right mastoid, diffusing in the mandible and long bones such as the distal humeri, radius, and ulnar, as well as the distal two thirds of femurs. CT of the head demonstrated a large expansile lytic lesion involving the right mastoid. Biopsy of the left maxillary gums showed Langerhans cell proliferation with positive BRAF staining. LCH is a disease with abnormal histiocytes proliferation, and subsequent various organs accumulation. The skeleton is the most commonly involved organ system in LCH, involving 50% of the skull (5).

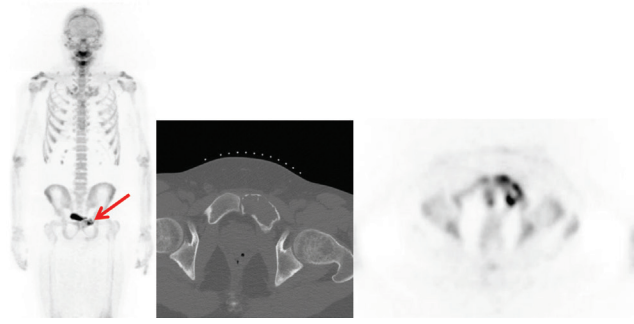

Figure 7. Desmoplastic fibroma: A 30-year-old male patient with a 1-year history of left hip/groin pain. NaF PET images demonstrated heterogeneous tracer uptake within the cortex of an expansile osseous lesion in the left superior pubic ramus. After the CT-guided biopsy which showed desmoplastic fibroma, the lesion was resected. Desmoplastic fibromas are extremely rare bone tumors that are histologically identical to soft tissue desmoid tumors (6).

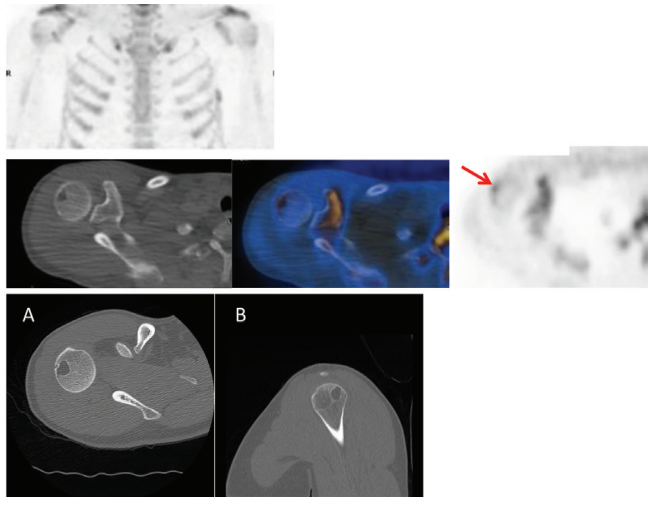

Figure 8. Intraosseous lipoma: A 35 year-old male patient presented with right shoulder sports injury, which led to an incidental 1.4x1.4 cm lucent osseous lesion in the subcortical lateral right humeral epiphysis with internal fat density (HU: -90), thin sclerotic margin, and narrow transition zone as demonstrated on diagnostic CT images (A and B). NaF PET demonstrated only minimally increased focal uptake at the site of the lucency in the right humeral head. No further investigation or treatment was deemed necessary as intraosseous lipomas that do not affect bone stability are treated conservatively (7).

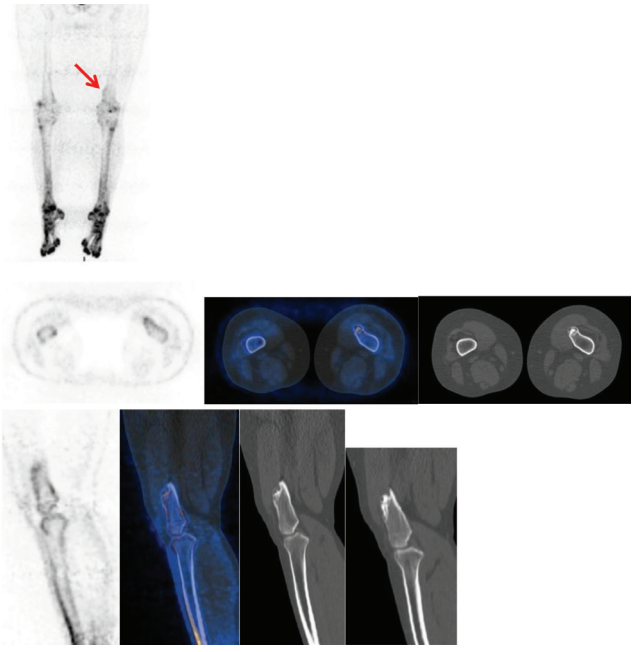

Figure 9. Osteoid osteoma: A 28 year-old male patient with indolent right shoulder pain, which worsens at night and improves with non-steroidal anti-inflammatories. NaF PET images demonstrate focal intense increased uptake in the glenoid fossa of the right scapula, associated with sclerosis of the right glenoid and radiolucent nidus and central mineralization. Patient underwent radiofrequency ablation of the lesion, which led to symptom improvement (8).

Ethics

Informed Consent: Informed consent was waived.

Peer-review: Externally and internally peer-reviewed.

Authorship Contributions

Concept: N.A., G.A., Design: N.A., G.A., Data Collection or Processing: N.A., G.A., Analysis or Interpretation: N.A., M.H., J.N.D., V.D., G.A., Literature Search: N.A., Writing: N.A.

Conflict of Interest: No conflict of interest was declared by the authors.

Financial Disclosure: The authors declared that this study received no financial support.

References

1. Persaud T. The polka-dot sign. Radiology 2008;246:980-981.
2. Rubin AN, Byrns K, Zhou D, Freedman L. Fibrous Dysplasia of the Rib: AIRP Best Cases in Radiologic-Pathologic Correlation. Radiographics 2015;35:2049-2052.
3. Erickson JK, Rosenthal DI, Zaleske DJ, Gebhardt MC, Cates JM. Primary treatment of chondroblastoma with percutaneous radio-frequency heat ablation: report of three cases. Radiology 2001;221:463-468.
4. Murphey MD, Nomikos GC, Flemming DJ, Gannon FH, Temple HT, Kransdorf MJ. From the archives of AFIP. Imaging of giant cell tumor and giant cell reparative granuloma of bone: radiologic-pathologic correlation. Radiographics 2001;21:1283-1309.
5. David R, Oria RA, Kumar R, Singleton EB, Lindell MM, Shirkhoda A, Madewell JE. Radiologic features of eosinophilic granuloma of bone. AJR Am J Roentgenol 1989;153:1021-1026.
6. Frick MA, Sundaram M, Unni KK, Inwards CY, Fabbri N, Trentani F, Baccini P, Bertoni F. Imaging findings in desmoplastic fibroma of bone: distinctive T2 characteristics. AJR Am J Roentgenol 2005;184:1762-1767.
7. Campbell RS, Grainger AJ, Mangham DC, Beggs I, Teh J, Davies AM. Intraosseous lipoma: report of 35 new cases and a review of the literature. Skeletal Radiol 2003;32:209-222.
8. Chai JW, Hong SH, Choi JY, Koh YH, Lee JW, Choi JA, Kang HS. Radiologic diagnosis of osteoid osteoma: from simple to challenging findings. Radiographics 2010;30:737-749.

Interesting Image
Mol Imaging Radionucl Ther 2021;30:117-118 DOI:10.4274/mirt.galenos.2020.90377

PET/CT Findings of a Patient with Striped Muscle Metastasis of Invasive Breast Carcinoma

İnvaziv Meme Karsinomu Tanılı Hastanın PET/BT Görüntülemesinde Saptanan Çizgili Kas Metastazı

Rabiye Uslu Erdemir[1], Özlem Elmas[2]

[1]*Zonguldak Bülent Ecevit University Faculty of Medicine, Department of Nuclear Medicine, Zonguldak, Turkey*
[2]*Zonguldak Bülent Ecevit University Faculty of Medicine, Department of Radiation Oncology, Zonguldak, Turkey*

Abstract

A 37-year-old female with a history of invasive breast carcinoma was referred to our department for an ^{18}flor-fluorodeoxyglucose (^{18}F-FDG) positron emission tomography/computed tomography whole-body scan. An intense ^{18}F-FDG uptake in striped muscles anterior to the left thigh region was noted. Excisional biopsy outcome from the left vastus medialis muscle was found to be consistent with striped muscle metastasis from breast carcinoma.

Keywords: Breast carcinoma, ^{18}F-FDG PET/CT, striped muscle, metastasis

Öz

İnvaziv meme karsinomu tanılı 37 yaşında kadın hasta tüm vücut ^{18}flor-florodeoksiglukoz (^{18}F-FDG) pozitron emisyon tomografi/bilgisayarlı tomografi görüntülemesi için birimimize başvurdu. Sol uyluk bölgesi anteriorundaki çizgili kaslarda yoğun artmış ^{18}F-FDG tutulumları saptandı. Bu bölgeden yapılan (sol vastus medialis kası) eksizyonel biyopsi sonucu meme karsinomu çizgili kas metastazı ile uyumlu olarak raporlandı.

Anahtar kelimeler: Meme karsinomu, ^{18}F-FDG PET/BT, çizgili kas, metastaz

Address for Correspondence: Asst. Prof. Rabiye Uslu Erdemir, MD, Zonguldak Bülent Ecevit University Faculty of Medicine, Department of Nuclear Medicine, Zonguldak, Turkey
Phone: +90 372 250 03 29 **E-mail:** doktorhanim6@gmail.com ORCID ID: orcid.org/0000-0002-5542-7453
Received: 29.01.2020 **Accepted:** 06.05.2020

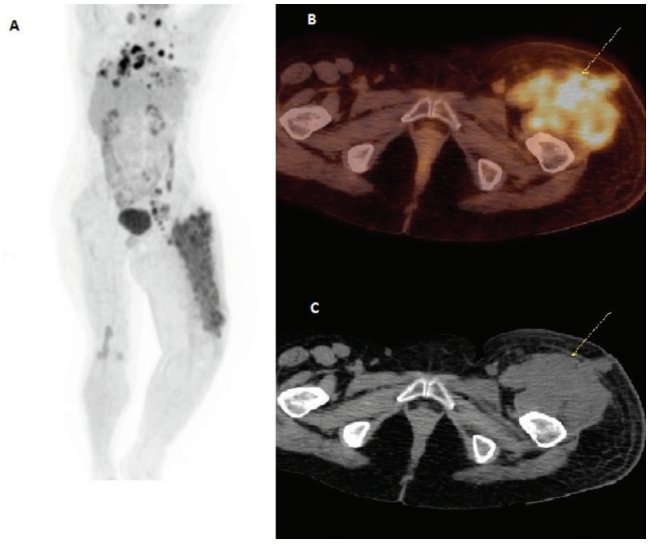

Figure 1. A 37-year-old female with invasive breast carcinoma was referred to our positron emission tomography/computed tomography (PET/CT) department for re-staging. Her medical history revealed a radical mastectomy for breast carcinoma in the left breast 2 years ago. The patient received chemotherapy and radiotherapy 1 year ago. The ^{18}fluorine-fluorodeoxyglucose (^{18}F-FDG) PET/CT scanning was performed 60 minutes after IV injection of 395 MBq ^{18}F-FDG, on an integrated 16 slice PET/CT, scanning from the base of the skull to the knee. The obtained images from ^{18}F-FDG PET/CT maximum intensity projection (A), axial fusion (B), and axial CT (C) showed tracer accumulation in the striped muscles anterior to the left thigh region (maximum standard uptake value, 7.1; mean density, 8 Hounsfield units) (B, C yellow arrows). Excisional biopsy indicated striped muscle metastasis from breast carcinoma in the left vastus medialis muscle. Furthermore, radiation therapy application was started.

Although muscle tissue makes up approximately half of the total body weight, metastatic extension to the skeletal muscle is an exceptional event in neoplasms, with an incidence of 0.8%-1.5% in autopsy series (1,2,3,4). Muscular contractile actions, lactic acid accumulations, and protease inhibitors affect the blood flow and inhibit the growth of tumor cells in the muscles. This potentially explains the rarity of this phenomenon (5). However, it has been reported that the incidence of metastasis is increased in trauma patients. In trauma, skeletal muscle function is impaired and focal hyperemia occurs, resulting in decreased ability of the muscle to eliminate lactic acid and increased possibility of metastatic cells to settle in the muscle. Therefore, patients should be assessed for trauma and hematoma and muscle rupture, and infection should be considered in differential diagnosis (6). Despite these protective mechanisms, soft tissue (striated muscle) metastasis secondary to lung cancer, kidney cancer, and colon cancer were reported in the literature (7). Intramuscular metastases can be seen in advanced and poorly differentiated tumors and worsen prognosis (8).

Ethics

Informed Consent: Consent was obtained patient.

Peer-review: Externally peer-reviewed.

Authorship Contributions

Concept: R.U.E., Design: R.U.E., Data Collection or Processing: R.U.E., Analysis or Interpretation: R.U.E., Literature Search: Ö.E., Writing: R.U.E., Ö.E.

Conflict of Interest: No conflict of interest was declared by the authors.

Financial Disclosure: The authors declared that this study received no financial support.

References

1. Damron TA, Heiner J. Distant soft tissue metastases: a series of 30 new patients and 91 cases from the literature. Ann Surg Oncol 2000;7:526-534.
2. Pop D, Nadeemy AS, Venissac N, Guiraudet P, Otto J, Poudenx M, Mouroux J. Skeletal muscle metastasis from non-small cell lung cancer. J Thorac Oncol 2009;4:1236-1241.
3. Tuoheti Y, Okada K, Osanai T, Nishida J, Ehara S, Hashimoto M, Itoi E. Skeletal muscle metastases of carcinoma: a clinicopathological study of 12 cases. Jpn J Clin Oncol 2004;34:210-214.
4. Sridhar KS, Rao RK, Kunhardt B. Skeletal muscle metastases from lung cancer. Cancer 1987;59:1530-1534.
5. Acinas García O, Fernández FA, Satué EG, Buelta L, Val-Bernal JF. Metastasis of malignant neoplasms to skeletal muscle. Rev Esp Oncol 1984;31:57-67.
6. Magee T, Rosenthal H. Skeletal muscle metastases at sites of documented trauma. AJR Am J Roentgenol 2002;178:985-988.
7. Damron TA, Heiner J. Management of metastatic disease to soft tissue. Orthop Clin North Am 2000;31:661-673, ix.
8. Emlik D, Gök M, Ödev K, Kıreşi DA. Akciğer malign tümörüne bağlı iskelet kası metastazı. Selçuk Tıp Der 2005;21:25-28.

Interesting Image
Mol Imaging Radionucl Ther 2021;30:119-121 DOI:10.4274/mirt.galenos.2020.48278

^{18}F-FDG PET/CT Imaging in an Unusual Case of Cutaneous Melanoma Arising From Congenital Melanocytic Nevus in a Two-year-old Girl

İki Yaşındaki Bir Kız Çocuğunda Konjenital Melanositik Nevüsten Kaynaklanan Nadir Bir Kutanöz Melanom Olgusunda ^{18}F-FDG PET/BT Görüntüleme

Seval Erhamamcı[1], Mehmet Reyhan[1], Nebil Bal[2], Neşe Torun[1], Ali Fuat Yapar[1]

[1]*Başkent University Faculty of Medicine, Department of Nuclear Medicine, Ankara, Turkey*
[2]*Başkent University Faculty of Medicine, Department of Pathology, Ankara, Turkey*

Abstract

Childhood malignant melanoma (MM) is extremely uncommon. We report an unusual case of cutaneous melanoma that developed from a medium-sized congenital melanocytic nevus (CMN) in a two-year-old girl. The patient had a history of CMN on the right hip, and she presented with a new ulcerative area with irregular borders and bleeding on CMN. Histopathological examination of the nevus revealed a MM. ^{18}Flor-fluorodeoxyglucose (^{18}F-FDG) positron emission tomography/computed tomography was performed for metastatic evaluation. The scan demonstrated metastatic increased ^{18}F-FDG uptake in the right external iliac and inguinal lymph nodes.

Keywords: ^{18}F-FDG PET/CT, childhood, cutaneous melanoma, congenital melanocytic nevus

Öz

Çocukluk çağı malign melanomu (MM) oldukça nadirdir. İki yaşında bir kız çocuğunda orta büyüklükte konjenital melanositik nevüsten (KMN) gelişen nadir bir kutanöz melanom olgusunu sunduk. Sağ kalçada KMN öyküsü olan hasta, KMN üzerinde düzensiz sınırlı ve kanamalı yeni bir ülseratif alan ile başvurdu. Nevüsün histopatolojik incelemesi MM gösterdi. Metastatik değerlendirme için, ^{18}flor-florodeoksiglukoz (^{18}F-FDG) pozitron emisyon tomografi/bilgisayarlı tomografi görüntüme yapıldı. Görüntüleme sağ ekternal iliak ve inguinal lenf nodlarında metastatik artmış ^{18}F-FDG tutulumunu gösterdi.

Anahtar Kelimeler: ^{18}F-FDG PET/BT, çocukluk çağı, kutanöz melanoma, kongenital melanositik nevüs

Address for Correspondence: Seval Erhamamcı MD, Başkent University Faculty of Medicine, Department of Nuclear Medicine, Ankara, Turkey
Phone: +90 216 554 15 00 **E-mail:** sevaler@yahoo.com ORCID ID: orcid.org/0000-0001-5016-4650
Received: 22.04.2020 **Accepted:** 31.05.2020

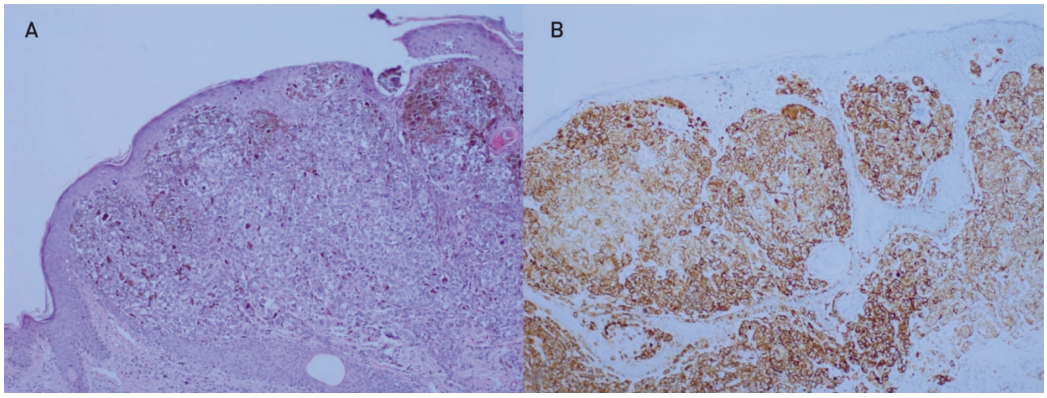

Figure 1. A 2-year-old girl with a medical history of congenital melanocytic nevus (CMN) on the right hip presented with a new ulcerative area with irregular borders and bleeding. At three months after the birth, histopathological examination of the nevus revealed CMN. She had no significant family history of atypical nevus or melanoma. Physical examination demonstrated hyperpigmentation of the right sclera, congenital hairy pigmented nevus of 11 cm in size on the right hip, multiple cafe au lait spots, and bilateral palpable inguinal lymphadenopathy. A recent histopathological examination of the nevus revealed a malignant melanoma (MM) with Breslow 1.2 cm and Clark level V (A). Nests of atypical melanocytes that filled the papillary dermis (hematoxylin and eosin staining, x100) (A). In immunohistochemical studies, tumor cells revealed positive expressions for HMB-45 (HMB45, x100) (B).

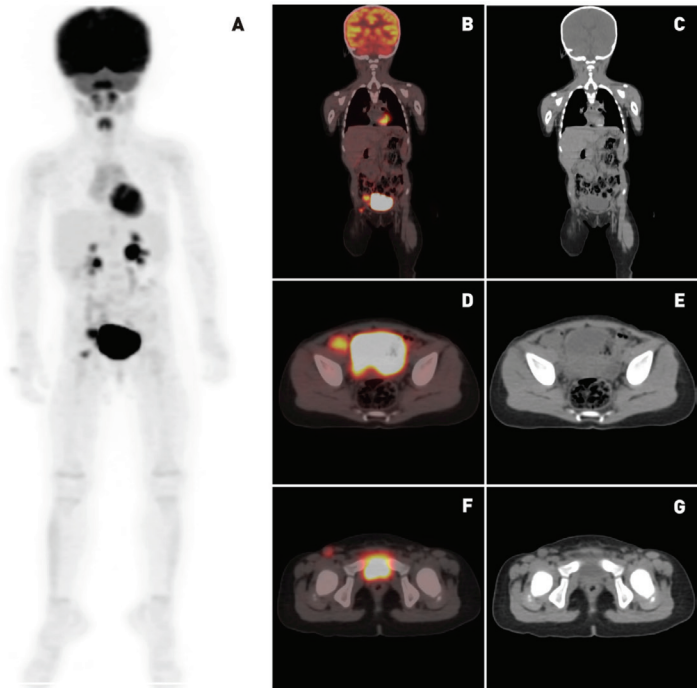

Figure 2. For metastatic evaluation, ^{18}flor-fluorodeoxyglucose (^{18}F-FDG) positron emission tomography (PET) imaging with non-contrast and low-dose computed tomography (CT) was performed. ^{18}F-FDG PET/CT maximum intensity projection (A), fusion PET/CT (B), CT (C), transaxial fusion (D, F), and transaxial CT (E, G) images show increased ^{18}F-FDG uptake in the right external iliac [largest 25x14 mm, maximum standardized uptake value (SUV_{max}) 7.6] and right inguinal (largest 10x9 mm, SUV_{max} 5.6) lymph nodes, consistent with metastases. Nasopharyngeal and tonsillary ^{18}F-FDG uptake were considered normal variant (SUV_{max} 7.1), and mild ^{18}F-FDG uptake in bilateral cervical lymph nodes at the 2B level was considered reactive (SUV_{max} 2.4).

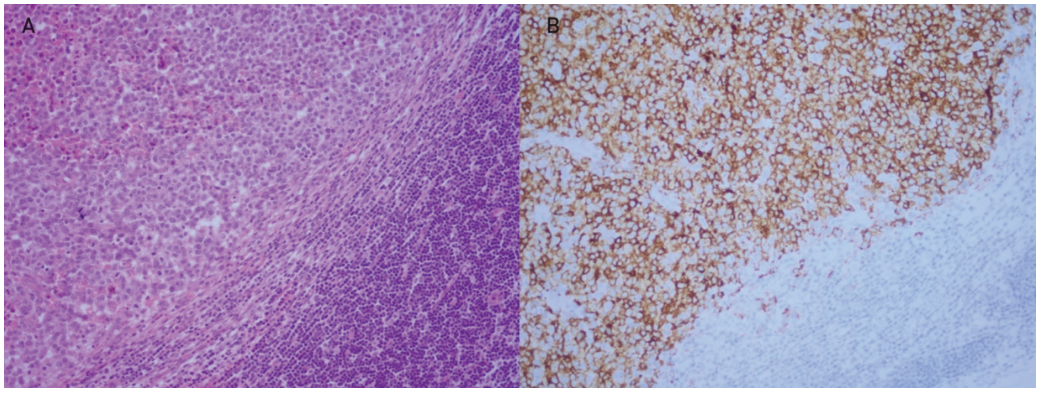

Figure 3. The patient underwent excisional biopsy of the inguinal lymph node, and the pathologic diagnosis was consistent with metastatic MM (hematoxylin and eosin staining, x200) (A). HMB45 positivity in atypical melanocytes that metastasized to the lymph node (HMB45, x200) (B). The patient underwent a combined wide local excision with negative margins and inguinal and parailiac lymph node dissection. The skin defect in the hip was reconstructed with a split skin graft. Pathologic examination demonstrated that the MM infiltrated into the entire dermis and metastasize into the lymph node. Two months later, magnetic resonance imaging showed soft tissue mass of 5x3.5x3 cm in size in the right pelvic region, considered conglomerate lymph nodes. The patient underwent surgery for this mass, and pathological examination revealed melanoma metastasis to the lymph node with extranodal soft tissue involvement. The patient was treated with chemotherapy, interferon, and radiotherapy. The patient died 12 months after the diagnosis of MM.

Childhood MM is extremely uncommon, representing only 0.3%-0.4% of all melanomas in prepubertal children aged <15 years (1). Depending on the size of the lesion, CMN carries an increased risk for the development of childhood melanoma. Giant CMNs (>20 cm) have been reported to have increased risk of developing melanomas, particularly during the first and second decades of life (2). However, cutaneous melanomas rarely arise from small (≤1 cm) and medium (1.5-20 cm) CMNs. Risk factors for developing melanoma from a CMN include irregular borders, increased diameter, color change, surface ulceration, and bleeding. Cutaneous MM poses a high risk of dissemination to regional lymph nodes and visceral organs. Childhood MM is a potentially fatal disease. Accurate staging of patients with melanoma is especially important if clinically occult systemic metastasis is present, which may preclude them the benefit of a complex lymph node dissection for locoregional control (1). The most appropriate imaging approach for diagnosing and following pediatric patients with MM has been adopted usually from adult guidelines because of its rarity (3). In staging melanoma, ^{18}F-FDG PET/CT is often employed to evaluate distant metastatic disease, as melanoma is very ^{18}F-FDG avid (3). In addition to staging, PET/CT plays an important role in patient management, such as deciding on the extent of surgery, determination of radiation field, and evaluation of treatment response. The current case also underlines the importance of whole-body oncologic assessment by ^{18}F-FDG PET scan in pediatric MM, which is a rare but a serious clinical entity.

Ethics

Informed Consent: Waived.

Peer-review: Externally peer-reviewed.

Authorship Contributions

Concept: S.E., Design: S.E., Data Collection or Processing: S.E., M.R., N.B., N.T., A.F.Y., Analysis or Interpretation: S.E., M.R., N.B., N.T., A.F.Y., Literature Search: S.E., Writing: S.E.

Conflict of Interest: No conflict of interest was declared by the authors.

Financial Disclosure: The authors declared that this study received no financial support.

References

1. Han D, Zager JS, Han G, Marzban SS, Puleo CA, Sarnaik AA, Reed D, Messina JL, Sondak VK. The unique clinical characteristics of melanoma diagnosed in children. Ann Surg Oncol 2012;19:3888-3895.
2. Schaffer JV. Update on melanocytic nevi in children. Clin Dermatol 2015;33:368-386.
3. Veit-Haibach P, Vogt FM, Jablonka R, Kuehl H, Bockisch A, Beyer T, Dahmen G, Rosenbaum S, Antoch G. Diagnostic accuracy of contrast-enhanced FDG-PET/CT in primary staging of cutaneous malignant melanoma. Eur J Nucl Med Mol Imaging 2009;36:910-918.

Interesting Image
Mol Imaging Radionucl Ther 2021;30:122-125 DOI:10.4274/mirt.galenos.2020.49091

Magnetic Resonance Imaging Signal Changes Mimicking Bone Metastasis in Patients Receiving Bisphosphonate Therapy

Bifosfonat Tedavisi Almış Hastalarda Kemik Metastazını Taklit Eden Manyetik Rezonans Görüntüleme Sinyal Değişiklikleri

İpek Tamsel[1], Mehmet Argın[1], Ayşegül Akgün[2]

[1]*Ege University Faculty of Medicine Hospital, Department of Radiology, İzmir, Turkey*
[2]*Ege University Faculty of Medicine Hospital, Department of Nuclear Medicine, İzmir, Turkey*

Abstract

Bisphosphonates are inorganic pyrophosphate agents that reduce bone turnover. These agents reduce bone pain and delay skeletal complications, such as fractures in patients with metastatic lytic lesions, malignant-related hypercalcemia, multiple myeloma, Paget's disease of bone, and osteoporosis. Osteonecrosis, developing in the jaw bones specifically, has been described as a complication associated with the use of bisphosphonates. In this report, we presented osteonecrosis-like magnetic resonance imaging findings that can be confused with bone metastasis in two patients who underwent long-term bisphosphonate treatment and the value of bone scan and ^{18}flor-fluorodeoxyglucose positron emission tomography/computerized tomography in the differential diagnosis.

Keywords: Bisphosphonate, osteonecrosis, long bone, magnetic resonance imaging, bone scan, ^{18}F-flourodeoxyglucose positron emission tomography/computerized tomography

Öz

Bisfosfonatlar, kemik döngüsünü azaltan inorganik pirofosfat maddelerdir. Bu ajanlar, metastatik litik lezyonları, malign ilişkili hiperkalsemi, multipl miyelom, kemik Paget hastalığı ve osteoporozu olan hastalarda kemik ağrısını azaltmak ve kırık gibi iskelet komplikasyonlarını geciktirmek için kullanılır. Özellikle çene kemiklerinde gelişen osteonekroz, bisfosfonatların kullanımı ile ilişkili bir komplikasyon olarak tanımlanmıştır. Bu bildiride, uzun dönem bifosfonat tedavisi almış iki olguda kemik metastazını taklit eden osteonekroza ait olabilecek manyetik rezonans görüntüleme bulguları ile birlikte kemik sintigrafisi ve ^{18}flor-florodeoksiglukoz pozitron emisyon tomografi/bilgisayarlı tomografinin tanıya katkısı sunulmuştur.

Anahtar kelimeler: Bisfosfonat, osteonekroz, uzun kemik, manyetik rezonans görüntüleme, kemik sintigrafisi, ^{18}F-florodeoksiglikoz pozitron emisyon tomografi/bilgisayarlı tomografi

Address for Correspondence: İpek Tamsel MD, Ege University Faculty of Medicine Hospital, Department of Radiology, İzmir, Turkey
Phone: +90 533 234 11 24 **E-mail:** ipektamsel@yahoo.com ORCID ID: orcid.org/0000-0003-3629-2386
Received: 15.03.2020 **Accepted:** 31.05.2020

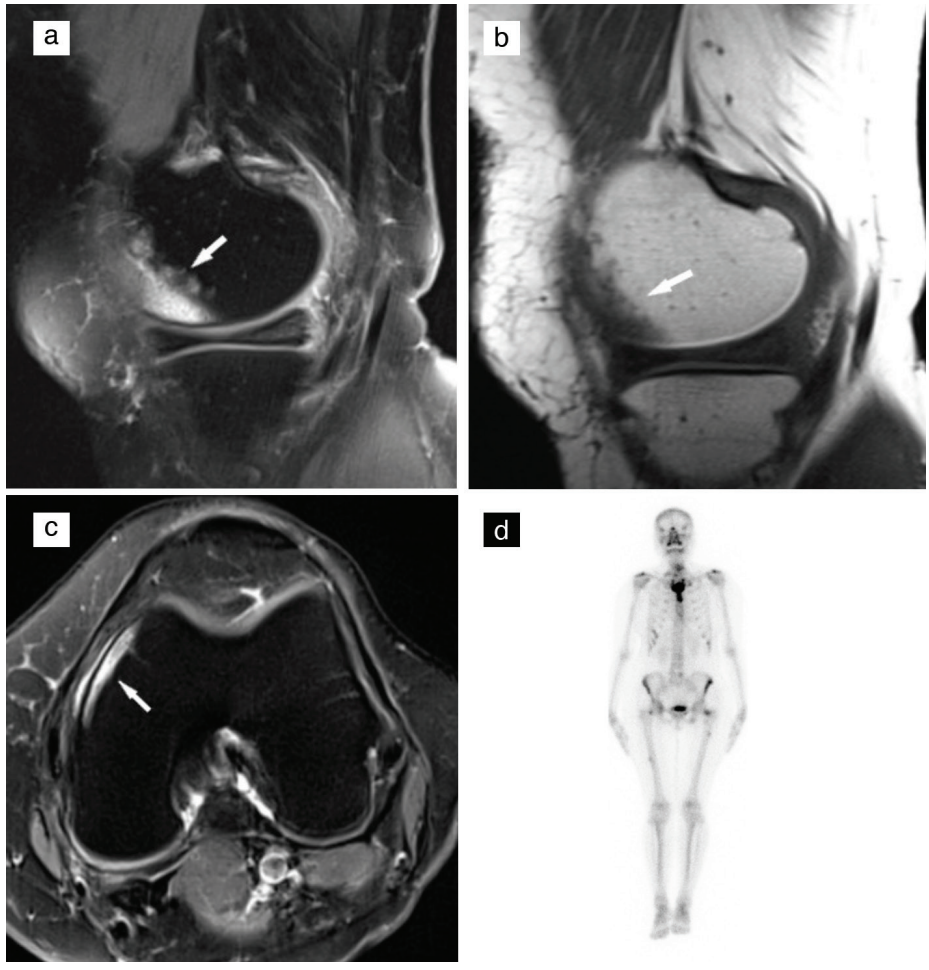

Figure 1. Magnetic resonance imaging (MRI) of a 55-year-old woman with breast cancer who has been on intravenous bisphosphonate for two years. (a, c) Fat-saturated T2-weighted MRI showing increased signal intensity in the femoral medial condyle at the subcortical area (arrow); (b) T1-weighted image showing decreased marrow signal intensity in the femoral medial condyle at the subcortical area (arrow); (d) anterior views of the planar bone scan showing multiple areas of intensely increased activity in the skeleton, representing metastatic involvement. Despite this, there are no metastatic findings on scanning the knee.

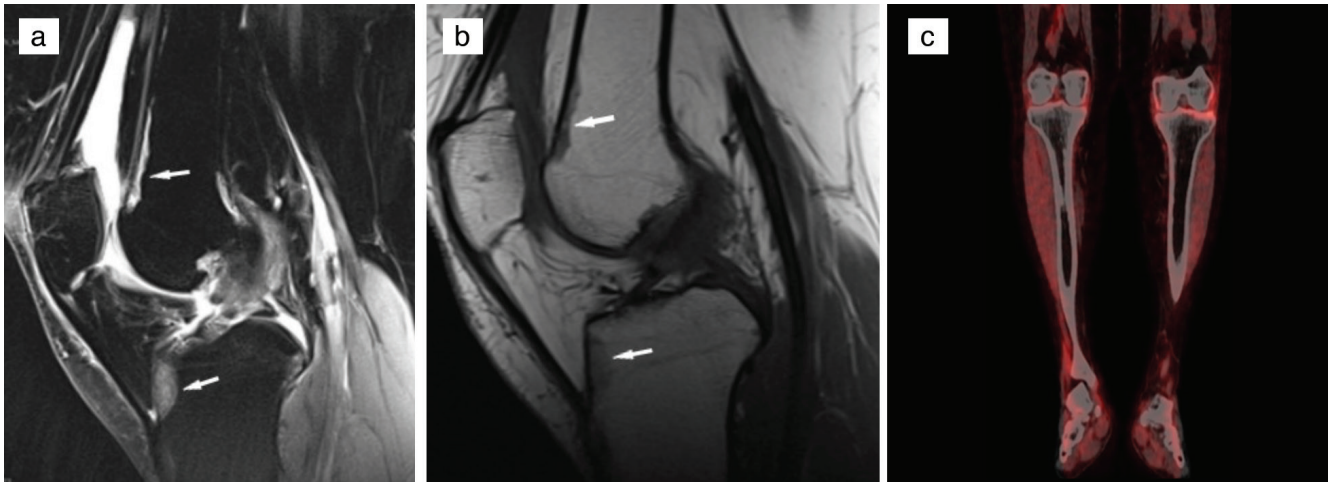

Figure 2. MRI of a 61-year- old woman with breast cancer who received intravenous bisphosphonate therapy for two years. (a) Fat-saturated T2-weighted MRI showing increased signal intensity; (b) T1-weighted image showing decreased signal intensity in the femur and tibia at the subcortical areas (arrows); (c) there is no metastatic ^{18}flor-fluorodeoxyglucose (^{18}F-FDG) uptake on coronal fused positron emission tomography/computerized tomography (PET/CT) image in the knee region.

Bisphosphonate treatment is increasingly used in patients with osteoporosis and metastatic carcinomas (1). Bisphosphonates inhibit osteoclast function and normal bone turnover. Bisphosphonate-related ischemic changes in the mandible and maxilla were reported in several studies in the literature (2). Bisphosphonate-related osteonecrosis of the jaws was first reported by Marx (3) in 2003. In our report, all lesions were located at the subcortical areas of long bones with low signal intensity on T1-weighted images and high signal intensity on T2-weighted images. Osteonecrosis and metastatic lesions show similar signal abnormalities on MRI. Because of this fact, nuclear medicine imaging or histopathologic examination is required to exclude metastatic lesions. Saito et al. (4) recently reported that histopathologically proven osteonecrosis appeared as abnormal multiple focal bone lesions in the femur and tibia, mimicking metastasis.

The duration of intravenous bisphosphonate treatment was more than one year in all patients, and there was no history of other drug use causing bone marrow signal change, such as erythropoietin or granulocyte stimulating factor, in these patients. In the follow-up of these patients, the bone scan and PET/CT supported the diagnosis of MRI by excluding metastatic involvement in these bones. Bone scan findings might vary according to the stage of osteonecrosis disease. In the acute phase of osteonecrosis, bone scintigraphy may not show technetium-99m methylene diphosphonate accumulation. After one to three weeks, increased radiotracer uptake is seen during the bone remodeling process (5). The uptake of ^{18}F-FDG is a marker for the tissue metabolism of glucose and represents the benign and malignant lesions as well as infections and sterile inflammation. In most cases reported in the literature, osteonecrosis revealed focal ^{18}F-FDG uptake. Talamo et al. (6) reported osteonecrosis in long bones, including the femoral and humeral heads, without ^{18}F-FDG uptake (7). In our patients, bone lesions defined on MRI did not show ^{18}F-FDG uptake and lytic/sclerotic density on PET/CT examination.

As a result, abnormal signal intensities detected on MRI can mimic metastatic bone lesions in patients with primary malignancy. In this report, we described osteonecrosis-like signal abnormalities of the long bones in patients that used long-term intravenous bisphosphonate treatment. The exclusion of metastatic involvement of these sites described on MRI was made using nuclear medicine examinations. Radiologists should keep in mind the probable diagnosis of osteonecrosis mimicking metastatic lesions in patients with primary malignancy. Bone scan and ^{18}F-FDG PET/CT are useful examinations in the evaluation of bone lesions detected on MRI, suspicious for metastatic disease.

Ethics

Informed Consent: Consent was obtained from the two cases in the study.

Peer-review: Externally peer-reviewed.

Authorship Contributions

Surgical and Medical Practices: İ.T., M.A., A.A., Concept: İ.T., M.A., A.A., Design: İ.T., M.A., A.A., Data Collection or Processing: İ.T., M.A., A.A., Analysis or Interpretation: İ.T., M.A., A.A., Literature Search: İ.T., M.A., A.A., Writing: İ.T., M.A., A.A.

Conflict of Interest: No conflict of interest was declared by the authors.

Financial Disclosure: The authors declared that this study received no financial support.

References

1. Obinata K, Shirai S, Ito H, Nakamura M, Carrozzo M, Macleod I, Carr A, Yamazaki Y, Tei K. Image findings of bisphosphonate related osteonecrosis of jaws comparing with osteoradionecrosis. Dentomaxillofac Radiol 2017;46:20160281.
2. Ruggiero SL, Mehrotra B, Rosenberg TJ, Engroff SL. Osteonecrosis of the jaws associated with the use of bisphosphonates: a review of 63 cases. J Oral Maxillofac Surg 2004;62:527-534.
3. Marx RE. Pamidronate (Aredia) and zoledronate (Zometa) induced avascular necrosis of the jaws: a growing epidemic. J Oral Maxillofac Surg 2003;61:1115-1117.
4. Saito A, Nakamura Y, Tanaka R, Inoue S, Okiyama N, Ishitsuka Y, Maruyama H, Watanabe R, Yoshida K, Ishiko A, Fujimoto M, Shinkuma S, Fujisawa Y. Unusual Bone Lesions with Osteonecrosis Mimicking Bone Metastasis of Squamous Cell Carcinoma in Recessive Dystrophic Epidermolysis Bullosa. Acta Derm Venereol 2019;99:1166-1169.
5. Agrawal K, Tripathy SK, Sen RK, Santhosh S, Bhattacharya A. Nuclear medicine imaging in osteonecrosis of hip: Old and current concepts. World J Orthop 2017;8:747-753.
6. Talamo G, Angtuaco E, Walker RC, Dong L, Miceli MH, Zangari M, Tricot G, Barlogie B, Anaissie E. Avascular necrosis of femoral and/or humeral heads in multiple myeloma: results of a prospective study of patients treated with dexamethasone-based regimens and high-dose chemotherapy. J Clin Oncol 2005;23:5217-5223.
7. Choi KH, Oh JK, Kim SH, Yoo ID, Choi EK, Han EJ. Osteonecrosis Mimicking Bone Metastasis in Femoral Head on (18)F-FDG PET/CT: A Case Report. Nucl Med Mol Imaging 2011;45:68-71.

Interesting Image
Mol Imaging Radionucl Ther 2021;30:126-128 DOI:10.4274/mirt.galenos.2020.51422

Systemic Sarcoidosis Induced by Chemotherapy, Mimicking Metastatic Testicular Carcinoma with ^{18}F-FDG PET/CT

^{18}F-FDG PET/BT Görüntülemede Metastatik Testis Karsinomunu Taklit Eden Kemoterapi Tedavisinin İndüklediği Sistemik Sarkoidoz

Esra Arslan[1], Tamer Aksoy[1], Süheyla Ekemen[2], Tevfik Fikret Çermik[1]

[1]*University of Health Sciences Turkey, İstanbul Training and Research Hospital, Clinic of Nuclear Medicine, İstanbul, Turkey*
[2]*Bahçeşehir University Faculty of Medicine, Department of Pathology, İstanbul, Turkey*

Abstract

A 34-year-old male patient who had left orchiectomy and received three cycles of chemotherapy for testicular mix germ cell carcinoma was referred for ^{18}fluorine-fluorodeoxyglucose (^{18}F-FDG) positron emission tomography/computed tomography (PET/CT) for complaints of weight loss and fever. PET/CT showed multiple and progressive ^{18}F-FDG uptakes in supra and infra diaphragmatic lymphatic regions, and multiple abnormal ^{18}F-FDG uptakes were noted in the lytic formed skeletal lesions. Clinicians remain in doubt regarding the multiple metastatic lesions without elevated serum tumor marker levels (alpha-fetoprotein, beta-human chorionic gonadotrophin, CA19-9, and carcinoembryonic antigen).

Biopsy of the lytic lesion in the iliac bone revealed granulomatous inflammation suggestive of sarcoidosis. Systemic prednisone at 20-40 mg/daily was started. ^{18}F-FDG PET/CT images showed complete metabolic response to prednisone 8 months following the start of treatment.

Keywords: Systemic sarcoidosis, testis carcinoma, ^{18}F-FDG PET/CT

Öz

Orşiektomi yapılan ve testis mikst germ hücreli karsinomu tanısı nedeni ile 3 kür kemoterapi alan 34 yaşındaki erkek hastada, kilo kaybı şikayeti nedeniyle nüks hastalık şüphesi ile ^{18}flor-florodeoksiglukoz (^{18}F-FDG) pozitron emisyon tomografi/bilgisayarlı tomografi (PET/BT) görüntülemesi yapıldı. PET/BT'de supra ve infra diyafragmatik lenfatik istasyonlarda çok sayıda ve patolojik FDG tutulumu gözlendi. Ayrıca litik görünümlü çok sayıda iskelet lezyonlarında da anormal ^{18}F-FDG tutulumu kaydedildi. Klinisyen, serum tümör belirteç (alfa feto protein, beta insan koryonik gonadotropin, CA19-9 ve karsinoembriyonik antijen) düzeyi yükselmemiş metastatik multipl lezyonlar konusunda şüphelenerek olguya iliak kemikteki litik lezyondan biyopsi incelemesi önerdi. Histopatolojik sonuç sarkoidoz düşündüren granülomatöz inflamasyon gösteren odak olarak raporlanması üzerine günlük 20-40 mg/gün sistemik prednizon başlandı. Sistemik prednizon tedavisine başlandıktan 8 ay sonraki ^{18}F-FDG PET/BT görüntüleri tam metabolik yanıt göstermektedir.

Anahtar kelimeler: Sistemik sarkoidoz, testis karsinomu, ^{18}F-FDG PET/BT

Address for Correspondence: Esra Arslan MD, University of Health Sciences Turkey, İstanbul Training and Research Hospital, Clinic of Nuclear Medicine, İstanbul, Turkey
Phone: +90 212 459 64 55 **E-mail:** dresraarslan@gmail.com ORCID ID: orcid.org/0000-0002-9222-8883
Received: 10.11.2019 **Accepted:** 13.06.2020

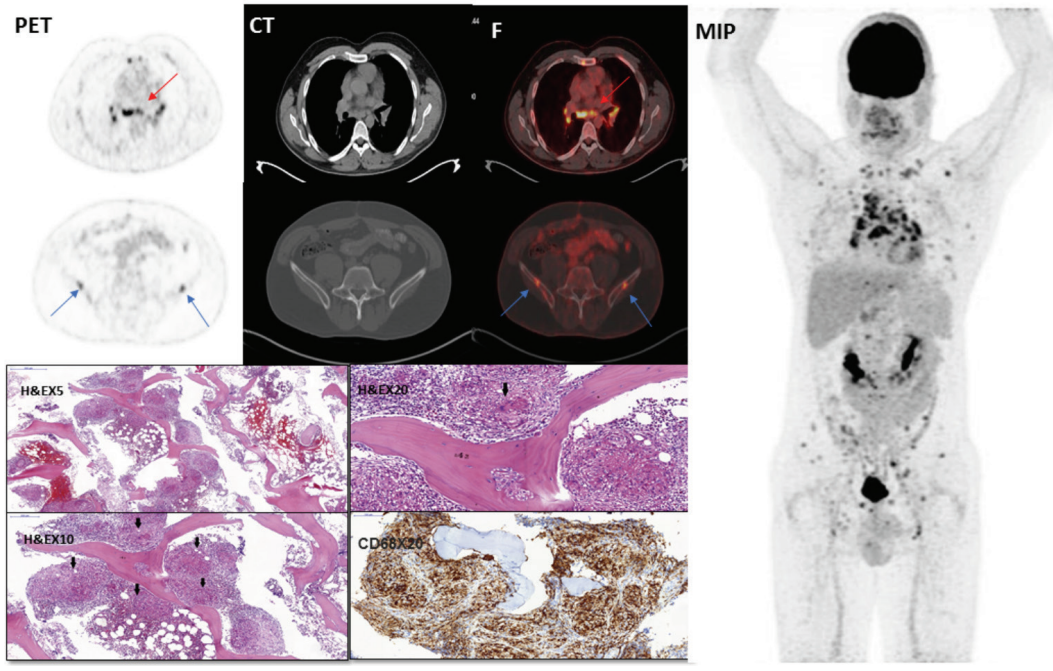

Figure 1. A 34-year-old male patient presented with fever, fatigue, and weight loss 4 months after left orchiectomy and three cycles of bleomycin, etoposide, and platinum chemotherapy due to testicular mix germ cell carcinoma (60% embryonal carcinoma, 30% teratoma, 10 % yolk sac tumor), pT1NxMx. Although the patient had no laboratory abnormalities (serum alpha-fetoprotein, beta-human chorionic gonadotrophin, CA19-9, and carcinoembryonic antigen levels were in normal ranges), ^{18}fluorine-fluorodeoxyglucose (^{18}F-FDG) positron emission tomography/computed tomography (PET/CT) was performed to evaluate metastatic disease as the patient suffered from excessive weight loss, fatigue, and fever. Written and verbal informed consents were obtained from the patient. Axial PET images and PET/CT fusion images show hypermetabolic mediastinal lymph nodes (red arrows), and abnormal focal ^{18}F-FDG uptakes were noted on the bilateral iliac bones (blue arrows). Multiple hypermetabolic supra and infra diaphragmatic lymph nodes and multiple bone lesions with increased ^{18}F-FDG uptakes were noted on maximum intensity projection images of PET examination. Biopsy of the lytic lesion in the iliac bone suggested granulomatous inflammation, instead of malignant cells. In H&EX5 staining, granuloma structures between bone trabeculae were seen. In H&EX10 image, black arrows show non-caseating granulomas. In H&EX20 image, black arrow shows multinuclear giant cells in the central of the granuloma. In CD68X20 staining, immunohistochemically positivity of histiocytes with CD68 was noted.

Sarcoidosis is a systemic granulomatous disease presenting with non-caseating epithelioid granuloma that primarily affects the lung and lymphatic systems of the body (1). The relationship between granulomatosis and cancer have been reported (2,3,4). Moreover, several reports have described the association between sarcoidosis and antineoplastic treatment (5,6,7,8). Another theory proposed that testicular cancers may be accompanied by a sarcoid-like reaction or can be associated with real sarcoidosis (8).

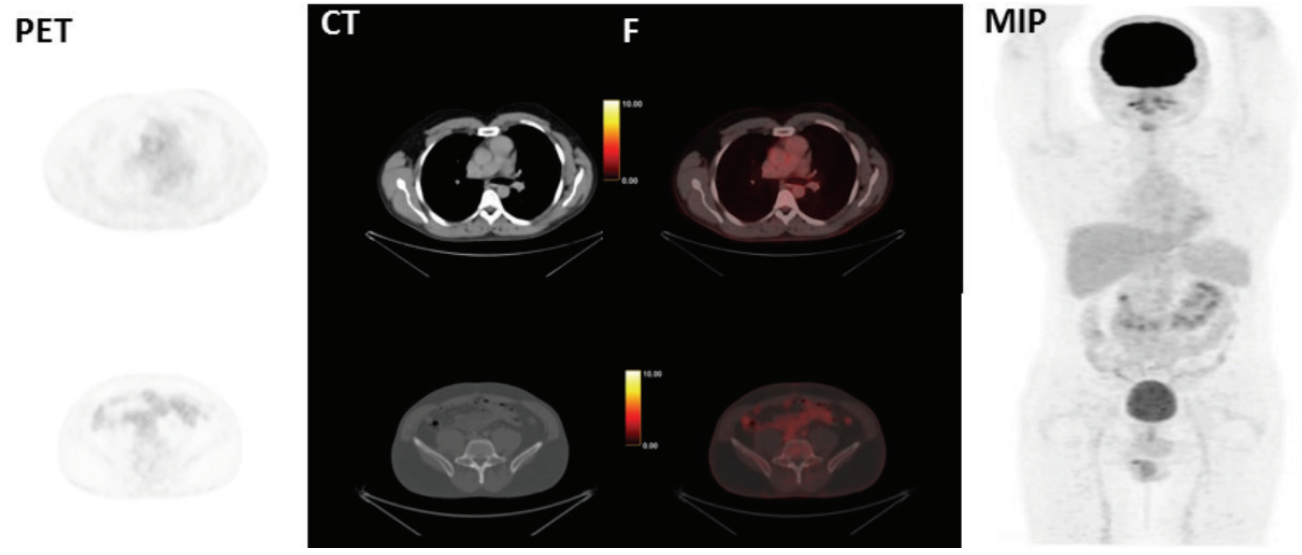

Figure 2. ^{18}F-FDG PET/CT images demonstrate complete metabolic response to systemic 20-40 mg/daily prednisone treatment after 8 months.

Ethics

Informed Consent: Was obtained from the patient.

Peer-review: Externally peer-reviewed.

Authorship Contributions

Surgical and Medical Practices: S.E., Concept: E.A., T.A., S.E., T.F.Ç., Design: E.A., T.A., S.E., T.F.Ç., Data Collection or Processing: E.A., T.A., S.E., T.F.Ç., Analysis or Interpretation: E.A., T.A., S.E., T.F.Ç., Literature Search: E.A., T.A., S.E., T.F.Ç., Writing: E.A., T.A., T.F.Ç.

Conflict of Interest: No conflict of interest was declared by the authors.

Financial Disclosure: The authors declared that this study received no financial support.

References

1. Statement on sarcoidosis. Joint Statement of the American Thoracic Society (ATS), the European Respiratory Society (ERS) and the World Association of Sarcoidosis and Other Granulomatous Disorders (WASOG) adopted by the ATS Board of Directors and by the ERS Executive Committee, February 1999. Am J Respir Crit Care Med 1999;160:736-755.
2. Rømer FK, Hommelgaard P, Schou G. Sarcoidosis and cancer revisited: a long-term follow-up study of 555 Danish sarcoidosis patients. Eur Respir J 1998;12:906-912.
3. Pavic M, Debourdeau P, Vacelet V, Rousset H. Place de la pathologie granulomateuse au cours des cancers [Sarcoidosis and sarcoid reactions in cancer]. Rev Med Interne 2008;29:39-45.
4. Grados A, Ebbo M, Bernit E, Veit V, Mazodier K, Jean R, Coso D, Aurran-Schleinitz T, Broussais F, Bouabdallah R, Gravis G, Goncalves A, Giovaninni M, Sève P, Chetaille B, Gavet-Bongo F, Weitten T, Pavic M, Harlé JR, Schleinitz N. Sarcoidosis Occurring After Solid Cancer: A Nonfortuitous Association: Report of 12 Cases and Review of the Literature. Medicine (Baltimore) 2015;94:e928.
5. Wirk B. Sarcoid Reactions after Chemotherapy for Hodgkin's Lymphoma. Clin Med Insights Case Rep 2010;3:21-25.
6. Inoue K, Goto R, Shimomura H, Fukuda H. FDG-PET/CT of sarcoidosis and sarcoid reactions following antineoplastic treatment. Springerplus 2013;2(1):113.
7. Sanan P, Lu Y. Multiorgan Involvement of Chemotherapy-Induced Sarcoidosis Mimicking Progression of Lymphoma on FDG PET/CT. Clin Nucl Med 2017;42:702-703.
8. Paparel P, Devonec M, Perrin P, Ruffion A, Decaussin-Petrucci M, Akin O, Sheinfeld J, Guillonneau B. Association between sarcoidosis and testicular carcinoma: a diagnostic pitfall. Sarcoidosis Vasc Diffuse Lung Dis 2007;24:95-101.